11-8-2016

Intraocular Pressure Sensing and Control for Glaucoma Research

Simon Antonio Bello
University of South Florida, simonabd@hotmail.com

Intraocular Pressure Sensing and Control

for Glaucoma Research

by

Simón Antonio Bello

A dissertation submitted in partial fulfillment
of the requirements for the degree of
Doctor of Philosophy in Electrical Engineering
Department of Electrical Engineering
College of Engineering
University of South Florida

Co-Major Professor: Christopher Passaglia, Ph.D.
Co-Major Professor: Wilfrido Moreno, Ph.D.
Paris Wiley, Ph.D.
Jing Wang, Ph.D.
Radouil Tzekov, Ph.D.

Date of Approval:
October 17, 2016

Keywords: telemetry, biomedical devices, IOP, wireless power, animal model

DEDICATION

To my parents, Antonio Bello and Kenndy Delgado, and my siblings Rodrigo and Ximena Bello. Thank you for being my inspiration, my source of comfort, my all. I love you with all my heart.

"It will forever live in my chest what I learned from their love.

From my mother: kindness. From my father: dedication.

From both…Hope"

- *Anonymous*

ACKNOWLEDGMENTS

I would like to express my most sincere gratitude to all of those that made this project possible. Firstly, Dr. Christopher Passaglia, my research advisor, who has been an invaluable mentor for me. He has taught me not only how to do research, but how to think critically and analyze every problem that comes my way. I deeply appreciate the patience, time and dedication that he took to ensure that I succeeded in this journey. I can only hope that my next boss is as affable as he has been, always making me feel like a colleague and an important part of the team. Secondly, Dr. Wilfrido Moreno without whom I would not be in the position that I am today. I will be forever grateful for his efforts and guidance to help me start my graduate studies. For the past five years he has been an instrumental advisor to me, always acting in my best interest without asking for anything in return. I would also like to thank the members of my dissertation committee, Dr. Jing Wang, Dr. Paris Wiley and Dr. Rad Tzekov, who have kindly lent me their time. Lastly, I would like to acknowledge my lab mates, especially Dr. Xiaolan Tang and Ashley Knight for their surgical assistance during my experiments, as well as Dan Capecci for his important software contributions and the time he volunteered to help move this project forward.

TABLE OF CONTENTS

LIST OF TABLES

LIST OF FIGURES

ABSTRACT

Animal models of ocular hypertension are important for glaucoma research but come with experimental costs. Available methods of intraocular pressure (IOP) elevation are not always successful, the amplitude and time course of IOP changes are unpredictable and irreversible, and IOP measurement by tonometry is laborious. This dissertation focuses on the development and implementation of two novel systems for monitoring and controlling IOP without these limitations. The first device consists of a cannula implanted in the anterior chamber of the eye, a pressure sensor that continually measures IOP, and a bidirectional pump driven by control circuitry that can infuse or withdraw fluid to hold IOP at user-desired levels. A portable version was developed for tethered use on rats. The system was fully characterized and deemed ready for cage- or bench-side applications. The results lay the foundation for an implantable version that would give glaucoma researchers unparalleled knowledge and control of IOP in rats and potentially larger animals.

Moreover, a novel mathematical technique was developed to efficiently analyze IOP records obtained using the pressure controlling device. The algorithm successfully yields the value of several parameters that influence ocular physiology and are commonly linked to glaucoma development. This unique methodology uses information regarding the amount of volume necessary to maintain IOP at different levels to quantify the outflow facility of perfused eyes. The use of this technology largely simplifies the investigator's experimental set-up and cuts procedural times in half.

The second device is an implantable pressure sensor for continuously monitoring IOP. The miniature system is equipped with pressure and temperature transducers, on-board amplifiers and a powerful microcontroller that ensure data quality. The sensor is able to obtain measurements with twice the accuracy and precision of any other IOP sensor used to date, avoid electronic drifts commonly seen in commercial sensing devices, and can potentially be used in a variety of animal models. The sensor was characterized and tested in alert rats for weeks on end. Data obtained with this device showed the presence of previously reported circadian rhythms, with IOP significantly increasing during nocturnal cycles. This technology provides researchers with an unprecedented tool to analyze IOP dynamics over time. The characterization of the amplitude, period and phase of the IOP profiles of normal and glaucomatous eyes may help establish a definitive correlation between ocular hypertension and glaucoma progression.

While implantable systems provide investigators with essential physiological data, their implementation can be difficult. Challenges such as reduced operational lifetimes and limited data acquisition capabilities are commonly faced by most bio-devices. These limitations are frequently linked to small battery capacities, however the implementation of bigger batteries is not usually viable due to size requirements. Energy harvesting technologies have surfaced in recent years in an attempt to replace battery applications; however, most technologies provide low power densities and cannot deliver continuous telemetric operation. An innovative wireless powering system was developed to overcome these limitations. The technology uses radio frequency (RF) energy transfer to continuously harvest high energy levels. Taking advantage of the controlled environment under which most research animals are housed, RF transmitters are placed around the cage to form strong, omnidirectional electric fields. An especial antenna was designed to be worn by the animal and collect large energy levels, irrespective of animal

movements and positioning. The system was tested on the implantable IOP sensor for weeks, providing robust performances and allowing the sensor to collect data continuously with high precision. The device consistently generated power densities much greater than those required by the sensor. The surplus of energy could be used to operate multiple sensors simultaneously, greatly increasing the investigator's leverage. The technology is easily adaptable to other bio-sensors and has the potential to revolutionize the biomedical field.

CHAPTER 1: INTRODUCTION

1.1 Background

Glaucoma is a set of ocular disorders that preferentially targets retinal ganglion cells and their axons within the optic nerves, causing a gradual loss of visual sensitivity and eventually blindness if left untreated. Glaucoma is the second leading cause of blindness in the world with over 2.2 million cases reported in the U.S. (Friedman, 2004). Even more alarming are the projections of over 80 million cases worldwide estimated to occur by the year 2020, up from a reported 60 million cases in 2010 (Quigley, 2006). The development of glaucoma is often associated with elevated intraocular pressure (IOP), which is considered its only modifiable risk factor (Sommer, 1989; Sommer 1996). Studies have shown that the risk of retinal and optic nerve damage increases with high IOP (Chauhan, 2002; Heijl, 2010), and that medicines which lower IOP in glaucoma patients can reduce or arrest disease progression (Kass, 2002; Quigley, 1982). Thus, IOP remains the focus of most glaucoma research studies and clinical treatments.

IOP is the result of the dynamic balance between fluid production by the ciliary body epithelium, and fluid drainage through pressure dependent and independent pathways in the eye. The increase in IOP that leads to glaucoma is caused by ineffective drainage through the outflow channels. As the eye is unable to release the extra fluid produced over time, pressure rises. The amount and rate of pressure change depends on the form of the disease presented. With angle-closure glaucoma the IOP increase can be large and rapid due to blockage of aqueous humor outflow through the iridocorneal angle by the iris; whereas, with open-angle glaucoma the IOP

increase is deceptively subtle and slow due to a gradual decline in outflow facility that can take months or years to be noticed. IOP values in a normal human eye range between 12-22mmHg, while some glaucoma patients experience ocular pressure levels that fluctuate between 22-30mmHg (Wilensky, 1991).

Even after decades of research little is known about the dynamics of IOP. Common clinical practices measure IOP during doctor's appointments every few months. These assessments are usually performed during business hours using Goldmann applanation tonometry, a tool that provides a snapshot of the patient's pressure profile. On the other hand, research has shown that IOP fluctuates throughout the day (Frampton, 1987; Gautam, 2016) and can be affected by ocular pulsations (Katsimpris, 2014) and even body posture (Gautam, 2016). The endogenous variability of IOP and the sparsity of data create important challenges when studying glaucoma. For instance, clinical studies that investigated the incidence of IOP fluctuations on the disease based on inter-visit data have been inconclusive (Bengtsson, 2007; Caprioli, 2008; Medeiros, 2007). Even in research settings, the investigator can only obtain measurements a few times a week via tonometry and, when used in animals, data tends to be less accurate and more variable due to the high corneal curvature of smaller eyes (Abrams, 1996). The absence of technology that can provide comprehensive IOP data over time has hampered our ability to answer questions regarding glaucoma onset and development.

To answer these questions researchers have developed several experimental models for glaucoma induction. The models aim to recreate the disease in order to study its behavior, as well as possible treatments avenues. Numerous animal species have been investigated based on accessibility, the proximity of their ocular anatomy to that of humans (Dawson, 1993; Van Der Zypen, 1977) and their ability to spontaneously manifest glaucoma (John, 2005; Kolker, 1963).

Most induction models work by increasing the hydraulic resistance of the aqueous outflow pathways of the eye through anatomical alterations, or by introducing a foreign body that blocks fluid channels and impedes normal drainage. The reduced aqueous fluid outflow leads to chronic ocular hypertension and progressive damage of the retina and optic nerve like that seen in human glaucoma.

1.2 Motivation

While experimental models provide much insight, available methods of glaucoma induction and pressure monitoring have important limitations that the field must strive to address. Some of these limitations are illustrated in Figure 1.1, which plots the IOP record of a rat in which a common experimental model was used. The episcleral veins of one eye were injected with hypertonic saline to cause IOP elevation. One limitation, particularly for surgical methods of induction, is that the treatment does not always lead to ocular hypertension and success may not be apparent for weeks. For instance, this animal required two injections (dashes), meaning that a month of effort was ostensibly lost. Our success rate with the saline injection procedure is ~50% on the first try and ~80% after the second try, which is typical. A second limitation is that the amplitude and time course of IOP changes are not predictable or reproducible. The treated eye of this animal, for example, took a month to settle at a level of ~40 mmHg while IOP in other animals might plateau at a higher or lower level, reach the plateau at different time points, or exhibit other dynamical behaviors. Such differences in IOP profile often get obscured when results are pooled across animals, and the detailed pressure history to which an eye is exposed could be meaningful to disease pathology. Additionally, during these procedures permanent damage is done to the trabecular outflow pathway so IOP changes are generally irreversible. As a consequence, comparatively little is known about the ability of the

retina and optic nerve to recover from glaucomatous insult. Most of these challenges are common across glaucoma induction models. Another limiting factor is that IOP data are usually collected by hand with a tonometer so the measurements are, as previously discussed, sparse, variable, and time consuming. The sparsity of data makes it is unclear, for example, whether the IOP of this animal rose to a peak then fell slightly or increased monotonically to a sustained level.

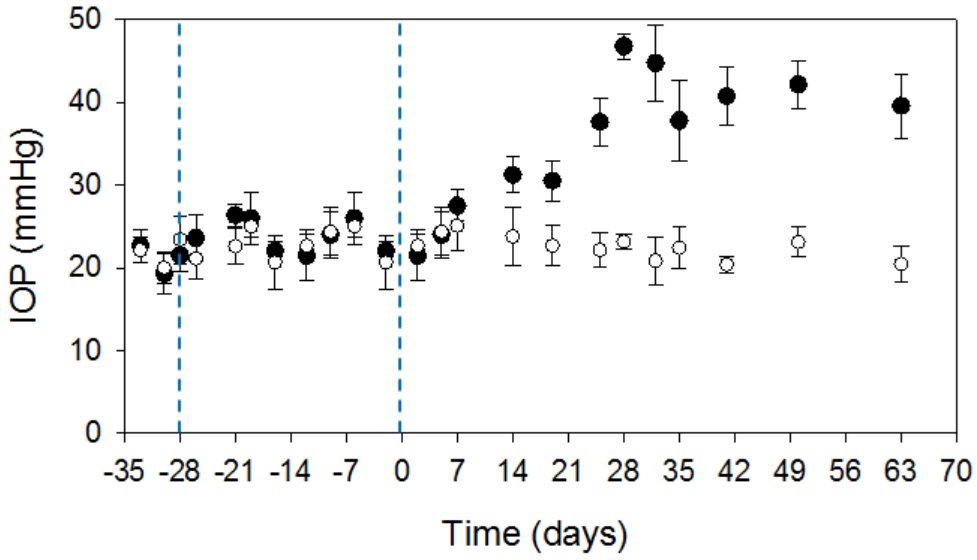

Figure 1.1 Rat glaucoma model. Mean IOP before and after hypertonic saline injection into one eye of a rat (unfilled circles: control eye, filled circles: treated eye). IOP was measured with a Tono-Pen XL tonometer. Each point is the average of 10 measurements. Error bars give the standard deviation. Dashed line indicates the day of saline injection.

Other technologies, besides tonometry, have been explored for more frequent IOP data collection; however, they present limitations of their own that makes them non-ideal. Commercial sensors used in the field for continuous IOP monitoring are adaptations of systems that were designed for other applications. As such, they are not optimized to work in normal IOP ranges. For instance, a sensor commonly used in glaucoma research (Li, 2008; McLaren, 1996)

was originally designed to measure blood pressure. The accuracy levels of this system are in the order of ± 3 mmHg, which are adequate to measure blood pressure signals that normally range between 120 and 130 mmHg in rodents (Parasuraman, 2012). However, when used to measure IOP signals that oscillate in the teen values, an error of 6mmHg is less than desirable. Moreover, these devices are powered by unregulated batteries that have an adverse effect on the sensor's calibration over time. Battery drainage frequently results in electronic artifacts that compromise data quality (Downs, 2011) and, in some cases, severely limit the length of the experiments. An inclusive review of the available IOP measuring technologies and glaucoma induction methods is presented in chapter 2. To conduct effective and comprehensive glaucoma studies, we must aim to develop better induction models, as well as more accurate means to continuously monitor IOP.

1.3 Aims and Objectives

This dissertation work describes novel IOP sensing and control systems that can overcome the limitations of current glaucoma models and pressure measuring technologies. The project was focused on the design, development and testing of two devices. The first one consists of an autonomous bidirectional pressure-sensing pump, connected to a cannula that is chronically implanted in the eye. The device offers closed-loop pressure control, without altering ocular anatomy, and aims to serve as a hypertension model for glaucoma studies. The iPump, as we have named this device, offers a simple implementation to actively manipulate fluid levels in the eye in order to increase or decrease pressure. This feature will allow researchers, for the first time, to steadily maintain IOP at different levels and correlate pressure dynamics and mean values to specific damage at the ocular nerve. An innovative mathematical technique was developed to analyze data obtained using the iPump. The algorithm yields the values of important physiological parameters that affect IOP and are often associated with glaucoma

development. This technique enables researchers to accurately measure the outflow facility of an eye while halving experimental times and reducing the size and complexity of the necessary equipment.

The second device consists of an implantable sensor that continuously measures intraocular pressure. The system aims to facilitate the study of IOP dynamics in normal and glaucomatous eyes, while serving as a bridge for the future miniaturization of the iPump. The device is equipped with an embedded microcontroller and a Bluetooth module for data processing and wireless transmission. On board amplifiers ensure clean and accurate data. A unique wireless powering system was designed and implemented to continuously run the sensor without batteries. The robust performance of the energy transfer technology provided the sensor with unlimited functional lifetime and eliminated electronic artifacts commonly seen in battery-operated sensors. No other sensor available today offers these capabilities. Both of these devices serve as enabling technology to improve the current state of the art and advance the knowledge in the field, potentially affecting the lives of millions of people.

1.4 Dissertation Outline

The design, construction and testing of these devices is explained in the subsequent chapters as follows:

- Chapter 2 presents a comprehensive list of the currently available sensors that have been used to monitor IOP, as well as the reported techniques for ocular hypertension induction. The advantages and disadvantages of each one of them are discussed.
- Next, chapter 3 covers the development and testing of the iPump. Its individual components are described and characterized. Similarly, a careful assessment of the system's ability to accurately measure and regulate IOP in rats is presented.

- In chapter 4 we describe a mathematical model to calculate the individual physiological parameters that affect IOP. This methodology provides accurate measurements of outflow facility in a rat eye in half the time of traditional outflow experiments and avoids the use of bulky equipment.
- Following the iPump implementation, chapter 5 focuses on the development and testing of the implantable IOP sensor. An electronic description of the sensor is provided, its properties are characterized and its performance is examined in fully awake rats. This chapter also presents statistical analysis of the IOP data obtained using the sensor.
- Chapter 6 presents the construction of a novel system for wirelessly powering biological sensors. Its properties were characterized and the system was tested by remotely powering an IOP sensor in an alert rat.
- Lastly, Chapter 7 presents the concluding remarks of the project, as well as recommendations for possible future research in glaucoma, and other avenues, using the devices described in this document.

CHAPTER 2: STATE OF THE ART

This dissertation addresses the need for improved IOP sensing technology and more effective glaucoma induction models. In order to truly understand the requirements of both of these processes, one must first analyze the current state of the art. The following section details the pressure transduction systems that have been employed to continuously measure IOP, as well as the glaucoma models that have been reported in the literature. The advantages and disadvantages of each are explored. Similarly, a description of the "ideal" system for glaucoma research is described to provide a template to which the technology developed in this project intended to adhere.

2.1 IOP Telemetry

2.1.1 T30-13B by Konigsberg Instruments

This sensor has been implemented to measure and characterize IOP dynamics in monkeys (Downs, 2011). The system allows for continuous data collection of IOP, heart rate and body temperature at 500Hz. The device provides excellent accuracy levels of ± 0.5 mmHg and non-restrictive transmission distances. The high sampling rate allows the user to obtain IOP fluctuations due to blinks, saccades and possibly ocular pulsations due to heart beat modulation of the venous system (Downs, 2011). The sensor has been extensively implemented to measure acute IOP responses to varying conditions such as stress levels (Downs, 2016), eye rubbing (Turner, 2016) and anesthesia induction (Jasien, 2016). These studies have yielded important results for researchers studying IOP variability.

For chronic data collection using this system, some limitations must be considered. One concern lies on the device's unregulated battery supply, which causes artificial drifts in pressure measurements over time. These drifts have been documented to be in the order of -17mmHg/month during the first six week of operation and 6mmHg/month thereafter (Downs, 2011). Considering that normal IOP levels in monkeys in the order of 12-20 mmHg (Yu, 2009), the downward trend exhibited by this system represents an important challenge. For instance, if an implanted animal had an initial IOP baseline of 18 mmHg on day 1, one month after implantation pressure readings will have declined to ~1mmHg, even though actual IOP is most likely still close to the original value. To counteract the effects of artificial drifts, periodic recalibration is necessary. Subcutaneous implantation of the system makes direct troubleshooting unviable. Therefore, recalibration is performed by cannulating the eye using a needle connected to an additional pressure transducer and digitally adjusting the system's readings. The steep slope of the pressure drifts and their nonlinear behavior require bi-weekly recalibrations. This is not only laborious, but recurrent cannulation could be detrimental to the ocular health. Moreover, leakage caused by the perforation of the anterior chamber disrupts normal IOP dynamics, forcing investigators to avoid data collection on the days following calibration (Downs, 2011). Additionally, the system's manufacturer recommends that data collection be kept in blocks of 24 hours at a time in order to avoid write-to-disk errors. Following post-recalibration guidelines and the data collection requirements, researchers have been limited to collecting data only 6 days per month for up to 9 months (Downs, 2011). The low number of data-available-days may present limitations for long term glaucoma studies. Another challenge is the system's size, which makes it unsuitable for smaller, more affordable and easily manageable animal species (e.g. rodents, rabbits, etc.).

2.1.2 C10/C40 by Data Science International (DSI)

The C10 and C40 wireless sensors are probably the most widely used IOP telemetry systems. The biggest advantage of the DSI sensors is their size, which has granted their implantation in rabbits (Akaishi, 2005; McLaren, 1996), and mice (Li, 2008). These sensors obtain 15 seconds of pressure data, sampled at 100Hz, every two minutes. While less powerful than the Konigsberg system in terms of sampling frequency and multi-parameter monitoring, DSI sensors do not suffer from the 24-hour data collection restriction, permitting it to run for several consecutive days. The research studies that have employed these sensors have provided us with pioneering data on IOP circadian variations (McLaren, 1996) and the effects of certain drugs on lowering IOP (Akaishi, 2005).

DSI sensors are also powered with unregulated supplies, which make them vulnerable to artificial pressure drifts similar to those seen in the Konigsberg systems. According to the manufacturer's specifications, the C10 and C40 sensors experience downward trends of 2-5mmHg/month, can operate continuously for 1-2 months before the batteries are depleted and experience accuracy levels of ± 3 mmHg. A window of error of 6mmHg severely compromises the validity of IOP data, given that the eye is naturally oscillating in teen values of pressure. Lastly, the DSI sensors have a transmission distance of only 18 inches, which can create data losses as the animals move away from the receiver. This limitation makes them unsuitable for implementations in larger animals that are kept in more spacious cages (e.g. monkeys).

2.1.3 Triggerfish by Sensimed

The Sensimed's triggerfish device is one of the most promising systems available today. It consists of a custom designed contact lens with an embedded strain-gauge that is able to

measure corneal deformations due to pressure variations (Leonardi, 2009). The electronics are inductively powered using a coil attached to a plastic frame that the patient wears. This device has been implemented successfully in humans, allowing researchers to continuously track IOP variations throughout the day (Mansouri, 2011; Mansouri 2012). The noninvasive nature of the technology allows for an easier implementation, however, transcorneal IOP measurements present some drawbacks. For instance, corneal properties such as thickness, curvature and elasticity are known to vary from subject to subject (Liu, 2005; Luce, 2005), and to accurately measure corneal deflections, they must be considered. While these parameters can be estimated in general, their variability could compromise the accuracy of the data across individuals (Liu, 2005; Whitacre, 1993). As a result, the triggerfish is able to track relative changes in IOP but it does so in arbitrary units created by the manufacturer, which cannot be easily converted into standard pressure units. Additionally, since the lenses are fabricated in standard human size, they cannot be implemented in lower level animals that are most commonly used for glaucoma or IOP studies.

2.1.4 WIT by Implant Data

The WIT sensor is a wireless telemetry system consisting of multiple capacitive-pressure cells and a microcoil antenna that are coated in a silicon package and implanted in the anterior chamber of the eye. The device couples inductively with an external reader which powers the sensor and collects IOP data at 10Hz. System operation requires the reader to be placed within 5 cm of the eye (Todani, 2011) which limits continuous data collection and requires an operator. The sensor's placement directly in the anterior chamber makes it independent of corneal physical properties that affect other IOP transducers (e.g. Triggerfish, tonometers, etc.). Although accurate readings have been reported via manometry using the WIT (Todani, 2011), data

collected in humans showed significant variability compared to tonometry (Koutsonas, 2015). The authors could not identify the source of this variability. Unexpected drifts were also observed, presumably due to fibrous reactions of the eye interfering with the sensor's performance (Koutsonas, 2015). The size of the WIT was designed for implantation in humans and large animals, but is not suitable for implementation in rodents whose research value has been discussed.

2.2 Animal Models for Glaucoma Induction

2.2.1 Hypertonic Saline Injection

As mentioned in chapter 1, this technique injects a hypertonic saline solution into the episcleral veins towards the limbus. The solution causes sclerosis of the outflow pathways of the eye, resulting in elevation of IOP (Morrison, 1997). This technique can recreate ocular outflow obstruction at the site of blockage seen in human glaucoma (Morrison, 2015), but it presents certain limitations. First of all, the methodology requires a complex microsurgical technique that can result difficult to master, and even the most skilled researchers experience a success rate of just around 50-60% (Morrison, 1997). Secondly, this method often needs repeating in order to achieve IOP elevations and induction success might not be apparent for weeks after experimental treatment (figure1.1; Morrison, 1997; Morrison, 2015). Moreover, in some cases, the procedure can result in excessive inflammation that generates IOP levels much higher than desired (Morrison, 1997). Lastly, in those animals in which the procedure is successful, the researcher has no control over the amount or time course of IOP elevation. The detailed pressure profile of the treated eye ranges widely across experiments, making it a challenge to draw definitive conclusions of the relationship between IOP dynamics and cell damage.

2.2.2 Microbead and Ghost Red Blood Cell (RBC) Injection

These two methodologies are very similar in nature and use the same principle. A foreign body is introduced in the eye through an injection into the anterior chamber. In both cases, the microbeads or RBC's obstruct normal outflow facility and result in IOP elevation. In most animals a single RBC injection is needed, however, the viscosity of the RCB's and the volume necessary to achieve IOP elevation can create poor visibility of the optic disk (Quigley, 1980), which is a crucial element in the clinical assessment of glaucoma progression. On the other hand, microbead occlusion techniques can be more time consuming as periodic injections are necessary to achieve chronic IOP elevation (Sappington, 2009; Weber, 2001), but does not compromise the visibility of the optic nerve (Weber, 2001). Both of these techniques have the added benefit of producing no intraocular inflammation, common in other glaucoma induction models. Although the mean IOP elevation can be somewhat adjusted by modifying the volume of microbeads/RBC's injected in the eye (Quigley, 1980; Sappington, 2009; Weber, 2001), these models offer no control over the variability if IOP during the experiment, which can limit the researchers ability to establish significant correlations between IOP levels and optic disk damage.

2.2.3 Laser Photocoagulation and Episcleral Vein Cauterization

Another way to induce ocular hypertension is to mechanically alter the outflow channels of the eye instead of blocking them. As aqueous humor leaves the anterior chamber, it flows through the trabecular meshwork and into the venous system via the episcleral veins (Tamm, 2009). The use of lasers (Gaasterland, 1974; Levkovitch-Verbin, 2002; Ueda, 1998) and cautery (Grozdanic, 2003; Shareef, 1995) to change the properties of these structures has been explored as a glaucoma model. While both techniques result in rapid elevation and less variable IOP

(Grozdanic, 2003; Levkovitch-Verbin, 2002; Shareef, 1995), their effect is limited as IOP returns to baseline levels within 2-3 weeks after the surgery (Gaasterland, 1974; Grozdanic, 2003; Levkovitch-Verbin, 2002; Shareef, 1995), which may not be sufficient for most glaucoma studies. Repeating the procedure may result in unwanted damage to the eye. While failure rates for photocoagulation models are fairly low, others have reported success rates of just 35% in cauterization models (Grozdanic, 2003).

2.2.4 Genetic Mutations

This model is the only one to manifest glaucoma spontaneously. Although multiple animal species have been studied, mice genetic models are the most widely used. Several strains have been identified with high IOP and inbred for research use. The most studied is the DBA/2J line which has a genetic mutation that causes iris pigment to slough off and accumulate in the trabeculum at 6-8 months of age (John, 2015). The pigment gradually obstructs fluid outflow, causing a gradual rise in IOP of moderate amount.

While the mouse model has the advantage that obstruction happens automatically, without the need for surgical interventions, a drawback is that the IOP increase is bilateral and the onset time is uncertain. Since both eyes experience hypertensive conditions, there is no internal control group for statistical comparisons. Moreover, frequent monitoring is needed to determine the duration of pressure exposure, which is difficult given the small size of mouse eyes. Induced glaucoma models are more laborious, but present the advantage of having the non-treated eye serve as a useful control for hypothesis testing. Additionally, the animal is genetically normal so any damage inflicted upon the eye can be directly linked to the experimental treatment itself.

2.3 The Ideal Research Model

Through this literature review, several characteristics have been identified as desirable for an ideal model to induce glaucoma and monitor intraocular pressure. In terms of IOP measuring, the technology must provide: i) continuous data, ii) have accuracy levels well-suited for low pressure ranges, iii) not present electronic pressure drifts, iv) allow implementation in a variety of animal species, iv) provide non-restrictive data transmission distances, v) be independent of corneal properties, vi) deliver extensive operational lifetimes, vii) monitor multiple physiological functions simultaneously and viii) present data in mmHg. On the other hand, the perfect glaucoma induction model should: i) offer high success rates, ii) sustain IOP elevation over time, iii) offer IOP controllability, iv) not produce detrimental biological responses, v) be unilateral, vi) be reversible and, vii) induce rapid IOP changes. Tables 2.1 and 2.2 compare available technologies to the ideal models.

Table 2.1 Ideal IOP Sensor vs. Available Technology

Feature	Ideal Sensor	Tonometer	Konigsberg	DSI	Triggerfish	WIT
Continuous data	Yes	No	Yes *	Yes	Yes	No
Accuracy	< 1 mmHg	± 3mmHg	± 0.5	±3mmHg	± 0.4	± 0.81
Drift	None	N/A	6-17 mmHg/month	2-5 mmHg/month	N/A	0-2 mmHg/month
Animal species	Rodents, rabbits, monkeys	Rodents, rabbits, monkeys	Monkeys	Rodents, rabbits	Humans	Rabbits, monkeys
Transcorneal	No	Yes	No	No	Yes	No
Operational Life	> 3 months	N/A	9 months	1-2 months	Unlimited	Unlimited
Multi-sensor	Yes	No	Yes	No	No	No
Pressure Unit	mmHg	mmHg	mmHg	mmHg	Arbitrary	mmHg

* Data only obtained in 24h blocks, 6 days a month.

Table 2.2 Ideal vs. Traditional Glaucoma Models

Feature	Ideal Model	Saline inject.	Micro bead Injection	RBC injection	Photo-coagulation	Vein Cautery	Genetic
Success Rate	100%	60%	90% multiple treatments	100%	85% multiple treatments	35%	100%
Sustained elevation	Yes	Yes	No	No	No	No	Yes
IOP control	Yes	No	No	No	No	No	No
Bio-response	None	Inflama-tion	None	Occlusion	Inflammati-on	Inflammati-on	Mutation
Unilateral	Yes	Yes	Yes	Yes	Yes	Yes	No
Reversible	Yes	No	No	No	No	No	No
Time before elevation	Immediate	2 weeks	1 week	1 day	2 weeks	1 week	6-8 months

CHAPTER 3: IPUMP SYSTEM

3.1 Note to Reader

This chapter has been previously published as an article in the Annals of Biomedical Engineering journal (Bello, 2016) and has been reproduced with permission from the Springer editorial. Authorization is included in Appendix A.

3.2 Introduction

Elevated intraocular pressure (IOP) has been identified as a major risk factor for glaucoma (Leske, 1995; Sommer, 1989), an eye disease that causes gradual loss of vision and eventually blindness if left untreated. To better understand the etiology and pathophysiology of the disease, several experimental models have been developed in mice, rats, rabbits, pigs, and monkeys. The models raise IOP by increasing the resistance of aqueous outflow pathways of the eye through a variety of techniques, including laser photocoagulation of trabecular meshwork (Gaasterland, 1974; Ueda, 1998) hypertonic saline injection into limbal vessels (Chauhan, 2002; Morrison, 1997), cauterization of episcleral veins (Ruiz-Ederra, 2005; Shareef, 1995), and ghost red blood cell (Quigley, 1980) or microbead (Sappington, 2010; Weber, 2001) injection into the anterior chamber. The reduced aqueous outflow leads to chronic ocular hypertension and progressive injury of the retina and optic nerve like that seen in human glaucoma.

Experimental glaucoma models are widely used by researcher with great success, but it is recognized that they have important limitations (Morrison, 2011). Firstly, the failure rate is high so many animals do not experience a significant IOP increase. Secondly, some methods need

repeating to achieve chronic IOP elevation and induction success might not be apparent for weeks after treatment (Chauhan, 2002; Morrison, 1997; Weber, 2001), while other methods produce a rapid IOP change that returns to baseline levels over time (Shareef, 1995; Ueda, 1998). Thirdly, the researcher has no control over the amplitude or time course of IOP elevation. The detailed pressure history to which treated eyes are exposed can range widely across animals, making it more difficult to correlate IOP exposure with glaucoma onset and progression. Fourthly, damage done to aqueous outflow pathways cannot be experimentally reversed so the capacity of the eye to recover from glaucomatous injury cannot be investigated. And fifthly, IOP is usually measured by hand with a tonometer. Tonometers can provide only an indirect and sporadic record of the pressure history of an eye, which is less accurate and more variable in smaller eyes having high corneal curvature (Abrams, 1996). The sparse pressure data hamper examination of relationships between glaucoma and IOP dynamics (Asrani, 2000; Bengtsson, 2000), which have been shown to fluctuate on multiple time scales due to blood pulsation, respiration, and endogenous biological rhythms (Akaishi, 2005; Downs, 2011; Li, 2008; Mansouri; 2012; McLaren, 1996).

This chapter describes a novel IOP control system that can overcome limitations of existing glaucoma models. We refer to the system as iPump because it consists of an autonomous pressure-sensing pump connected to a cannula implanted in the eye. Data are provided on: i) the resolution, noise level, and long-term stability of pressure measurements *in vitro*, ii) and the ability of the system to maintain IOP of anesthetized rats at any level desired by the user. The results demonstrate that a portable iPump system is ready for tethered use on rats and for miniaturization into an implantable device. The technology promises, for the first time, to provide researchers complete knowledge and control of IOP in conscious behaving animals.

3.3 System Overview

The iPump system includes a cannula, a pressure sensor, control circuitry, and a fluid pump (figure 3.1A). The cannula is implanted in the anterior chamber of the eye using an especial surgical technique (Bello, 2016) and conducts IOP to the pressure sensor. The controller circuit compares sensor output with a target IOP level specified by the user and commands the pump to withdraw or inject fluid through the cannula so as to set and hold IOP at the user-specified level. A 7-ml reservoir is connected to the pump that can be drained or refilled as needed. A portable system was constructed for research use (figure 3.1B). The cannula is a fine polyimide tube (ID: 100 µm, OD: 130 µm, MicroLumen, Oldsmar, FL) filled with sterile artificial aqueous humor (130 mM NaCl, 5 mM KCl, 5 mM $NaHCO_3$, 1 mM $CaCl_2$, 0.5 mM $MgCl_2$, 5 mM glucose, 20 mM HEPES, pH 7.25, McNulty, 2004). The cannula runs subdermally to a custom head mount (10 mm) that connects to the iPump via 30G Teflon tubing (length: 35cm, Zeus, Branchburg, NJ) and prevents animal movements from retracting the cannula tip from the eye.

The system interfaces with a computer via a USB connection, which provides power and data lines. A custom LabVIEW program sends the desired IOP set point to the device and records IOP and pump command signals at 1 Hz. The sampling rate can be adapted by the used through the LabVIEW interface. The iPump can operate in two modes. In open-loop mode, only the sensing elements are powered and IOP is reported. In closed-loop mode, the control circuitry and pump are also powered and IOP is clamped within a user-specified window of the set point. In the experiments describer throughout this chapter a ±2 mmHg window was used. IOP control is achieved by varying the pump rate or pump duty cycle. In the latter case, pump rate was fixed at 2 µL/min.

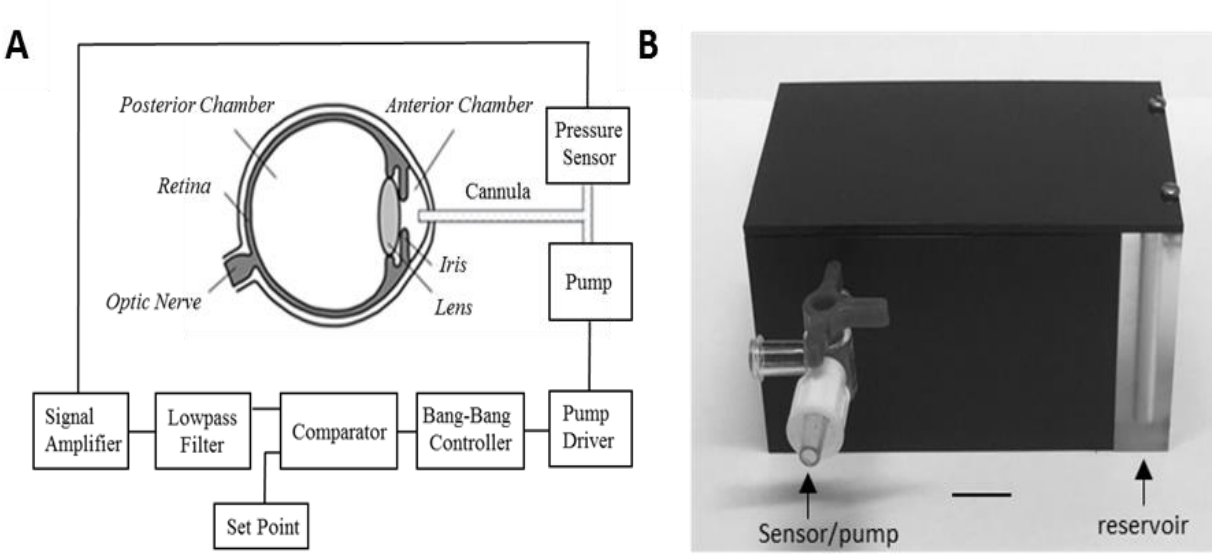

Figure 3.1 IOP control system. (A) Block diagram of the system. A pressure sensor measures IOP via a fine cannula implanted in the anterior chamber of the eye. A controller circuit amplifies and filters the pressure signal and compares the result against a user-specified set point. If IOP deviates from the desired level, the system produces a command signal that drives a small pump to inject or withdraw fluid through the cannula until IOP returns to the set point. (B) Picture of portable iPump system. All electronic components are housed in a small plastic box (8 x 5 x 4 cm) that contains a fluid reservoir which can be filled or drained. The box tethers to the animal via tubing that runs inside a protective spring to a plastic head mount which connects subdermally to the implanted cannula. Bar: 1 cm.

3.4 Electronic Description

Figure 3.2 illustrates the electronic schematics of the iPump system. The system is equipped with: i) a pressure transducer, ii) a low pass filter, iii) a microprocessor, iv) a pump driver, v) a micropump , vi) a flow restrictor and, vii) an optional flow meter. The device operates on a single-rail 5V supply that is stepped up or down throughout the circuitry to power the different stages. The implanted cannula serves as an interface between the eye and the iPump. Each component is described in more detail in the section below.

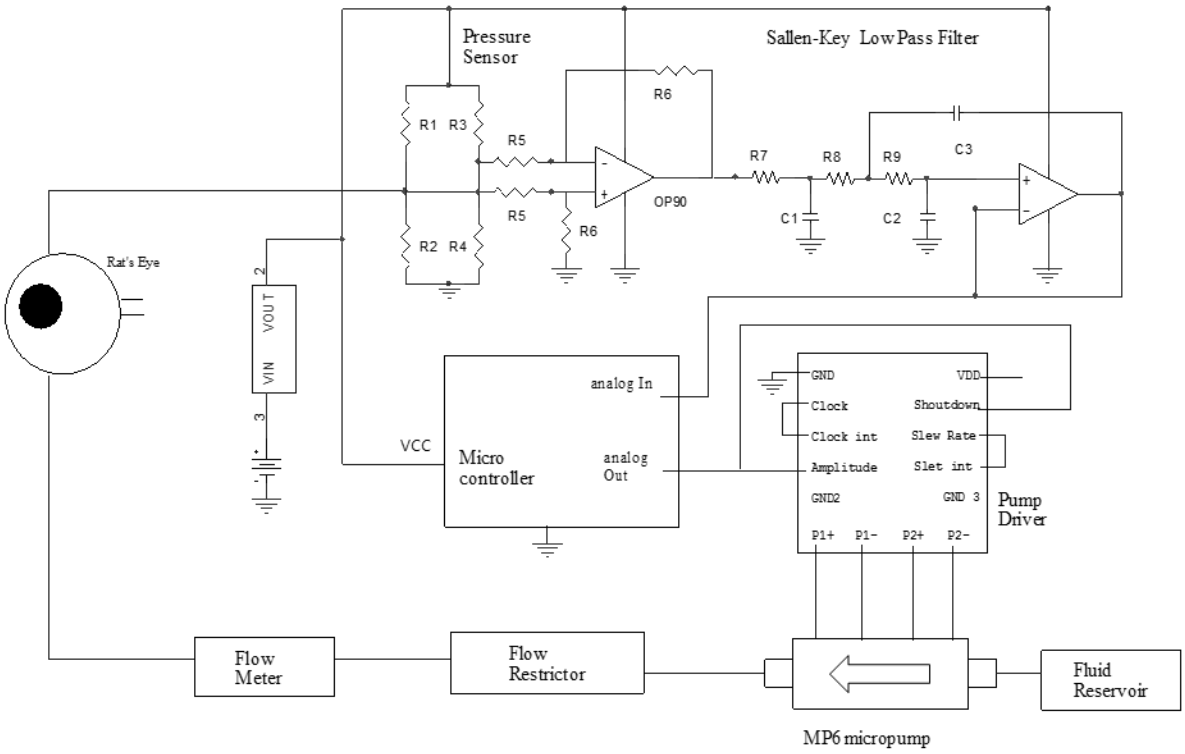

Figure 3.2 Electronic schematics of the iPump. The pressure sensor operates in a temperature compensated Wheatstone bridge configuration. The signal is differentially amplified x1000 and low pass filtered at a cut-off frequency of 1Hz. The bang-bang controller is implemented digitally in the microprocessor and while a dual DC-DC converter circuit drives the actuator micropump. Fluid is pulled from the reservoir and injected into the eye until IOP reaches the set-point. A mechanical flow restrictor helps maintain flow at a constant 2µL/min. A USB port provides a 5V supply to the system, which is stepped down to 3.3V in certain parts of the circuit.

3.4.1 Sensing Elements

3.4.1.1 Pressure Transducer

The pressure sensor (TBPDANS005PGUCV, Honeywell, Morristown, NJ) is a piezoresistive strain gauge manufactured on an alumina ceramic substrate and covered by a silicone gel coating that protects the electronic components from fluid condensation in the line. The sensor has an operating range of 0-250mmHg, with an overpressure capacity of 1500mmHg in reference to atmospheric pressure. During pressure control experiments IOP will be varied between 0-50mmHg. The transducer is equipped with multiple gauges which allow for

temperature compensation in the range of 0-85 °C and can operate with power supplies ranging from 1.5 to 12V. In our application the sensors are powered using a constant 3.3V supply and draw a nominal 300µA current.

3.4.1.2 Differential Amplifier

The sensor is connected to a differential amplifier with a gain of 1000 that ensures data accuracy and resolution. The selected microchip (OPG90, Analog Devices, Norwood, MA) is a precision operational amplifier that can be powered using a single supply between 1.6 and 36V. The single rail and low working voltage were crucial requirements for operation using a standard USB port as the system's supply.

3.4.1.3 Sallen-Key Low Pass Filter

IOP readings are influenced by other physiological functions, such as heart palpitations and respiration, which can create pressure fluctuations in the anterior chamber. In the rat these occur at frequencies of 4-5 Hz (McLaren, 1996). The sensor can also detect vibrations in the tethering line between the animal and the system, which can create noise in the data recorded. In order to achieve pressure control, however, the system should react only to DC changes in IOP and not physiological or mechanical noise. Therefore, a 3rd order low pass filter with a cut-off frequency of 1Hz in incorporated during data acquisition, which eliminates noise and allows for consistent pressure control.

3.4.2 Control Elements

3.4.2.1 Microcontroller

The system is run by a small programmable microcontroller unit (RFD22301, RFDuino, Hermosa Beach, CA), which is equipped with 128kB of flash memory for application space and

8kB of RAM memory. The chip is equipped with an 8-bit analog-digital converter and 7 general purpose input-output channels (GPIO). The microprocessor has two main functions: i) collecting and transferring data and ii) implementing digital control processes. The device is equipped with a USB cable that connects directly to the data collection computer. The connection serves as a bilateral communication pathway between the data acquisition software and the on-chip microprocessor. IOP data is continuously printed to the computer's communication port, while user commands are set at the PC and relayed to the device. Using a custom designed LabView program, the user can indicate changes to the set-point, which are read and stored in the processor's memory. The microcontroller then computes the error between the actual and desired IOP and uses an analog output channel to activate the pump's driver when the error is greater than the allowed window. The window of error is programmable and is set at a default 2mmHg. The same USB cable used for data communication powers the sensor and pump with 5V, while an intermediate DC-DC buck converter delivers 3.3V to the microprocessor.

3.4.2.2 Code

Bilateral communication between the iPump and the data collection computer was stablished using a custom written hand-shaking protocol that links the microcontroller with a LabVIEW program via a USB serial port and a special data acquisition add-on library (VISA, National Instruments, TX). The LabVIEW program also serves as the user interface, where *set-point, window*, *open loop* and *closed loop* settings can be changed. Each setting was assigned a flag for identification purposes. Loop settings were assigned the letter *k*, while set-point and window variables were identify by the letters *s* and *w*, respectively. When any of these settings is changed, the LabVIEW program prints the flag, followed by the new setting value, to the serial port. (e.g. s30, when changing the set-point to 30mmHg). A special logic algorithm was designed

to only print information to the serial port when one or more settings were changed. This procedure eliminates the need of continuous reading and writing by the microcontroller, which increases efficiency and decreases processing times.

The microcontroller code was written using C++ and loaded into the microprocessor using a stack-on USB-connector and Arduino software (Arduino, Italy). The device is set to use serial port communications at a 9600 BAUD rate. The code operates in two main *while loops*. First, the microcontroller checks the serial port for flags indicating that a setting has changed. If there is a flag present the code proceeds to remove the ID letter from the string and leave only the new set value (e.g. s30 is converted to 30) and the parameter is redefined (e.g. set_point= 30). Once this process is completed, the system collects IOP data from the sensor at 50Hz and calculates the *error* between actual and desired IOP. If the *error* is greater than the allowed *window* and the system is operating in *closed-loop,* the pump is turned ON. The microfluidic elements remain active until the error is reduced to 0 or a setting is changed. A second inner while loop is implemented to ignore the window threshold when the pump is active. This allows the system to drive IOP to the exact set-point but then allow a window of error before restarting perfusion. Once per second the microcontroller prints all settings and current IOP values to the serial port where the LabVIEW programs reads and stores them.

3.4.2.3 Pump Driver

In order to operate the pump efficiently the system employs a specialized driving circuit. The mp6-OEM controller (Servoflo, Lexington, MA) employs a two stage DC-DC voltage converter to generate peak-to-peak voltages up to 235V. The driver outputs two pulsating voltages at a frequency of 100Hz, which are used to operate the actuators of the mp6 pump described in the next section. The pump rate is modulated via an analog voltage ranging from 0.6

to 1.3V at the *amplitude* pin, which is generated by the microprocessor. Due to the high voltages generated by the driver, care should be taken when troubleshooting as they can be harmful to the body.

3.4.3 Pumping Elements

3.4.3.1 Micropump

The pump (mp6, Servoflo, Lexington, MA) uses two piezoelectric diaphragms in combination with passive check valves to move fluid from the reservoir to the eye. The voltage generated by the driver causes a downward deformation of the pump's piezoelectric membrane, resulting in a displacement of fluid out of the pump in the direction defined by the valve. Alternatively, when voltage decreases, the membrane experiences and upwards deformation that draws fluid from the reservoir into the pump. Oscillation between high and low voltages generates steady flow rates. Those flow rates, however, can be affected by external conditions such as the backpressure generated by the eye and conducted to the pump via the tethering tubing. According to the manufacturer, when operating at maximum performance, the mp6 generates flow rates of 7000 µL /min at no backpressure. Flow decreases linearly with backpressure and stops completely when it reaches 450mmHg (figure 3.3A). In order to effectively control IOP, the pumping rate must be kept within 1-4 µL/min (as shown in the results section of this chapter). Decreasing the driving voltage of the pump results in slower infusion rates, but also decreases the maximum backpressure handled by the device. This voltage reduction keeps the slope of the operating line constant at approximately -15 µL/min/mmHg, which results in a backpressure sensitivity level not viable for IOP control. In order to decrease the system's flow rate while maintaining maximum backpressure levels, a flow restrictor is incorporated between the pump and the eye.

3.4.3.2 Flow Restrictor

A change of slope in the characteristic curve of the pump can be achieved by incorporating a flow restrictor, which is a piece of tubing with a reduced lumen that connects the outlet of the pump to the cannula. Following Hagen-Poiseuille's law the volume flow through a conductor is:

$$Q = \frac{\Delta P}{R} \quad (1)$$

and

$$R = \frac{8 \cdot \eta \cdot L}{\pi \cdot r^4} \quad (2)$$

where Q is the volume flowrate, ΔP is the change is total pressure (e.g. 450mmHg at maximum performance for the mp6), R, r and L are the resistance, radius and length of the conductor, respectively, and η is the dynamic viscosity of the fluid (8.75 x 10^{-8} mmHg·min at body temperature; Fitt, 2006). To calculate the total flow rate, the inner resistance of the pump (5.1429E+11 Pas / m^3, per manufacturer indication, must also be taken into consideration, making equation (1)):

$$Q = \frac{\Delta P}{\mathrm{RTubing} + \mathrm{RPump}} \quad (3)$$

for instance, using a flow restrictor with and inner diameter of 40µm and a length of 10cm while operating the pump at maximum performance, results in a maximum flow rate of approximately 2.3µL/min while handling a maximum backpressure of 450mmHg. The slope of this new characteristic curve is 0.005µL/min/mmHg (figure 3.3B), which is negligible in the pressure ranges that IOP is expected to be maintained.

3.4.3.3 Flow Meter

In applications in which exact flow rates are required, a flow meter can be incorporated between the restrictor and the eye, however this component is optional. The meter (LG16-0150A, Sensirion, Switzerland) can detect flowrates ranging 0-7µL/min with nL/min resolution. The module operates with a 9V power supply, which cannot be achieved via USB powering. Therefore, the flowmeter is not incorporated within the iPump case and it is rather used as an add-on accessory.

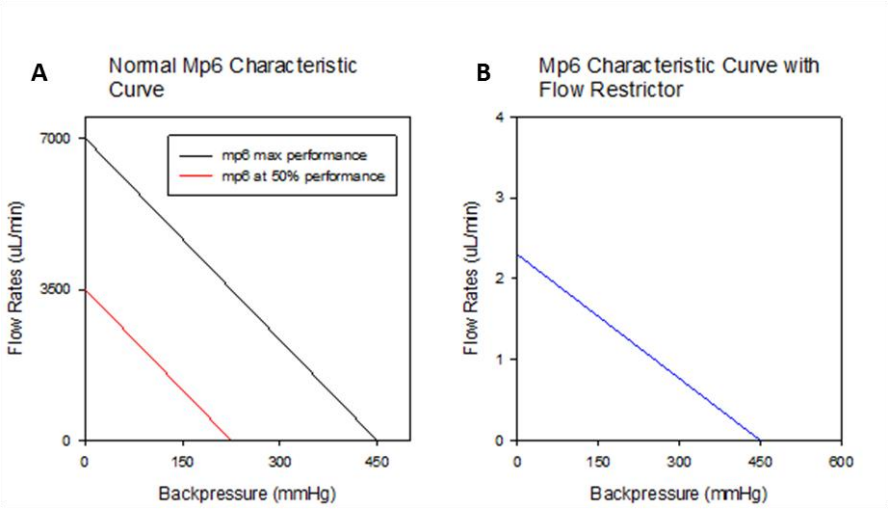

Figure 3.3 Backpressure vs. flow rate operating curve of the mp6. (A) When the system is operated at maximum performance (black line) it can pump at 7mL/min when opened to air and can withstand a maximum backpressure of 450mmHg. When the driver circuit is set to operate the pump at 50% of max performance, max flowrate decreases to 3.5mL/min and the max backpressure becomes 225mmHg. (B) When fluid is pumped through a flow restictor (ID:40µm, length: 10cm) the mp6 can move fluid at 2.3µL/min when opened to air and endure a mximum pressure of 450mmHg.

3.4.4 Circuit Board and Packaging

Figure 3.4 shows the circuit board of the iPump with hand soldered elements and a schematic of its custom designed case. The circuit is organized in two vertical levels that

separate the electronic and fluidic elements. A plastic case was designed using CAD software (SolidWorks, Waltham, MA) and machined in acetal homopolymer (Derlin, Interstate plastics, Sacramento, CA). The bottom part of the case houses the electronic circuitry, while the pump and restrictor are placed on a plastic shelf that rest on four beams built on the box's corners. The flow restrictor is connected to the sensor and the exit port via 16G tubing and a 3-way connector. The pump is connected to the driver using a special flexible connector (Molex FCC 39532045, Lisle, IL) that is routed to the circuit board and soldered in placed.

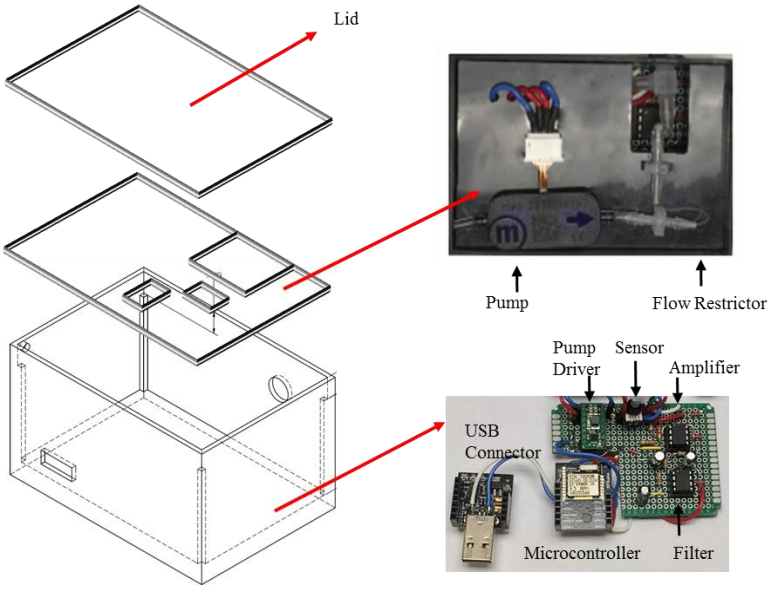

Figure 3.4 iPump system circuit board and case. Plastic case was designed using CAD software (left). The bottom of the case houses all electronic elements (bottom right). The USB connector and the microprocessor are stacked up using a 12 pin built-in connector. A custom shelf holds the micropump and restrictor in place (top right). A plastic lid is held in place using 4 screws.

3.5 Materials and Methods

3.5.1 Animal Preparation

Experiments were performed on adult Brown-Norway rats (300-400 g, Harlan Laboratories Inc.) housed under a 12hr-12hr (6am - 6pm) light-dark cycle and fed a standard

daily diet. Animals were kept in a temperature controlled room (22°C) and were under regular veterinarian supervision. All procedures were approved by the Institutional Animal Care and Use Committee of the University of South Florida in accordance with NIH guidelines.

3.5.2 Calibration and Bench Testing

The iPump system was calibrated by connecting the cannula (length: 10 mm) to a saline reservoir and mercury manometer via a three-way stopcock. Reservoir height was varied, and the offset voltage and gain of the pressure transducer were mapped to mmHg. Long-term stability was evaluated by fixing reservoir height and recording pressure continually for 90 days. The reservoir was covered to prevent evaporation, and fluid level was regularly checked to verify that hydrostatic pressure stayed constant. Room temperature was concurrently monitored with a thermistor. Drift in transducer output was approximately linear and quantified by regression. System accuracy was evaluated by recording IOP in dead rats with an independent commercial pressure transducer (5110, Stoelting, Wood Dale, IL). Animals were anesthetized with a mixture of ketamine and xylazine (50 and 7 mg/kg, IP), and an eye was cannulated with two 33G needles mounted on micromanipulators. One needle was connected to the iPump cannula (length: 10 mm) and the other to the commercial transducer. Animals were then euthanized with Euthasol (>50 mg/kg, IP), and sensor outputs were digitized to computer. After IOP fell to 0 mmHg the system was run at pump rates of 1-4 µL/min for several minutes each, and sensor differences in IOP onset and amplitude were quantified. System dynamics were separately evaluated by measuring the time needed for each rate setting to raise IOP by 20 mmHg.

3.5.3 System Testing in Anesthetized Animals

The *in vivo* performance of the complete iPump system was assessed in 5 rats. After implanting a cannula (length: 20 mm) for >3 days to allow for wound closure, animals were

anesthetized with the ketamine-xylazine mixture. A catheter was inserted in the femoral vein, and anesthesia was maintained for remainder of the experiment via intravenous infusion of ketamine (30 mg/kg/hr), dextrose (600 mg/kg/hr), and physiological saline. The head was mounted in a stereotaxic, and the body was rested on a heating blanket under temperature control via a rectal thermometer. Needle electrodes were inserted to record the ECG. Eyes were instilled with mydriatic and fitted with clear contact lenses to prevent corneal drying. The scalp was opened to expose the implanted cannula, which was then connected to a fluid-filled 30G needle tethered by PTFE tubing and a three-way stopcock to the iPump system. The third port was closed except to extract bubbles in the line or null the system to atmospheric pressure. Data were collected while vitals (heart rate, ECG waveform, body temperature) remained at healthy levels. The system was run in open-loop mode for two animals and closed-loop mode for three animals. Before activating feedback control the implanted eye was undisturbed for 15 minutes to determine baseline IOP. Afterwards, the system was programmed to step IOP to levels ranging from 5-35 mmHg and hold IOP within ±2 mmHg of the target level for 2-4 hours.

3.5.4 Data Analysis

Statistical significance was assessed by a two-sample *t*-test with an alpha level of 0.05 using SigmaPlot software (San Jose, CA). Results are expressed in terms of mean ± standard deviation.

3.6 Results

3.6.1 Specification of System Properties

The IOP control system was calibrated by connecting the cannula to a variable-height fluid reservoir and mercury manometer. Figure 3.5A plots the recorded pressure as hydrostatic

pressure was raised from 0 to 100 mmHg in steps of 20 mmHg and then released. It can be seen that the iPump system responds instantly to pressure changes with a step-like waveform as well. Figure 3.5B plots the average pressure reading for each pressure step. Sensor output is linear over the range tested, which more than spans normal and glaucomatous IOP levels. Sensor output is also very accurate. The standard deviation of the noise in the pressure record is <0.5 mmHg for all applied pressures. Long-term stability was evaluated by applying constant hydrostatic pressure to the system for several weeks via a water column (n = 3). Figure 3.5C shows the output of an iPump system exposed to 40 mmHg for 90 days. Linear regression of the data yielded an average pressure reading of 40.4 ± 0.4 mmHg. The regression slope was -0.05 mmHg/week for this prototype and +0.04 and -0.02 mmHg/week for two others, amounting to a total pressure drift of <1 mmHg over 3 months. Throughout the recording the ambient room temperature was monitored. Figure 3.5C (inset) shows that sensor output was insensitive to temperature changes between 22 to 26 °F (R^2 = 0.003). Sensor output was not examined for temperatures outside the range in which the system would normally operate. These results indicate that the iPump system can record pressure with high accuracy for months on end.

IOP measurement accuracy was evaluated by cannulating the anterior chamber of rat eyes *in situ* with two needles, one of which was connected to the cannula and the other to a calibrated commercial pressure transducer. The animal was euthanized prior to data collection to eliminate biological disturbances. Figure 3.6A shows the IOP signals recorded by the sensors as the iPump system perfused the eye at different rates, each of which increased IOP by 10 mmHg. Between the steps in perfusion rate the pump was turned off until IOP declined naturally by 5 mmHg. It can be seen that the system accurately tracked pump-induced changes in IOP level, as measured directly and independently by the commercial sensor. Figure 3.6B shows the average

discrepancy in the IOP records across a group of animals (n = 4). The difference was virtually zero at rest and when the pump was off (0.2 ± 0.2 mmHg). It grew linearly with pump rate, with the system overestimating IOP by 1.4 ± 0.4 mmHg for a rate of 4 µL/min ($p < 0.05$). The rate dependence reflects the hydraulic impedance of the cannula and tether tubing, which causes a hydrodynamic pressure drop between the eye and iPump sensor. Figure 3.6C shows that IOP dynamics scale nonlinearly with pump rate. It took the system nearly 30 min to raise IOP by 20 mmHg at 1 µL/min and just 5 min at 2 µL/min. The exact dynamics depend on aqueous volume, outflow facility, ocular compliance, and system tubing compliance. These parameters are analyzed in more detail in the next chapter. A tradeoff thus exists between accuracy of IOP measurement and speed of IOP alteration, so the pump rate of the iPump system was fixed at 2 µL/min to achieve maximum speed with minimal loss of accuracy.

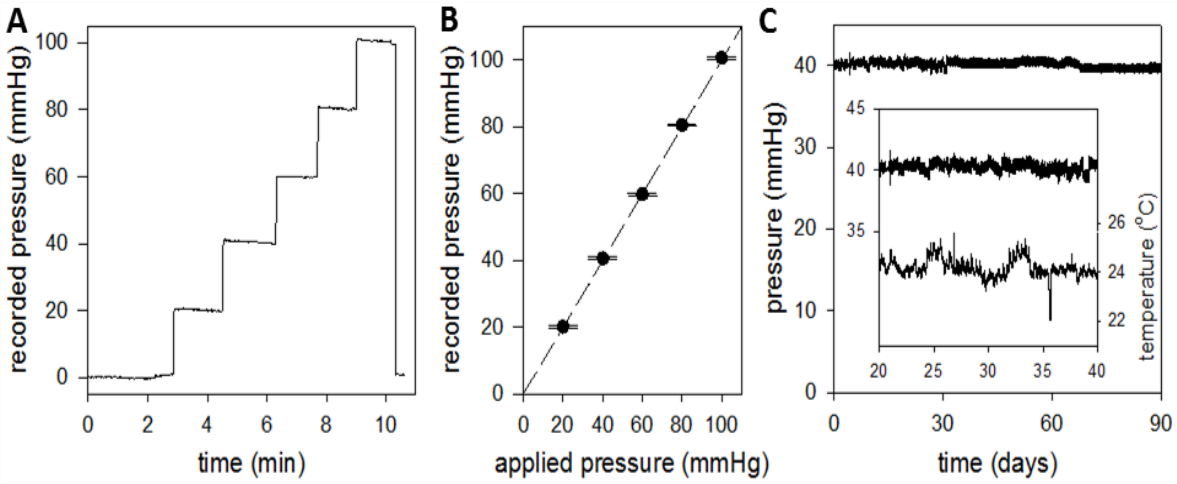

Figure 3.5 iPump sensor system properties. (A) System output as applied pressure was raised in steps of 20 mmHg. (B) Mean (symbols) and standard deviation (bars) of pressure readings for each step in applied pressure. (C) Signal recorded with applied pressure set at 40 mmHg. Data were fit by the regression line: f(x) = 40.7 - 0.0077x. Inset, segment of the pressure record during which room temperature fluctuated greatest

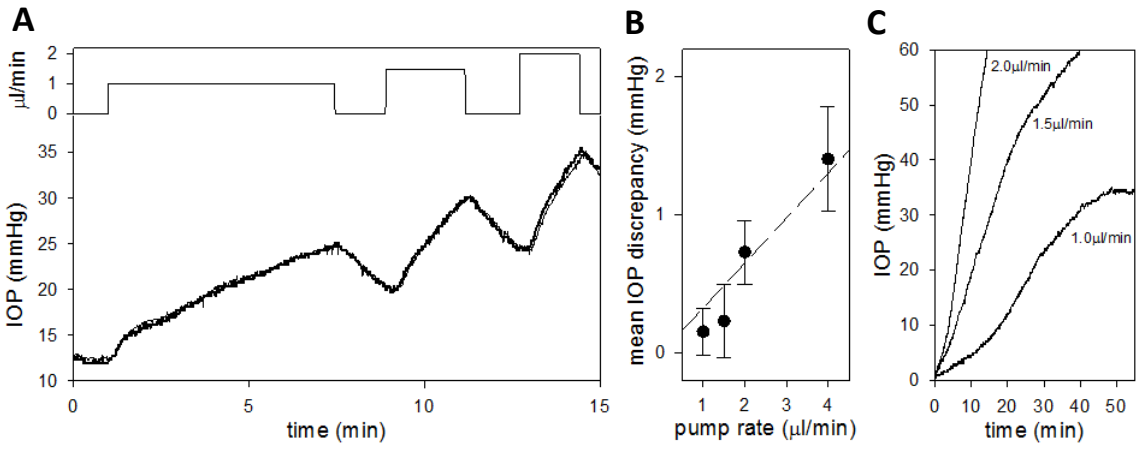

Figure 3.6 iPump perfusion properties. (A) Top: Time course of pump rates applied by the system to a dead rat eye in situ. The rate was stepped on and off to 1, 1.5 and 2uL/min. Bottom: Pump-induced IOP changes recorded simultaneously by the iPump (thick line) and a second pressure sensor (thin line) independently connected to the eye. (B) Mean and standard deviation of the difference record obtained by subtracting the simultaneously-recorded IOP signals for pump rates of 1 to 4uL/min. (C) IOP dynamics following the perfusion rate steps.

3.6.2 System Performance on Anesthetized Animals

Once device electronics were tested and cannulation procedure was developed, the performance of the complete system was evaluated *in vivo* from anesthetized rats in a sound- and light-proof room. Figure 3.7A shows the IOP record of an implanted eye over a 28-hour period recorded with the iPump in open-loop mode. After cannula insertion at noon, IOP settled at a daytime level of ~16 mmHg as resting aqueous outflow and fluid volumes were restored. IOP later increased to ~22 mmHg after daytime lighting would normally have turned off at 6PM, and it remained at this level until the following morning when IOP decreased to ~14 mmHg after daytime lighting would normally have turned on at 6AM. The nighttime elevation is consistent with prior observations of circadian IOP rhythms in rodents (McLaren, 1996; Moore, 1996). It can be seen that IOP also fluctuated at faster time scales, especially at night in this recording, although the animal was anesthetized for the entire experiment. Figure 3.7B shows that the

fluctuations are irregular and ranged 2-4 mmHg in amplitude in this rat. The in vivo variability averaged 2.1 ± 1.5 mmHg across all IOP recordings (n = 5). This is significantly greater than the ex vivo variability (figure 3.5), which implies that the IOP noise is produced by the animal. Figure 3.8A shows the IOP record of an implanted eye in which the iPump was programmed to hold pressure for 2 hours at 25, 45, and 35 mmHg. Upon activation of closed-loop control (asterisk), IOP increased from its resting level of ~15 mmHg to ~25 mmHg as the system injected fluid into the eye. Figure 3.8B shows that, once target IOP was reached, the system ceased pumping and IOP slowly decreased as the eye cleared the excess fluid. When IOP fell 2 mmHg below the target level, the system resumed pumping and returned IOP to ~25 mmHg. The cycle repeated until the target level was switched, at which time the system adjusted the pump duty cycle and IOP was maintained at ~45 and ~35 mmHg. Figure 3.8C summarizes the distribution of measured IOP values across animals for an iPump control window of ±2 mmHg. The distribution was comparable to the window size for all target IOP levels. For example, IOP was kept between 22.4 to 27.8 mmHg over a 2-hr period when the system set point was 25 mmHg.

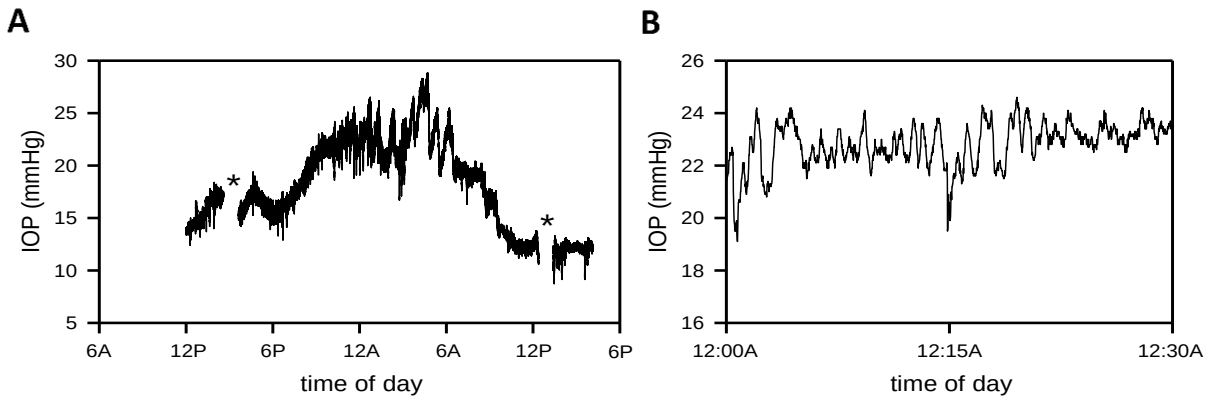

Figure 3.7 IOP monitoring with the iPump system. (A) IOP record of the implanted eye of an anesthetized rat. Asterisks mark data periods that were excluded because IOP was manipulated to examine system behavior. (B) Short (30-min) segment of the IOP record at midnight.

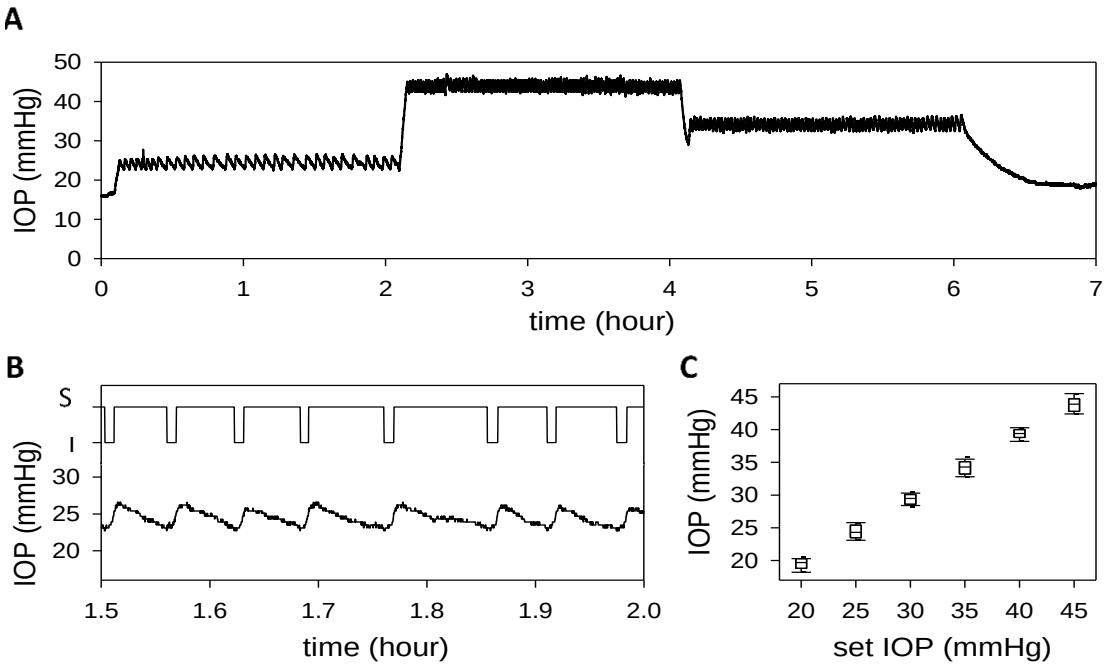

Figure 3.8 IOP control with the iPump. (A) IOP controlling with the iPump system record of the implanted eye of an anesthetized rat during which the system was programmed to hold pressure at 25, 45, and 35 mmHg for 2 hours each. (B) Top, record of pump action (I: injection, A: Stop) for a 30-min period. Bottom, IOP dynamics over the same period. (C) Box-and-whiskers plot of the distribution of IOP readings for each IOP step. Center line: mean IOP, lower and upper edges: 25% to 75% range, lower and upper whiskers: 10^{th} and 90^{th} data percentiles.

3.7 Discussion

This study introduces a portable telemetric system that can continuously monitor and autonomously control IOP in rats, and potentially larger animals. The iPump system was extensively tested and its performance specifications were quantified. We show that:

i) The system can accurately read pressure for months without drift while compensating for ambient fluctuations in barometric pressure and room temperature.

ii) The system can measure and hold IOP of rat eyes within a programmable window of any set point desired by the user.

3.7.1 Broader Applications of the Technology

The iPump system was conceived as a tool for reliably inducing ocular hypertension or for restoring hypertensive eyes to normal IOP levels. Recent work has indicated that glaucoma onset and progression may depend not just on IOP but more specifically on the pressure gradient across the lamina cribrosa (Berdahl, 2008; Nusbaum, 2015; Ren, 2010), a web-like collagenous structure through which optic nerve fibers exit the eye. The translaminar gradient is a function of IOP and intracranial pressure (ICP), raising interest in a possible role of ICP dynamics in the disease. By implanting the cannula in cerebral ventricles, the iPump system can also be used to monitor and control ICP. It could even be used to set the translaminar gradient. Since the system has two pressure sensors, it could simultaneously measure IOP and ICP while controlling one of them so as to hold the gradient at a user-specified amount.

Abnormal pressure level is a symptom of not just glaucoma. For example, Meniere's disease is associated with chronically high endolymphatic pressure, which distends fluid compartments of the cochlea and compresses the neurosensory organ (Mateijsen, 2001; Salt, 2010; Takumida, 2008). As with glaucoma, animal models of Meniere's disease attempt to induce cochlear hypertension via surgical, mechanical, or pharmacological methods oftentimes with inconsistent and irreversible results. The iPump system could thus provide a useful tool for investigating the etiology and pathophysiology of a myriad of pressure-induced neurodegenerative diseases.

3.7.2 Comparison to Existing Technologies

Several noninvasive and invasive technologies are commercially available for IOP measurement. Noninvasive technologies like the gold-standard applanation tonometer and cutting-edge wireless contact lens sensors (Leonardi, 2009; Mansouri, 2011; Mansouri, 2012) are

appealing because data can be obtained quickly with minimal subject preparation or trauma. However, the IOP readings are indirect and thus not absolute (Abrams, 1996). With tonometers they are also sparse and sporadic since readings are made by hand. Invasive technologies exist that can be placed inside the eye (Ha, 2012; Koutsonas, 2015; Todani, 2011; Walter, 2000) or connected to the eye via a tube (Akaishi, 2005; Downs, 2011; Liu, 2003; McLaren, 1996). They require surgical training and open the eye to surgical complications but also give round-the-clock streams of IOP data with little need for experimenter involvement. The iPump system measures IOP with open-loop accuracy of 0.2 mmHg and closed-loop accuracy of 0.7 mmHg, which meets or exceeds commercial systems (Konigsberg and DSI) that have been used for chronic IOP recording (Akaishi, 2005; Downs, 2011; Liu, 2003; McLaren, 1996). The iPump is not yet implantable like those systems, but it is only available technology that can automatically regulate IOP. Traditional ocular hypertension induction models are difficult to master, not always effective, time consuming and in many cases fail to maintain pressure elevated for extended periods of time. Table 3.1 shows a comparison between the most commonly used animal models and the iPump. Our system offers the most comprehensive tool for IOP manipulation and glaucoma studies.

Table 3.1 iPump vs. Ocular Hypertension Models

Feature	iPump	Hypertonic saline injection	Microbead injection	RBC injection	Photo-coagulation	Vein cauterization
Success rate	100%	60% [5]	90% (multiple treatments)[1]	100%	85% (multiple treatments)[2]	35%
IOP Control	Yes	No	No	No	No	No
Time before elevation	Minutes	2 weeks	1 week[1]	1 day[3]	2 weeks[2]	1 week [4]
Remains elevated	Yes	Yes	No	No	No	No
Records Pressure	Yes	No	No	No	No	No

[1] Urcola (2006); Sappington (2010); [2]Ueda (1998); [3]Quigley (1979); [4]Grozdanic (2003); [5]Morrison (1997).

3.7.3 Current Limitations of the Technology

The iPump system is intended for use on conscious animals, which presents design issues for consideration. One is reservoir size. The aqueous humor volume and outflow facility of rat eyes is ~10 μl^3 and ~0.05 µl/min/mmHg (Kee, 1997; Mermoud, 1996), respectively, meaning that a sustained IOP increase of 10 mmHg translates to an outflow of ~0.7 ml/day or ~7 eye volumes/day. The reservoir will thus need weekly refilling and perhaps resizing for other research applications or animals. Another is system tethering. Since the iPump sensor is outside the eye, vertical animal movement can cause hydrostatic pressure differences between the eye and sensor and introduce motion artifacts into the IOP record. Rats are small and live mostly in one horizontal plane, so the artifacts would be a few mmHg at most and minimally affect iPump operation. They would get filtered by control circuitry and the programmable window about which the system holds IOP. Larger animals also used in glaucoma (e.g. primates) present a significant challenge for iPump implementation, as their mobility is greater than that exhibited by their smaller counterparts. The use of our system in such animals may require miniaturization of the device to make it suitable for implantation, which is part of the future scope of this project. Bacterial growth in the line over time is a possibility and while the periodic operation of the pump should clear the tubing and avoid clogging, this is not the case when operating in open-loop conditions.

CHAPTER 4: OUTFLOW FACILITY

4.1 Introduction

IOP is the result of aqueous humor movement into and out of the eye (figure 4.1). The ciliary body continuously produces fluid, which flows from the posterior into the anterior chamber. Once there, fluid exits the eye via two main pathways: i) through the trabecular meshwork and into Schlemm's canal and the episcleral veins (Tamm, 2009). The resistance of the trabecular tissue opposes fluid flow, creating a pressure drop which we identify as IOP. The reciprocal of this resistance, or conductance, is defined as *conventional outflow facility.* ii) Through the ciliary muscle and other tissues (Barany, 1962; Johnson, 2016). This drainage is independent of IOP (Johnson, 2016) and is defined as the *uveoscleral or unconventional outflow facility.* These dynamics are modeled using the Goldmann equation:

$$IOP = \frac{Fin-U}{C} + EVP \qquad (1)$$

where F_{in} is the ocular fluid production, EVP is the episcleral venous pressure, U and C are the unconventional and conventional outflow facility, respectively. Understanding the dynamics of these parameters is crucial for glaucoma research since ocular hypertension is frequently traced to an abnormality in one of them, making outflow facility and fluid production the target of most IOP-lowering drugs and surgical treatments. To study outflow facility several methods have been reported in mouse (Aihara, 2003; Lei, 2011; Millar, 2011), rat (Mermoud, 1996) and human eyes (Karyotakis, 2015), most of which act by injecting additional fluid into the eye and analyzing the IOP response. These procedures have provided researchers with valuable data for decades.

Nevertheless, such experiments require several pieces of equipment that can be bulky and hard to set up, which renders the user's ability to easily transport it. Equipment transportation becomes particularly important in research facilities where animals are housed in a dedicated vivarium outside of the investigator's laboratory, where space can be survival experiments are conducted but space is usually limited. Moreover, several of the traditional outflow facility methodologies require a skilled operator to correctly assess IOP dynamics during the experiment and can be lengthy to perform. Therefore, a more compact and easy-to-use system would greatly facilitate chronic outflow facility studies.

This chapter presents the implementation of the iPump system described previously, in combination with a novel mathematical technique, to overcome the limitations of traditional outflow measuring techniques. Data are presented on the ability of the methodology to accurately measure outflow facility, as well as length of experiments. The results show that the iPump can effectively measure the flow through conventional and unconventional drainage pathways.

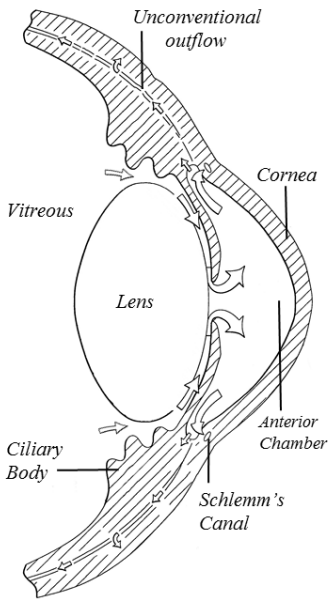

Figure 4.1 Diagram of the outflow facility of an eye. Fluid is produced by the ciliary body, flowing into the anterior chamber. Fluid exists the eye conventionally via pressure dependent channels or unconventionally through pressure independent pathways. Adapted from Shields (2004)

4.2 Materials and Methods

Experiments were performed on rats anesthetized with a ketamine-xylazine mixture (50 and 7 mg/kg, IP). A catheter was inserted in the femoral vein, and anesthesia was maintained for remainder of the experiment via intravenous infusion of ketamine (30 mg/kg/hr), dextrose (600 mg/kg/hr), and physiological saline. The head was fixed in a stereotaxic mount, and the body was rested on a heating blanket under temperature control via a rectal thermometer. Needle electrodes were inserted to record the electrocardiogram (ECG). A 33G needle mounted on a micromanipulator was used to cannulate the anterior chamber of the eye. The needle was connected to the iPump via 25G tubing (length: 25cm). Two different techniques were used to measure outflow facility. In 5 animals aqueous drainage was measured using a commonly used technique termed the *constant rate perfusion method*. In other 4 animals we measured outflow using our innovative procedure which we named the *constant pressure perfusion method.*

4.2.1 Constant Rate Perfusion Method (CRP)

When the eye is perfused at a fixed rate, its steady state is disturbed causing IOP elevation. The additional fluid infusion modifies the Goldmann equation, becoming:

$$IOP = \frac{Fpump+Fin-U}{C} + EVP \quad (2)$$

where F_{pump} is the pump's perfusion rate. Over time IOP will settle at a new level. When the rate of IOP change falls by 90%, IOP is considered to have stabilized and, at this plateau level, the amount of fluid entering and exiting the eye are equal. That is:

$$Fpump = Fout \quad (3)$$

where F_{out} is the total fluid outflow via conventional and unconventional pathways. Solving equation (2) for F_{pump} and setting it equal to equation (3) we obtain:

$$Fout = Fpump = C \cdot IOP + (U - Fin - C \cdot EVP) \quad (4)$$

plotting equation (4) we find that C is the slope of the line, while the y-intercept is the sum of IOP independent flows from *U*, F_{in} and *EVP*.

When using this methodology, eyes were perfused with 0.9% saline solution using at least 5 different rates ranging from 0.1 to 1.5 μL/min, while a Labview program recorded IOP. After data were collected, the pump was turned OFF and IOP was allowed to decay to its normal baseline. Pressure data was averaged for every plateau level and conventional outflow facility was calculated as the slope of the IOP vs. Perfusion Rate curve.

4.2.2 Constant Pressure Perfusion Method (CPP)

This novel technique was developed using the unique functions of the iPump to modify IOP levels. The iPump systematically maintains IOP within 2 mmHg of a user specified set-point. When the set point is manually changed, the system dispenses fluid into the eye at a constant rate (F_{pump}, 2μL/min) until IOP reaches the desired value, at which point the pump stops. The system remains idle until aqueous drainage lowers IOP by 2mmHg below the set-point, at which point the pump automatically resumes perfusion. This cycle is repeated until the set-point is changed or the system is turned OFF. The CPP technique analyzes volume dynamics during each individual pressure cycle. The fluid volume change during the rise phase of the cycle must equal the volume change during its fall phase. For instance, the volume of fluid injected by the pump to elevate IOP from 24 to 26mmHg must be equal to the volume of fluid drained by the eye (outflow facility) to lower IOP from 26 back to 24mmHg (figure 4.2). Additionally, we must consider the volumetric changes of the eye itself as its biomechanical properties allow the ocular globe to expand or contract as fluid moves in and out of the anterior chamber. Equation (5) illustrates this relationship.

$$(T1 \cdot Fpump) + \Delta Vrise = (T1 \cdot Fout) + (T2 \cdot Fout) + \Delta Vfall \quad (5)$$

where T1 is the perfusion time and T2 is the idle time of the pump. In other words, T1 is the amount of time required to raise IOP by 2mmHg while T2 is the amount of time that it takes the outflow facility to lower IOP by 2mmHg at each level (figure 4.2). This equation accounts for the amount of fluid delivered to the eye, as well as the fluid drained while the pump was active and after it stopped. Assuming that the changes in eye volume during the rise and fall phases are equal for small IOP variations ($\Delta V_{rise} = \Delta V_{fall}$), equation (5) becomes:

$$(T1 \cdot Fpump) = (T1 \cdot Fout) + (T2 \cdot Fout) \qquad (6)$$

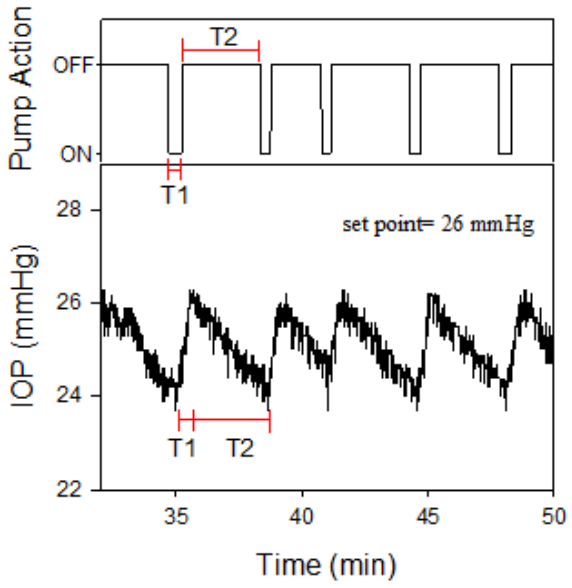

Figure 4.2 Constant pressure perfusion methodology. The iPump was used to maintain IOP within 2 mmHg of the set-point (26mmHg) using a 2µL/min perfusion rate. T1 is the amount of time required for the pump to drive IOP from 24 to 26mmHg. T2 is the amount of time needed by the eye to lower IOP from 26 to 24mmHg. This cycle is repeated until the iPump is disabled or the set-point is changed.

solving equation (6) for F_{out} we obtain that:

$$Fout = \frac{T1}{T1+T2} \cdot Fpump \qquad (7)$$

Note that in the case of the CPP technique, total outflow is equal to the perfusion-rate times the fraction of time that the pump was active. Modifying equation (4) to reflect this relationship we obtain:

$$Fout = Fpump \cdot \frac{T1}{T1+T2} = C \cdot IOP + (U - Fin - C \cdot EVP) \quad (8)$$

in a dead eye, cessation of vascular flow eliminates *EVP* as well as aqueous humor production. Therefore, repeating the same procedure on a dead eye yields equation:

$$Fout = Fpump \cdot \frac{T1}{T1+T2} = C \cdot IOP + U \quad (9)$$

in the new curve, the slope is equal to the conventional outflow facility, while the y-intercept indicates the value of the unconventional drainage.

During CPP experiments eyes were perfused with a 0.9% saline solution at 2μL/min. The iPump was used to set IOP to 5 different levels on each animal, ranging from 20 to 80mmHg. Each level was maintained for at least 5 full cycles. Outflow facility was calculated for each cycle (equation 8) and averaged across the same IOP level. In 3 animals the CPP method was perform before and after death. After the live data was obtained, the animals were euthanized via intraperitoneal euthasol injection (>50 mg/kg, IP) and the procedure was repeated *in-situ*.

4.2.3 Characterization of the Perfusion System

Outflow facility measurements calculated using any methodology are affected by the physical characteristics of the perfusion system. For instance, the hydraulic resistance of the perfusion needle, as well as the resistance and compliance of the tubing used to connect it to the iPump, could influence outflow facility measurements and, therefore, must be taken into consideration. The length (25 cm) and diameter (ID: 700μm) of the tubing and was standardized

and maintained across experiments. Tubing and needle resistance were calculated using Poiseuille's law which stated that:

$$R = \frac{8\eta L}{\pi r^4}$$

where R is the resistance of the tubing, r is its radius, L its length and η is the dynamic viscosity of the fluid. System compliance was determined by sealing the needle tip and injecting known fluid volumes into the line while recording pressure. The slope of the injected volume vs. change in pressure graph corresponds to the compliance of the tubing system. Ocular compliance can be measured by repeating this procedure with the needle tip open and inside the anterior chamber. 1, 2, 3 and 4 µL were systematically delivered into the eye while IOP was monitored and recorded. This procedure yields the compliance of the tubing and eye together. Ocular compliance is therefore the difference between total compliance and tubing compliance.

4.2.4 Data Analysis

Statistical significance was assessed by a two-sample *t*-test with an alpha level of 0.05 using SigmaPlot software (San Jose, CA). Linearity was assessed by fitting data to a curve of the form $f(x) = f_0 + ax$. Results are expressed in terms of mean ± standard deviation.

4.3 Results

4.3.1 System Characterization and Ocular Compliance

Needle resistance was calculated using Poiseuille's Law of fluid flow. The 33G needle had an inner diameter of 108µm and a length of 13mm. The dynamic viscosity of a saline solution is 8.75×10^{-8} mmHg·min at body temperature (Fitt, 2006). Using these values, needle resistance has a value of 0.340 mmHg·min/µL. On the other hand the rest of the tubing had an inner radius of 350 µm and a length of 25cm. The resistance of the tubing was 5.30×10^{-3}

mmHg·min/µL. Since the needle and tubing are connected in series, the values of their resistances can be added, summing a total system impedance of 0.345 mmHg·min/µL. This resistance is negligible compared to the expected ocular resistance of a rat eye (Mermoud, 1996) and can therefore be ignored when analyzing outflow results. System compliance was measured to be 0.120 ± 0.010µL/mmHg (n=3; data not shown). Figure 4.3 shows an experiment in which total compliance was measured. 1, 2, 3 and 4 µL were systematically delivered into the eye, causing pressure changes that ranged from 7 to 40 mmHg. The compliance of the eye-tubing bundle was calculated to be 0.1401 ± 0.0107 µL/mmHg (n=3). Ocular compliance is therefore in the order of 0.020 µL/mmHg.

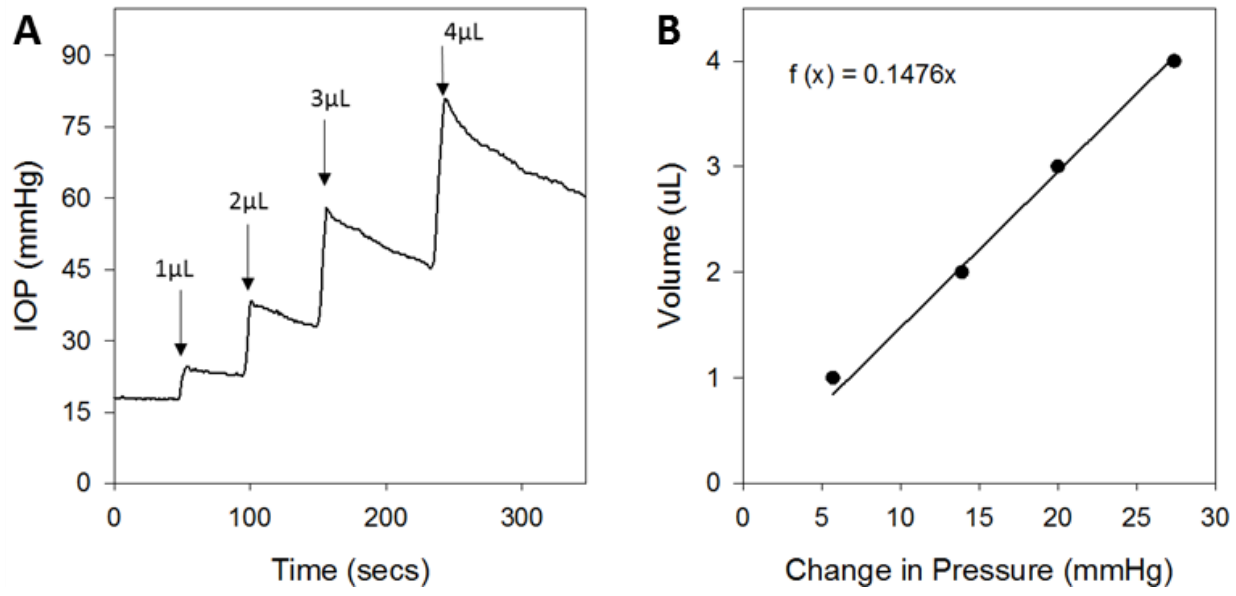

Figure 4.3 Ocular and system compliance. (A) IOP profile resulting from the injection of 1, 2, 3 and 4 µL saline boluses into a single rat eye. Pressure increases after each injection, followed by a slow pressure decrease as fluid exits the eye. (B) Linear regression of the volume vs. pressure relationship. Each data point was calculated as the injected volume divided by the resulting pressure change. The slope of the line yielded a compliance of 0.1476 µL/mmHg. Note that this is the equivalent compliance of the eye and the perfusion system bundled together.

4.3.2 Outflow Facility Using CRP

Outflow facility of the rat eye was evaluated via constant rate perfusion in 5 animals. Figure 4.4A shows one of these experiments. IOP had an original baseline of ~16mmHg. The eye was perfused at 0.1, 0.3, 0.5, 0.7 and 0.9 µL/min for 10 to 35 minutes until IOP stabilized. The lower perfusion rates generated the slowest IOP responses, taking almost 40 minutes to settle when perfusing at 0.1 µL/min (asterisk). During these slow IOP stages, assessment of plateau levels can be difficult. When all five levels were completed and the pump was turned off, IOP returned to the original baseline. In this experiment linear regression analysis of outflow data yielded a conventional outflow (C) value of 0.027µL/min/mmHg with a y-intercept of -0.64 µL/min (figure 4.4B).

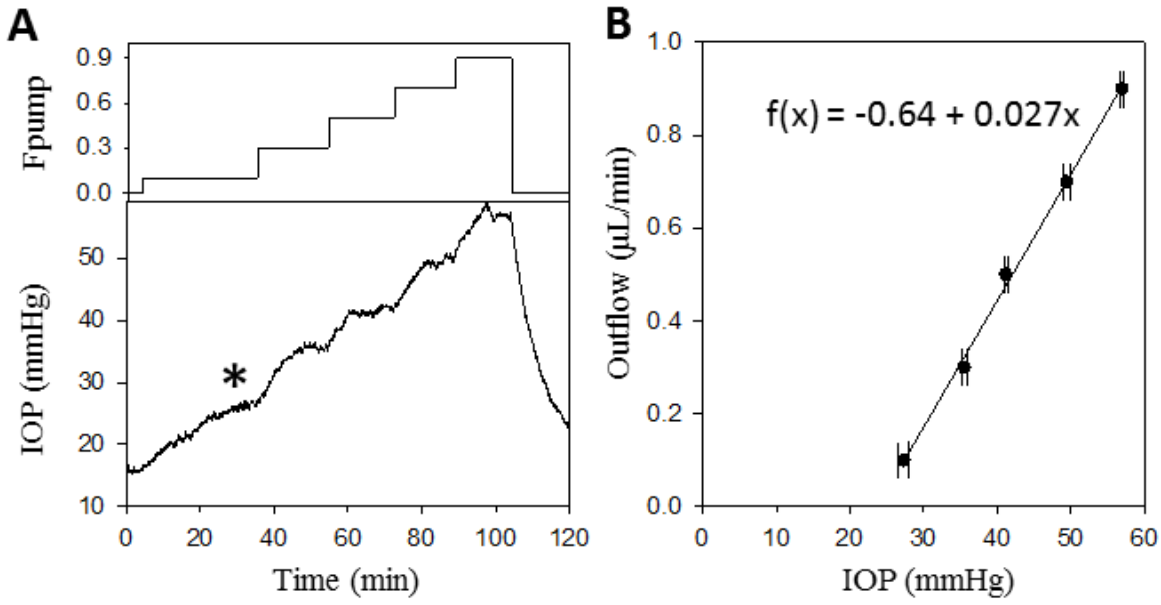

Figure 4.4 Outflow facility measurement via CRP. (A) Perfusion rates are set to a certain value for an extended period of time (top) causing an IOP response at each step (bottom). IOP must settle at one value before the perfusion rate is changed. The asterisk marks a level in which IOP may not have settled properly before the level was changed. (B) Linear regression of the IOP vs. outflow curve. Conventional outflow was 0.027µL/min/mmHg with an intercept of -0.64 µL/min.

4.3.3 Outflow Facility Using CPP

To test the ability of the iPump to measure outflow facility, experiments were performed in 4 rats. Figure 4.5 illustrates one experiment done using the CPP methodology. IOP had an original baseline around 16 mmHg, the set-point was varied between 5 and 30 mmHg above the baseline in steps of 5mmHg (figure 4.5A). After data were collected, the iPump was operated in open-loop, allowing IOP to return to its normal baseline. The simplicity of the procedure allows any user to conduct the experiment without previous training. Real time assessment of IOP is not necessary when using CPP and the operator is only responsible for switching set-point values when enough pressure cycles have elapsed. The linear regression of the data obtained revealed a conventional outflow facility of 0.0268 µL/min/mmHg with a y-intercept of -0.311 µL/min (figure 4.5B). These results are comparable to those obtained using the CRP method (see next section).

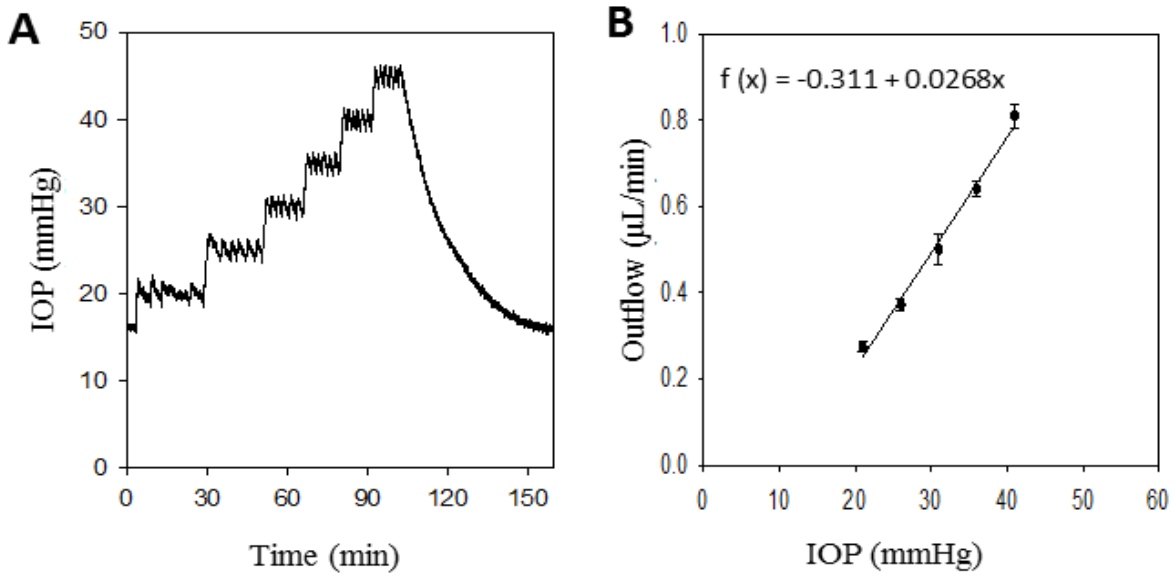

Figure 4.5 Outflow facility measurement via CPP. (A) The iPump was used to vary IOP in steps of 5mmHg. Once the experiment was finished IOP return to its initial baseline. (B) Linear regression of the IOP vs. Outflow curve. Conventional outflow was 0.0268 µL/min/mmHg with an intercept of -0.311 µL/min.

4.3.4 Comparison Between Methodologies

Several experiments were conducted using both the *constant-rate (CRP)* and the *constant pressure (CPP)* perfusion methods for outflow facility measurement. Figure 4.6 shows the regression data of all animals (n=9). The black circles represent data obtained using the traditional CRP technique, while the red circles show the outflow facility measured using our novel CPP methodology. CRP data revealed a conventional outflow facility of 0.0247 ± 0.003µL/min/mmHg and a y-intercept of -0.31 ± 0.34 (n = 5, mean ± SD). On the other hand, animals that underwent CPP showed a conventional outflow facility of 0.0243 ± 0.002 µL/min/mmHg and a y-intercept of -0.52 ± 0.17 µL/min (n=4, mean ± SD). Unconventional outflow facility was measured to be 0.1 ± 0.0533 µL/min (n=3, data not shown). No statistically significant difference was found between the slopes (P=0.832) and the y-intercepts (P=0.340) of the outflow data obtained using CRP and CPP. Similarly, conventional outflow facility in a live and dead rat eye was not statistically different (P=0.227). The results of all experiments are summarized in table 4.1. These data show that our novel methodology, CPP, is a reliable way of obtaining outflow facility measurements and its results are comparable to those obtained using traditional procedures.

Table 4.1 Ocular Physiological Parameters

Parameter	Mean	Standard Deviation
Conventional outflow, live (n=9) *Unit: µL/min/mmHg*	0.024	0.003
Conventional outflow, dead (n= 3) *Unit: µL/min/mmHg*	0.022	0.002
y-intercept, live (n=9) *Unit: µL/min*	-0.49	0.18
Unconventional outflow (n= 3) *Unit: µL/min*	0.10	0.053

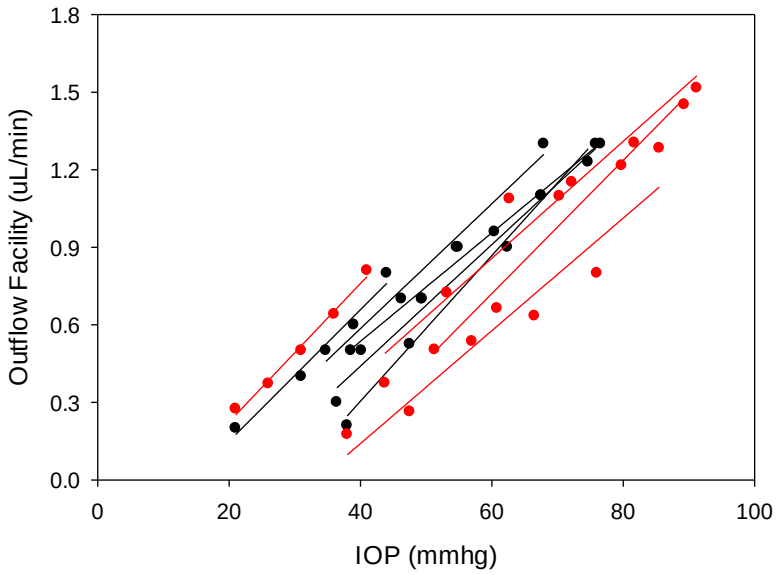

Figure 4.6 Outflow facility summary. Red lines denote experiments in which the constant pressure perfusion method was used. Five animals were analyzed using this technique. Black lines represent linear regressions of experiments done via constant rate perfusion. 4 animals were subjected to this method. Both methodologies yielded similar results.

Figure 4.7 shows a side by side comparison between the CRP and CPP methods. Figure 4.7A illustrates a CRP experiment in which IOP was set to 5 different levels. This experiment needed approximately two hours for completion and required subjective assessment of the IOP plateau levels, which can result in less accurate data. For instance, note that in the first stage IOP may not have properly settled before the next stage was started (asterisk). In some cases, correctly assessing IOP plateau levels during the experiment can be difficult and it is not until the data is processed that such conclusions can be made. Such evaluations often require an expert user and long waiting periods to ensure pressure equilibrium, which may result in even longer times for completion. For experiments that require outflow data in both the live and dead eye, experiments could last over 4 hours, not including preparation and euthanization times. On the other hand, as shown in figure 4.7B, experiments conducted using CPP allow for faster

completion, as the same five levels of IOP can be achieved in just an hour. Additionally, IOP can be systematically controlled by any user, regardless of experience, by adjusting the desired set-point in the iPump's user interface.

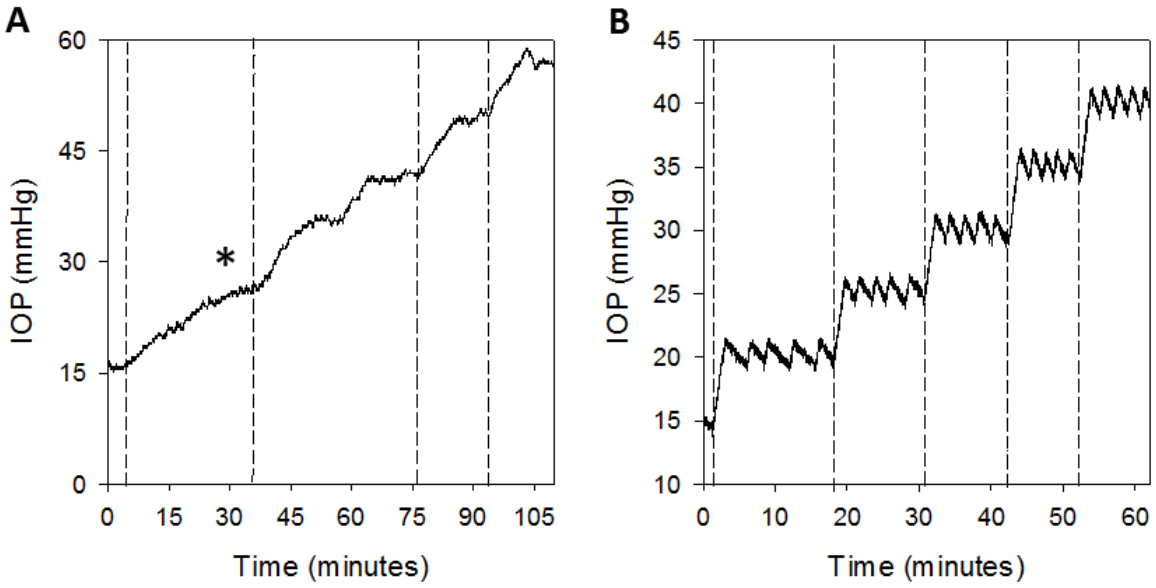

Figure 4.7 CRP vs. CPP. (A) IOP manipulation via constant rate perfusion. Experimental procedure lasts around 2 hours before completion of 5 IOP levels. Dash lines mark the beginning of a new pressure level. Asterisk denotes a level in which IOP plateau might not have been achieved. (B) IOP manipulation via constant pressure perfusion. Experiment takes around 1 hour to complete without the need of IOP plateau.

The differences between CRP and CPP methods are not only related to data quality. Figure 4.8 shows a comparison between the equipment necessary to perform CRP experiments (figure 4.8A) and the iPump, which is the only device needed for CPP procedures (figure 4.8B). CRP experiments require: i) a syringe pump (1000, New Era Pump Systems, NY; Dimensions: 22.86 cm x 14.60 cm x 11.43 cm; Weight: 3.6 lbs), which may require a controller box to be digitally operated (Ana-Box, New era Pump Systems, NY; Dimensions: 10cm x 6.1cm x 2.6cm;

Weight: 0.35 lbs). ii) A commercial pressure sensor (56360, Stoelting, IL; Dimensions: OD: 2.5cm, height: 3cm; Weight: 0.7 lbs). iii) A signal amplifier (50110, Stoelting, IL; Dimensions: 22cm x 15cm x 10cm; Weight: 2.8 lbs) and iv) a data acquisition card (6008, National Instruments, TX; Dimensions: 8.51cm x 8.18 cm x 2.21cm; Weight: 0.4 lbs). All components total a volume of 7442 cm^3 and a weight of 7.85 lbs, which can make equipment hard to transport. Conversely, the iPump consists of a single unit with a volume of 628 cm^3 and weighs only 0.5 lbs, making the system easily moveable and requiring minimal set-up.

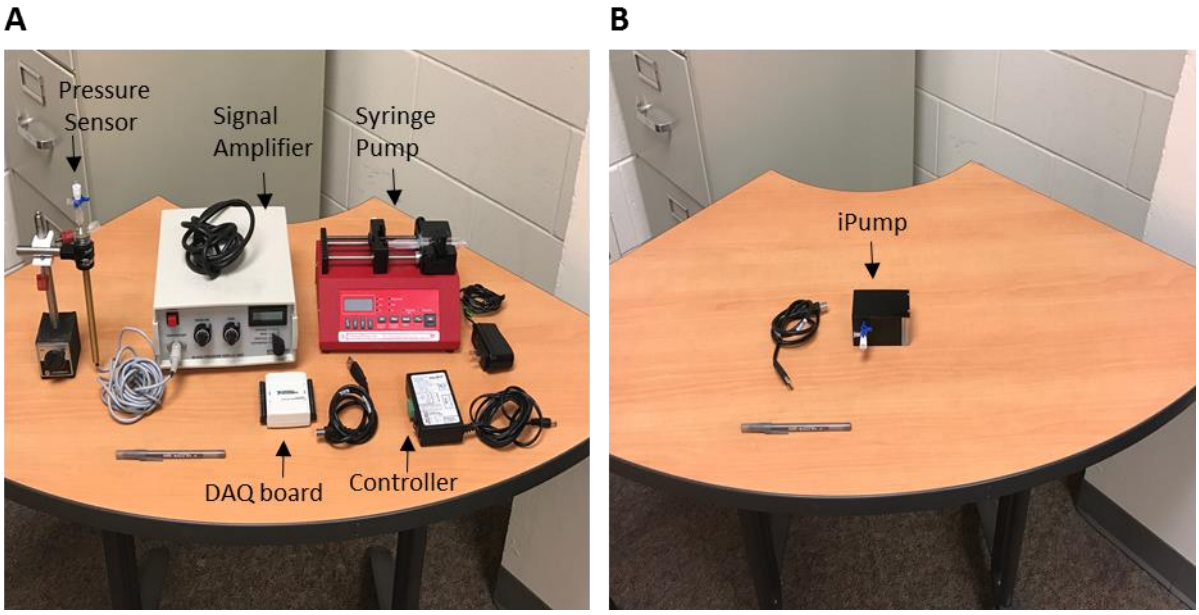

Figure 4.8 Equipment comparison CRP vs. CPP. (A) CRP methodologies require a commercial pump and controller, a pressure sensor, signal amplifier and a data acquisition card. The total volume of the items shown in the picture is 7442 cm^3 with a total a weight of 7.85 lbs. (B) Equipment necessary to perform CPP experiments. The only device required is the iPump system, which has a volume of 628 cm^3 and a weight of 0.5 lbs.

4.4 Discussion

This chapter outlines a novel methodology to measure ocular outflow facility, a set of physiological parameters that affect IOP dynamics. The iPump was used to regulate IOP levels

and an innovative mathematical model was developed to accurately calculate drainage rates based on volume variations. Our constant pressure perfusion (CPP) methodology empirically measured conventional and unconventional outflow facility of a rat eye to be 0.0243 ± 0.002 µL/min/mmHg and 0.1 ± 0.0533 µL/min, respectively. Although not explored in this study, other ocular parameters of the Goldmann equation can also be estimated using this technique. The difference between the live and dead y-intercepts is dependent only on EVP and F_{in}. EVP values have been reported to be in the order of 5 mmHg in mice (Aihara, 2003). Assuming such values mirror to rats, it could be possible to estimate F_{in}.

While our methodology yields similar results to those obtained using traditional techniques, CPP allows the user to overcome various limitations. Firstly, our methodology can cut experimental times in half when compared to commonly used constant-rate-perfusion models, which can take several hours for completion. Secondly, CPP procedures allow virtually any user to perform the experiments. The iPump system allows for precise controllability of IOP at every level, removing any subjectivity at the time of data collection and ensure data accuracy. Thirdly, another important advantage featured by the iPump is portability. Most of the equipment necessary to conduct outflow facility studies is bulky and require multiple components. On the other hand, the iPump provides a compact system with all necessary parts integrated in one easy-to-carry unit. These features are of increased interest since, due to most funding agencies' guidelines, many researchers are required to permanently house their animals in facilities others than their laboratories, such as specialized animal vivaria.

Moreover, the iPump provides the possibility of performing outflow facility measurements in awake animals through a tethered connection. This capabilities are possible due to our unique ocular implant and cannot be achieved using any other commercial equipment.

Although outflow measurements in awake animals have not been acquired to date, and its implementation is certain to bring unexplored challenges, the technology provided by the iPump opens the door for countless outflow studies that would certainly help advance our knowledge of glaucoma.

CHAPTER 5: IMPLANTABLE SENSOR

5.1 Introduction

The current gold standard for measuring intraocular pressure (IOP) is the Goldmann applanation tonometry (GAT), which has been proven a useful tool for monitoring glaucoma patients. GAT relies on corneal contact and requires an operator to obtain measurements, resulting in limited data collection. On the other hand, numerous studies have shown the dynamic behavior of IOP in normal (Frampton, 1987; Wilensky, 1991) and glaucomatous eyes (Asrani, 2000; Bengtsson, 2007; Gautam, 2015) due to circadian light cycles and body posture. The known variability of IOP and the sparsity of information available via tonometry makes this method unappealing for long term, comprehensive studies of ocular hypertension.

To overcome the limitations of tonometric measurements, researchers have focused their efforts on developing devices for continuous intraocular pressure measurements, most of which are intended for animal use. Continuous IOP telemetry has been reported in rabbits (Akaishi, 2005; McLaren, 1996) and mice (Li, 2005) using commercially available implantable pressure sensors. The devices used in these projects (DSI, St. Paul, MN) are battery powered, which severely limits their operational lifetime and introduces significant artificial pressure drifts into the recordings due to unregulated voltage levels draining overtime (McLaren, 1996). The presence of such drifts requires researchers to perform recurrent invasive recalibration procedures that are time consuming and can be damaging to the eye. Another study managed to implant a telemetric device in non-human primates (Downs, 2011), successfully recording IOP

and other physiological parameters simultaneously. The device used in this study was also subjected to battery related pressure drifts and its overall size makes it not suitable for implantation in smaller animal species, which are more commonly used in glaucoma research. The use of a pressure-measuring contact lens (Leonardi, 2009; Mansouri, 2011; Mansouri, 2012) has also surfaced in recent years, showing great potential for human glaucoma studies. To date, this technology has only been able to record IOP dynamics in arbitrary units that cannot be converted to conventional pressure units (Mansouri, 2013) and can only be implemented in animals with larger eyes, such as pigs or humans.

In this chapter we present the development of a wireless telemetry system for continuous IOP monitoring. We evaluated its performance in rats, however, the size and transmission distances of the device make it suitable for implantation in several animal species. The system is equipped with Bluetooth data transmission and voltage supply regulation that eliminates battery-related pressure drifts. The purpose of this section is to report the initial performance of the device in fully awake rats.

5.2 System Overview

The telemetry system used to measure IOP was custom designed for the application. The device consists six major components: i) a pressure transducer, ii) a differential amplifier, iii) a temperature sensor, iv) a microcontroller, v) a power circuit and vi) a Bluetooth module for data transmission (figures 5.1A and 5.1B). A head-mount was designed using CAD software (SolidWorks, Waltham, MA) and machined in acetal homopolymer (Derlin, Interstate plastics, Sacramento, CA). The head-mount is secured to the skull of the rat using four stainless steel miniature screws (#303, J.I. Morris, Southbridge, MA) and bone cement solution (figure 5.1C). The back of the head mount connects to the sensor (TBPDANS005PGUCV, Honeywell,

Morristown, NJ) via clear 16G PTFE tubing, surrounded by a metal spring that prevents kinking (figure 5.1D). The cannula (material: polyimide, ID: 100 μm, OD: 140 μm, MicroLumen, Oldsmar, FL) is inserted through a hole drilled in the front of the head-mount and sealed in place with cyanoacrylate (figure 5.1C). The other end of the cannula is implanted in the eye using a special surgical technique. Prior to implantation, the cannula and tubing are filled with 0.9% saline solution, which allows pressure waves inside of the eye to be conducted along the line and to the pressure transducer. Once the head mount is secured and the cannula is in place, skin sutures are used to close the scalp. The sensor, along with the rest of the system, is encased in a 25x25x10mm plastic box that attaches to a custom-designed vest worn by the animal (figure 5.1D).

The sensor is powered by a 3.3V coin-cell battery (CR2032, Duracell, Indianapolis, IN) which was located at the top of the system's case and held tightly in a battery socket. This positioning was designed to facilitate battery replacement while not allowing the animal to get a hold of the system. A DC-DC boost converter maintains a constant voltage supply to the system as the batteries drain. The microcontroller (RFD22301, RFDuino, Hermosa Beach, CA) runs the device in two modes: sleep and active. While in sleep mode the sensor and amplifier are OFF and the system consumes minimum power. During active mode circuitry becomes active, IOP data is collected and transmitted along with the system's temperature. The device alternates between active and sleep mode and the duration of each cycle can be adjusted depending on the application. The sensor's sampling rate can also be programmed up to 250Hz. A data receiver located within one meter of the animal's cage collects the information sent wirelessly and feeds it to a computer where it is displayed and stored using a custom LabVIEW program (National Instruments, Austin, TX). Though greater distances between the telemetric device and the data

receiver can be achieved, it may result in increased power consumption. One data receiver can synchronize with up to eight telemetric devices simultaneously. The individual electronic components of the system are described next.

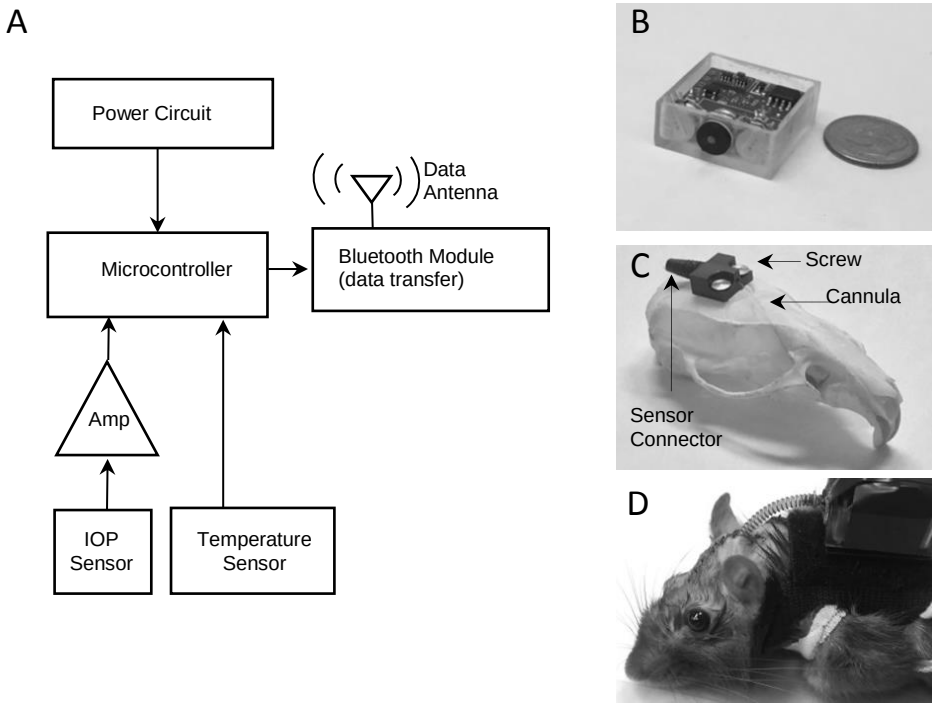

Figure 5.1 Implantable IOP sensor. (A) Block diagram of the implantable sensor. (B) Picture of the device. (C) Illustration of the head-mount connector. The head-mount is fixed to the skull using 4 stainless steel miniature screws. Cannula is inserted through a hole in the front of the mount and sealed in place. The other end of the cannula is implanted in the eye. The back of the mount is connected to the sensor via 16G tubing. (D) Picture of an implanted rat. The tubing connector is covered by a metal spring to prevent kinking, while the sensor is attached to the back of the animal using a custom designed vest.

5.3 Electronic Description

Figure 5.2 illustrates the electronic schematics of the telemetric system. The device is equipped with: i) powering circuitry. ii) a microcontroller. iii) pressure and temperature sensing

elements and iv) a Bluetooth module and antenna for data transmission. All components were carefully selected and customized in order to provide high accuracy, low power consumption and operate with a single power supply. Each component is described in detail in the following section.

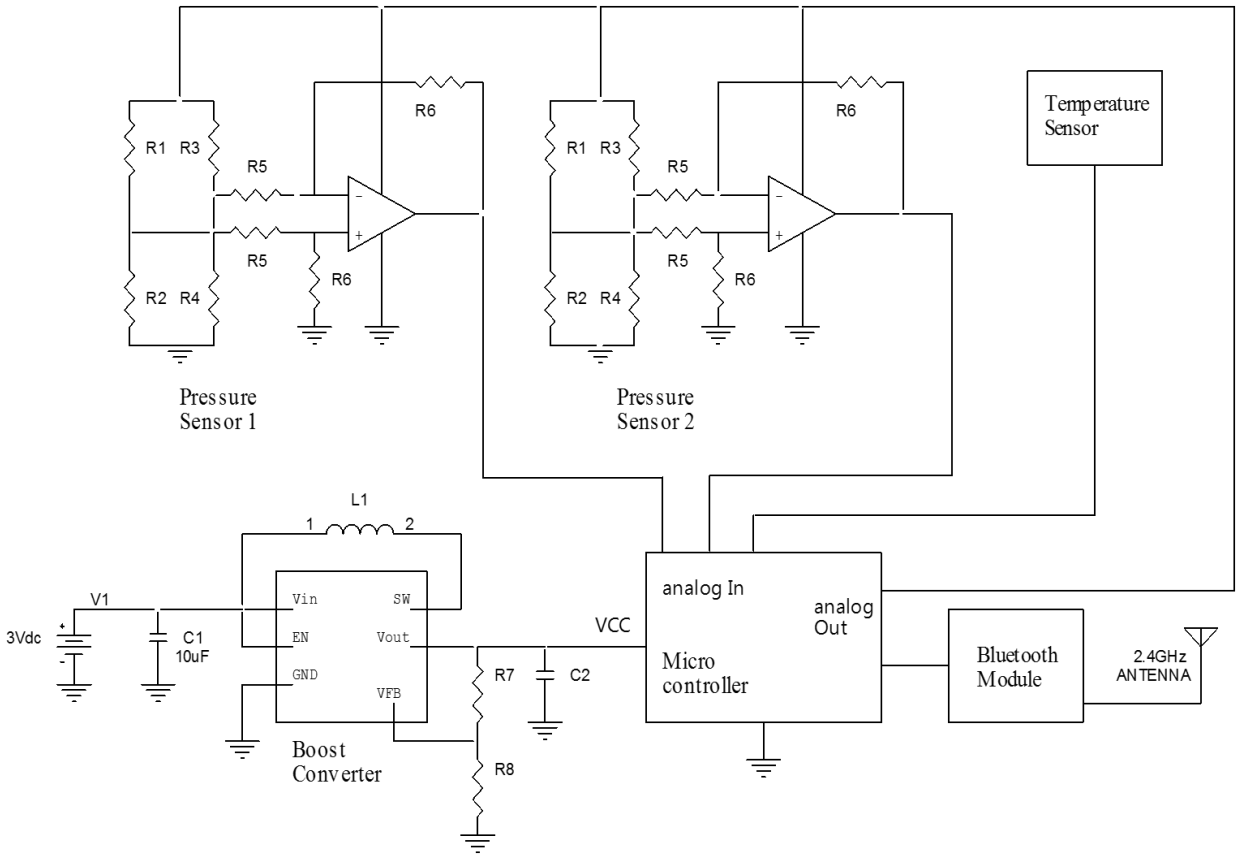

Figure 5.2 Electronic schematics of the implantable sensor. The system is powered with a 3.3V battery. A boost converter maintains voltage supply constant as the batteries drain. Two pressure transducers and a temperature sensor interact with the microcontroller to periodically obtain data and send it to a computer via Bluetooth.

5.3.1 Power Elements

The system is powered by a 3VDC coin-cell battery with a 220mAh capacity (CR2032, Duracell, Indianapolis, IN). As the battery drains with time, fluctuations in the voltage supply

can create artificial drifts in the data obtained. To avoid these artifacts a DC-DC boost converter (MCP1640DT, Microchip Technology, Chandler, AR) is implemented. The converter steps-up any voltage ranging between 0.65 and 3V to a stable 3V. Since a single battery is implemented, all electronics must operate with a single voltage rail.

5.3.2 Microprocessor

The system is run by a small programmable microcontroller unit (RFD22301, RFDUINO, Hermosa Beach, CA), which is equipped with 128kB of flash memory for application space and 8kB of RAM memory. The chip has a built-in, 8-bit analog-digital converter and 7 general purpose input-output channels (GPIO), 4 of which can be configured as pulse-width modulation (PWM) channels. The chip counts with an embedded 2.4GHz radio, compatible with Bluetooth 4.0 low power technology. To maximize battery efficiency, the sensors and amplifiers of the device are only ON when data is being collected. To achieve this, the microcontroller operates the system in alternating active and sleep cycles. During sleep mode, all sensors and amplifiers are OFF and current consumption is decreased to 4µA. The amount of time between data collection events is fully programmable and can be customized to the application. The data receiver consists of a second identical microcontroller connected to a computer via a USB port. After the receiver collects the wirelessly sent data, it prints it to the serial port of the computer, where it is read, plotted and stored by a custom-written LabVIEW program. Up to 8 different sensors can communicate with a single receiver.

5.3.3 Code

The data transmission and reception codes were written in C++ and loaded into the microprocessors using a stack-up USB module and an open source prototyping software

(Arduino, Italy). The sensor and receiver communicate wirelessly via Bluetooth using a wireless transmission protocol (Gazelle, Nordic Semiconductor, Norway). An especial library (RFduinoGZLL.h) is loaded into the code to allow protocol implementation. Device ID, IOP and Temperature data are sent using a single packet of information every second. A custom structure (*struct*) is defined using 17 bytes. On the transmitter side, data is collected and incorporated into the *struct* according to the sampling rate defined by the user. The analog-to-digital converter is disabled via coding after every data collection action and restored before the next cycle. This step is a redundant safety measure to preserve data quality in case of a write-to-disk error. After data collection, the system enters a low power consumption stage until the next data transmission cycle is active. In another safety measure, the Bluetooth module is disabled and restored in between transmission cycles. This action preserves battery life in case of an error in the hand-shaking protocol between the transmitter and receiver.

On the receiver side, the code maintains the device in a continuous *listening* mode. When communication is initiated by a transmitter, the receiver uses device ID information to identify what sensor is generating the signal (one receiver can interact with up to 8 implanted sensor simultaneously). IOP and temperature data are then copied into the receiver's internal memory before being converted from ASCII into voltage values and printed to the serial port. (e.g. rat:1;cap:3; IOP: 2.5; temp: 30). A custom LabVIEW program reads the serial port continuously at a BAUD rate of 9600 using a special add-on data acquisition library (VISA, National Instruments,TX). As data becomes available, the LabVIEW code reads the string and breaks it into different sub-strings based on the identifiers *rat* , *cap* , *IOP* and *temp* (note that the *cap* value is not used in this application, but was coded to facilitate transition between applications). Each data subset is plotted in an individual graph, in real time, and saved into a text file.

5.3.4 Sensing Elements

5.3.4.1 Pressure Transducer

One of the key components of this system is the pressure transducer used to measure IOP. The printed circuit board (PCB) has two 4-pin connections set up for any sensor that operates in a Wheatstone bridge configuration. In cases when only one sensor is necessary (e.g. IOP measurements) a single transducer is connected, which makes the system more power efficient. The pressure sensors (TBPDANS005PGUCV, Honeywell, Morristown, NJ) are piezoresistive strain gauges manufactured on an alumina ceramic substrate and covered by a silicone gel coating that protects the electronic components from fluid condensation in the line. The sensors have an operating range of 0-250mmHg, with an overpressure capacity of 1500mmHg. IOP variations are expected to be between 12-22mmHg in normal eyes, and reach 30-40mmHg in glaucomatous eyes. Each transducer is equipped with multiple gauges which allow for temperature compensation in the range of 0-85 °C and can operate with power supplies ranging from 1.5 to 12V. In our application the sensors are powered using a 3V supply and draw a nominal 300µA current. A key characteristic of any low-voltage system is a low initial voltage (offset) from the sensing elements. The PCB has integrated connections for shunt resistors that allow for external biasing of the sensing bridges in order to reduce their offset and maximize data resolution.

5.3.4.2 Differential Amplifiers

Each sensor is connected to a differential amplifier that maximizes data accuracy and resolution. The amplifier selection was based on two main features, the ability to operate using a single rail (e.g. single power supply) and low power consumption. The selected op-amp (LPV521, Texas Instruments, Dallas, TX) was specially designed for remote sensor nanopower

applications, consuming 350nA when powered by a single 3V cell. Moreover the amplifier has integrated electromagnetic interference (EMI) protection, which attenuates RF noise picked up by the PCB and running through the pins of the op-amp. The amplifier attenuates RF waves resonating at 2.4GHz by more than 120dB. Since this frequency is used for data transmission, the EMI rejection properties of the amplifier ensure cleaner data. While the PCB allows for customizable amplifier gain, the IOP data was collected using a gain of 1000.

5.3.4.3 Temperature Sensor

The on-chip temperature sensor has a resolution of 0.25°C and can operate in a range of 0-85°C. Temperature data is sampled and transmitted along with IOP order to monitor the chip's temperature. Although the temperature sensor is not subcutaneously placed, it can serve as an indirect monitor of body temperature. The readings obtained with the system could be rescaled to obtain accurate rises and falls in core animal temperature.

5.4 Materials and Methods

5.4.1 System Properties

The existence of artificial pressure drifts due to power supply fluctuations were evaluated by monitoring the hydrostatic pressure exerted by a reservoir of physiological saline kept at a constant height for the lifetime of the battery. The reservoir was covered to prevent evaporation and fluid levels were periodically checked to ensure the pressure applied to the sensor remained constant. The supply voltage was also recorded for the duration of the experiment. Pressure drifts were statistically evaluated using linear regression techniques. The operational lifetime of the battery was assessed by repeating the experiment using several sampling rates. 20 pressure data points were recorded at 50Hz every 1, 2 and 4 seconds and the length of battery life was

compared between experiments. Experiments were repeated in regulated and unregulated (no step-up converter) systems.

5.4.2 System Performance in Rats

The performance of the system was evaluated in 8 rats. The average of 20 data points sampled at 50Hz was transmitted every 20 seconds. In 3 experiments IOP readings were crosschecked hydrostatically using a reservoir of physiological saline and an in-line pressure sensor (5110, Stoelting, Wood Dale, IL) connected to a 33G needle via a three-way stopcock. The animals were anesthetized with an IP injection of ketamine (50 mg/kg) and xylazine (7 mg/kg), supplemented as needed, the head was secured in a stereotactic mount and the implanted eye was cannulated with the needle. The reservoir height was varied from 5 to 45mmHg while IOP was recorded using the telemetric system. In other animals IOP was also monitored using a handheld tonometer (Tono-Pen XL, Medtronic, Sarasota, FL). Measurements were taken, in both eyes, twice a week around noon-time with the animal under isoflurane anesthesia, while on a thermal blanket. On each session, 6-10 IOP measurements were taken and averaged. Tonometric pressure means and standard deviations were compared to those of data obtained using the telemetric system.

The correlation between chip temperature and core body temperature was also examined. A rat implanted with our sensor was anesthetized using a 2% isoflurane gas chamber and hose and placed on a temperature-controlled heating blanket. A rectal thermometer was used to continuously monitor core temperature while the sensor recorded IOP and chip temperature. The blanket settings were varied to modulate the animal's temperature between 35 and 39°C. Similarly, the effects of core temperature on IOP were also explored. The IOP and temperature records were plotted in the same time scale and the mean value of IOP was computed for every

1°C change. To serve as a control, the same procedure was repeated in a second animal after cutting the cannula at limbus and exposing it to atmospheric pressure. The difference of IOP values at every temperature level was computed between groups.

5.4.3 Data Analysis

In some animals daily data was divided into 1 hour blocks and the means and standard deviation of every hour were calculated. The means were averaged across several days to analyze highest and lowest IOP times. In other animals data was dived into 12 hour blocks. IOP data was averaged from 6am-5:59pm and from 6pm to 5:59am to obtain mean IOP day and night values. Statistical significance was evaluated with a two-sample t-test using SigmaPlot software (San Jose, CA). Results are expressed in terms of mean ± standard deviation.

5.5 Results

5.5.1 System Specifications

Artificial pressure drifts due to variability in the sensor's power supply were evaluated by connecting the sensor to different power sources while applying constant hydrostatic pressure to the sensor via a water column. Figure 5.3A shows the pressure recorded by a sensor exposed to 40mmHg for 90 days (bottom), while powered by a constant 3V line voltage (top). Data was obtained every 4 seconds. Regression data showed an average slope of -0.01 ± 0.046 mmHg/week (n=3). Figure 5.3B illustrates the same process while powering the sensor with a 3.3V coincell battery and using special circuitry to rectify the battery output to a constant 3.3V over time (top) (see power elements section). Under these conditions regression analysis indicated a mean drift of 0.01 ± 0.024 mmHg/week (n=3). The drift observed using our powering system is negligible and similar to that seen when powering the sensor with a 3V power supply

(figure 5.3A, p = 0.541). When sampling pressure every 4 seconds, the sensor was able to operate for 28 ± 2.65 days (n=3). Increasing the sampling rate to 1Hz decreased battery life to 7.33 ± 0.56 days (n=3). For most glaucoma studies, having IOP data available every 4 seconds is more than sufficient as the focus remains on mean IOP levels over time. Increasing the time between samples results in increased operational lifetimes and can be adjusted depending on the application. Other commonly used sensors can only record IOP every 2 minutes (McLaren, 1996) or 6 days per month (Downs, 2011).

Powering the sensor directly from the battery (bypassing the DC-DC step-up conversion) increases battery life but exposes the sensor to electronic drifts. Figure 5.3C shows the hydrostatic pressure data obtained every 2 seconds with a sensor of unregulated battery supply. The system was able to operate for 39 days at this increased sampling rate. Most batteries exhibit a three-phasic behavior (5.3C, top). First, a rapid voltage decay that settles at the nominal battery value (i.e. from 3.3 to 3V for a 3V coin-cell battery). Second, a period of slow drainage and stable power delivery. Finally, a stage in which power delivery is diminished and voltage supply is more variable. The last stage ends in a sudden drop of voltage when the battery can no longer deliver the power required by the circuitry. These stages result in an overall non-linear drift in pressure records (5.3C, bottom). The drift, however, can be analyzed piece-wise linearly. During the first two stages of battery drainage, pressure readings are stable and present noise levels of 0.23mmHg and a linear drift of -0.3 mmHg/week. This is followed by a sudden rise in pressure readings of 2.26 ± 0.49 mmHg (n=6), after which data stabilizes but experiences an increased noise level of 0.33 mmHg. The total drift and noise levels did not vary when the experiment was run at different sampling rates, but it did result in variations in the amount of time before the pressure increase. The results of multiple experiments are summarized in table 5.1.

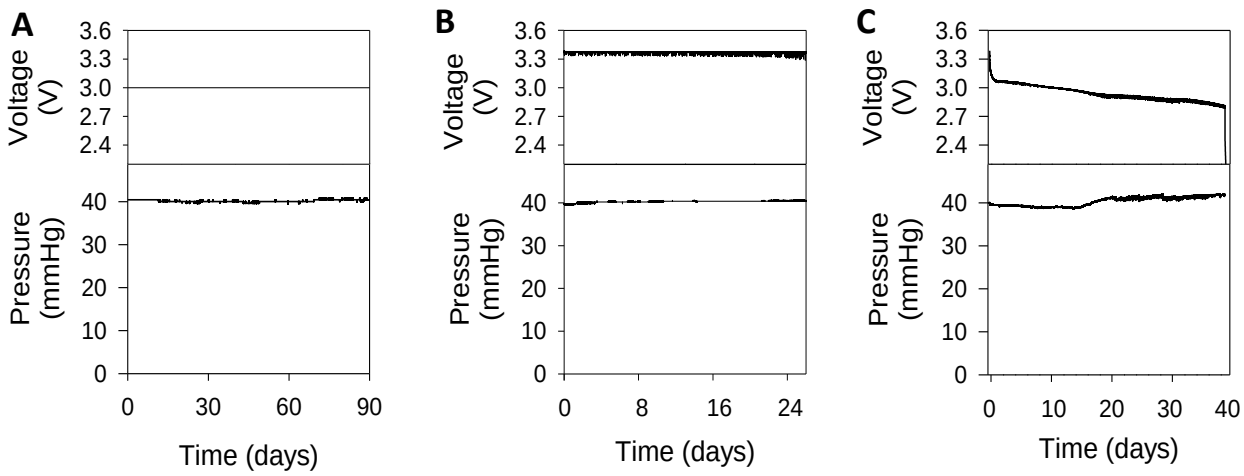

Figure 5.3 Pressure drift assessment of the implantable sensor. (A) Pressure record with applied pressure of 40mmHg (bottom). System was powered with a constant 3VDC (top). Data were fit by f(x) = 40.1 – 0.014x.0 (B) Signal recorded by the battery regulated implantable sensor when hydrostatic pressure was set at 40mmHg (bottom). Voltage supply was kept constant at 3.3V (top) using a DC-DC converter. Regression was fitted as f(x) = 40.05 +0.017x. (C) Hydrostatic pressure measurements using an unregulated battery powered sensor. Pressure records experience non-linear variations that results in a total drift of 2.26 ± 0.49 mmHg (n=6).

5.5.2 IOP Measurements on Awake Rats

Sensor accuracy was evaluated by manometric manipulation of IOP via anterior chamber cannulation (figure 5.4A). IOP was varied between 5 and 45mmHg, in steps of 5mmHg, and compared to the sensor readings. Manometric variations yielded a robust fit to the regression line (R^2=0.99, n=3), with a standard deviation of ± 0.27 mmHg across all pressure levels. The data ensures that the sensor readings are linear and highly accurate over this range, which is greater than normal IOP and glaucoma levels. Noise levels due to bending of the tubing system as the animal moves its head were evaluated in some animals by cutting the cannula at the entry point to the eye and exposing it to atmospheric pressure. Figure 5.4B shows two days of IOP data in one animal before the cannula was cut (black line) and two days of pressure data after it was cut (red line). With the system implanted in the eye, IOP measurements ranged from 7.4 to 25.6

mmHg with a mean value of 15.4 ± 4.1 mmHg. On the other hand, when the tube was out of the eye the system recorded a mean pressure of -0.03 ± 1.07 mmHg. This record indicates that pressure variations due to hydrostatic differences between the sensor and the eye, as well as bending of the tubing when the animal moves are much smaller than those seen when IOP is recorded. While some larger spikes are seen sporadically, presumably due to sharp movements of the head or changes in height while feeding, their duration is short and the mean values of IOP are preserved. This experiment demonstrates that the tubing connections employed in our sensor are adequate and allow accurate readings of IOP over time, even in an alert animal.

Table 5.1 Sensor Specifications (Unregulated Supply)

Sampling Rate (Hz)	Lifetime (days)	Total drift (mmHg)	Time to pressure rise (days)
1 (n=3)	23 ± 2	1.78 ± 0.33	9.33 ± 0.58
0.5 (n=3)	39 ±1	2.02 ±0.55	18.33 ± 1.52
0.25 (n=1)	91	2.1	40

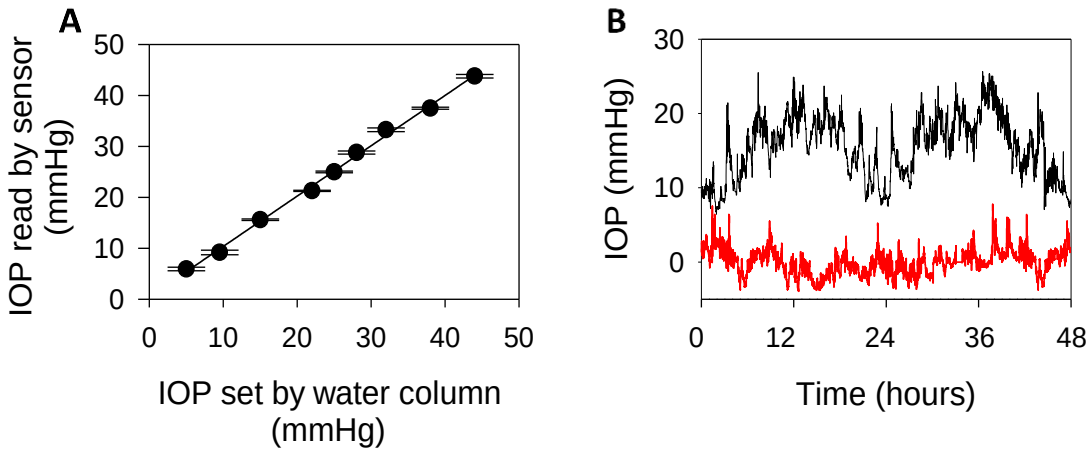

Figure 5.4 Accuracy and noise evaluation of implantable sensor. (A) IOP measurement with implantable sensor while pressure was set by manometry. The transducer's relationship was linear. (B) IOP measured with implantable sensor in an awake animal for 48 hours (black line). IOP showed pressure variations of ± 4.1 mmHg about the baseline. Pressure readings after the tube was pulled from the eye (red line) showed a decreased variability of ± 1.07 mmHg.

Once the electronics were tested and the system's accuracy was verified, long-term IOP data was recorded in several animals. Data was successfully acquired for 2 to 8 weeks in 6 of the implanted rats. In 2 other animals, fibrotic tissue grew around and inside the tip of the cannula, causing IOP readings to decrease after 4-6 days and eventually becoming negative. A crucial step to prevent clogging of the cannula was to flush the line with 50% moxifloxacin HCI ophthalmic solution (Vigamox, Alcon, Fort Worth, TX) daily during the first 3 post-operatory days. Fluid flow through the line, otherwise not present when measuring IOP, prevented tissue from adhering to the inside of the tube. After this period, physiological healing processes cease and fibrotic growth is less likely. Vigamox also prevented bacterial formation in the line. The positioning of the sensor facilitated flushing of the cannula and the whole procedure lasted just a couple of minutes with the animal under isoflurane anesthesia. After the flushing procedure was implemented, stable, long-term measurements were achieved in most animals.

Figures 5.5A and 5.5C show the IOP record of two rats for 4 and 8 weeks, respectively. In the first one, IOP fluctuated between 9.3 and 26.6 mmHg with a mean level of 16.5 ± 2.7 mmHg throughout the experiment. The second rat showed IOP values ranging from 11.9 to 25.9 mmHg with a mean value of 17.7 ± 1.8 mmHg. The IOP values read by the sensor were compared with tonometry data in both animals. The first animal (figures 5.5B) showed a mean IOP level of 18.46 ± 4.20 mmHg when measured with the Tono-Pen. On the other hand, the second rat (5.5D) had a mean IOP value of 19.40 ± 3.68 mmHg when using this method. The variability of IOP obtained via tonometry was much greater than that seen with the implantable sensor, even more so when normalizing data based on the time of day. Figure 5.6 shows a 1 hour record of IOP measured on a rat between 12:00 and 1:00 pm (a similar time of day in which tonometry data was acquired). Data shows a smooth pressure profile with a variability of ± 0.53

mmHg. The average variability in this animal between noon and 1pm across several days was ±0.42 mmHg (n=6). While tonometry measurements often yield variability values > 7mmHg (± 3.5 mmHg, figure 5.5), data demonstrates that the implantable sensor presented in this document offers a greatly more precise alternative.

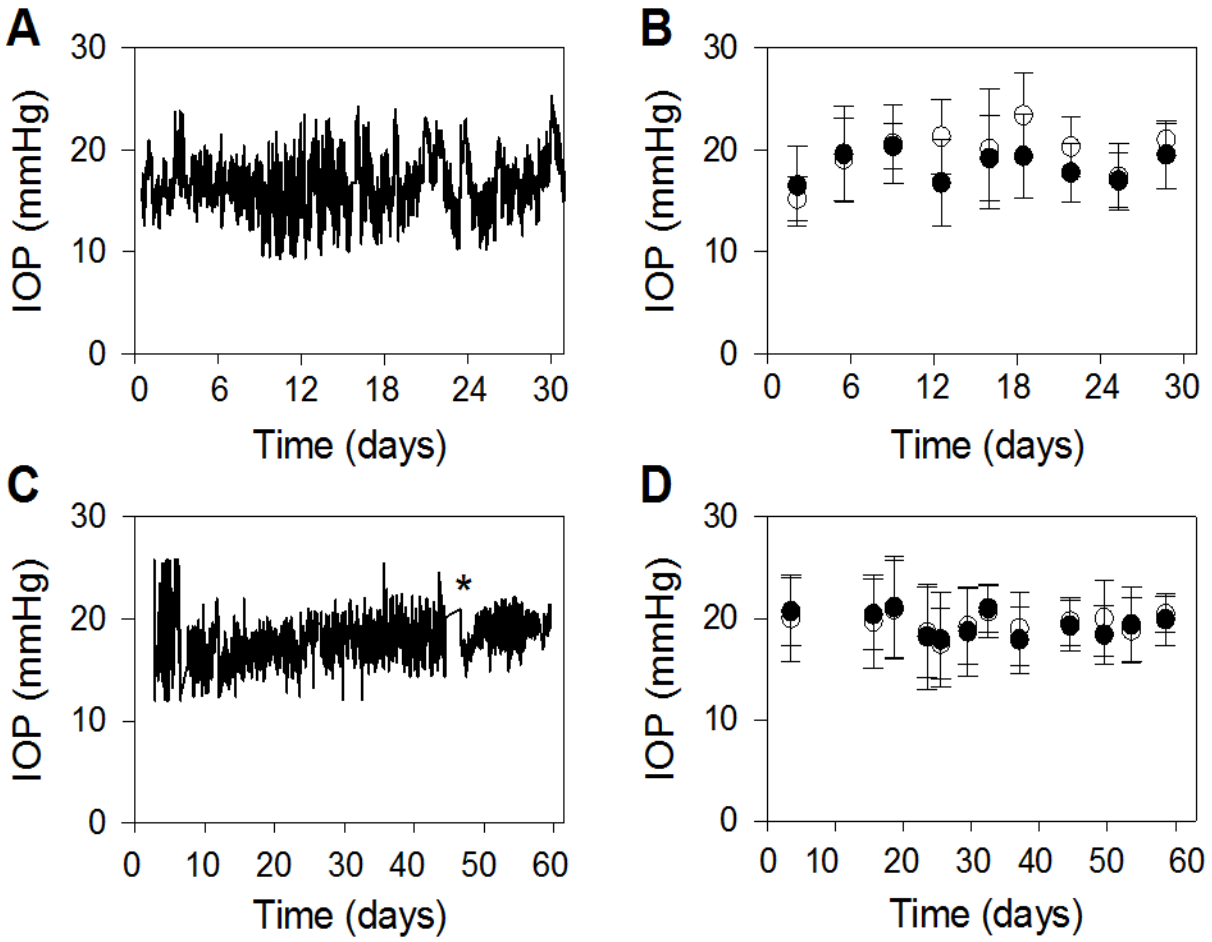

Figure 5.5 Long-term IOP measurements in live rats. (A, C) IOP measured with implantable sensor for 4 and 8 weeks in rats j26 and rat j22, respectively. IOP had values of 16.5 ± 2.7 mmHg (j26) and 17.7 ± 1.8mmHg (j22). Data was averaged in 10 minutes blocks. (B ,D) IOP measured by tonometry in rats j26 and j22. Black dots correspond to the implanted eye, while white dots illustrate the control (non-implanted) eye. Each data point is the average of 10 tonometer measurements. Data showed a mean value of 18.46 ± 4.20 mmHg (j26) and 19.40 ± 3.68 mmHg (j22).

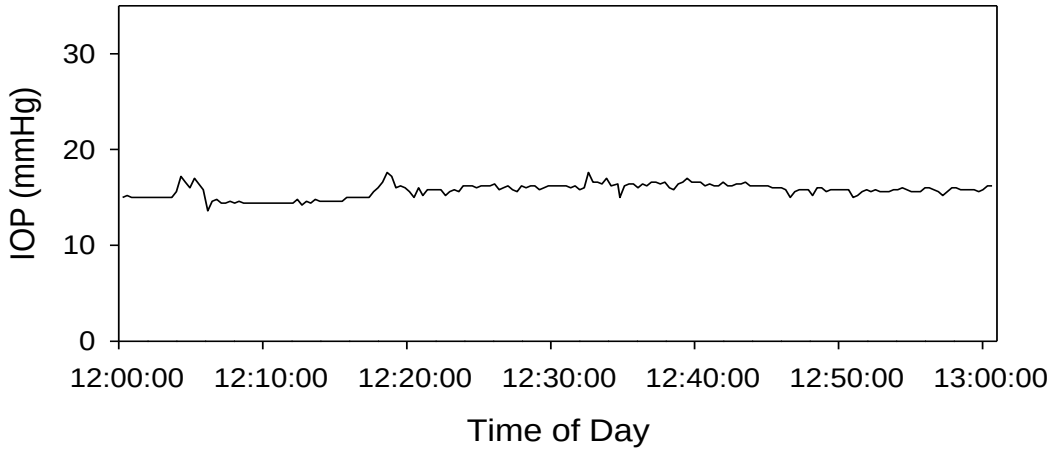

Figure 5.6 One hour IOP record of a rat. To recreate tonometric measurements conditions, data was obtained between 12:00 and 1:00pm using the implantable sensor on rat j26. Data was averaged every minute. Over this period, data oscillated around 15mmHg, with a variability of ±0.53 mmHg.

The effect of corneal applanation during tonometry on IOP was also explored. A rat implanted with our sensor was placed under isoflurane anesthesia and fixed on a heating pad to maintain body temperature. Once IOP readings were stable, tonometric readings were taken on the implanted eye. Figure 5.7 shows two IOP records obtained using this procedure. Red dots indicate tonometer data points (corneal tapping), while the black line indicates IOP measured by the sensor. In both cases, IOP rose considerably after the procedure began. Similar results have been reported in rabbits (McLaren, 1996). The length of experiments using tonometry can vary. In the first rat (left), 10 measurements were taken in approximately 3 minutes causing and elevation of around 4mmHg. In the second rat, the experiment lasted around 7 minutes and only 6 measurements were obtained. The change in pressure was 8mmHg in this animal. The non-systematic procedure makes it impossible to estimate how much IOP will vary every time. The results indicate that, although tonometers can be useful due to their non-invasiveness, they lack

precision and can create unwanted pressure increases during the procedure which may further compromise the accuracy of the data.

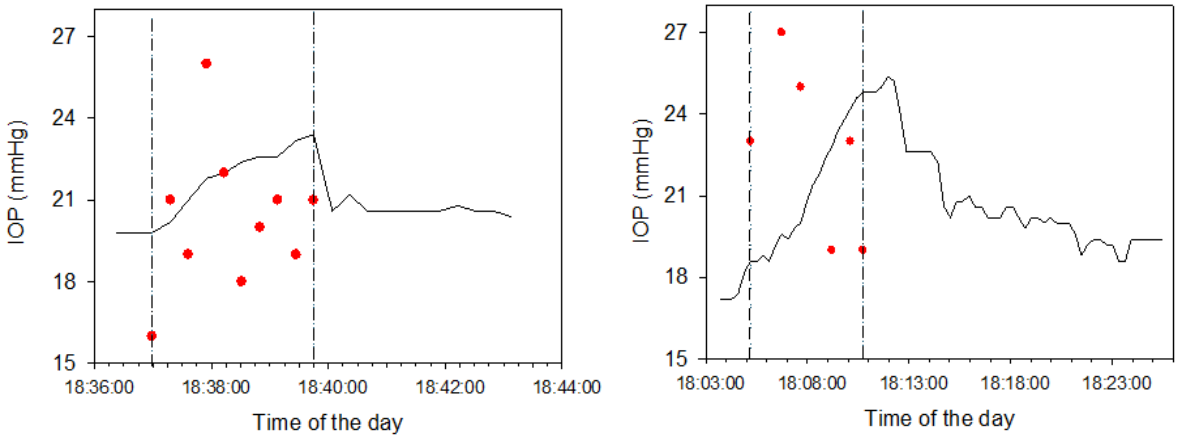

Figure 5.7 Effect of tonometry on IOP. Pressure was measured in two animas using both tonometry and the implantable sensor simultaneously while under isoflurane anesthesia. Core temperature was maintained at 37°C using a heating pad. Red dots indicate a single tonometer measurement. Solid black line indicated IOP measured via the implantable sensor. Dashed lines mark the beginning and end of tonometry measurements. In both cases IOP rose from its original baseline after tonometry started and decreased once it ended.

Circadian rhythms of IOP were present in most animals a couple of days post-surgery. Figure 5.8A shows a 24 hour IOP record of an implanted eye averaged every minute. During the light portion of the cycle, IOP had a mean level of 15.77 ±1.47 mmHg. Once the lights were turned off, IOP gradually increased and remained elevated through the night, exhibiting a mean pressure value of 19.91 ± 2.01 mmHg in this stage. Moreover, figure 5.8B illustrates the hourly averages of IOP for six consecutive days in this animal. IOP elevation patterns during periods of darkness were consistent from day to day, showing peak IOP values between 3 and 4 hours following the beginning of the dark cycle. IOP reached its lowest daily values between 4 and 6 hours after the lights were restored. The difference between IOP levels during the light and dark cycles across multiple animals was 5.02 ± 0.75 mmHg (n=5, figure 5.8C). These results are

consistent with previously reported light-induced IOP cycles in mice (Li, 2008) and rabbits (McLaren, 1996), showing that our sensor is able to detect physiological changes in pressure.

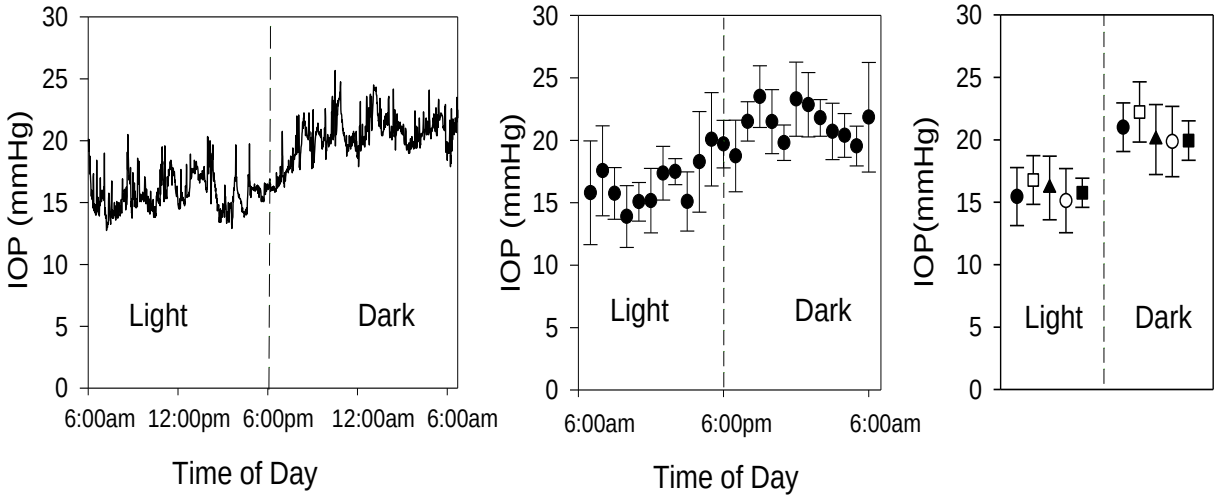

Figure 5.8 Circadian rhythm of IOP in awake rats. (A) 24 hour IOP record of rat j26. Data was averaged every minute. During the light cycle IOP: 15.77 ±1.47 mmHg. Dark cycle IOP: 19.91 ± 2.01 mmHg. (B) Hourly IOP average of 6 consecutive days of animal j26. (C) Day vs. night IOP of 5 different animals. Average difference in dark vs light IOP was 5.02 ± 0.75.

5.5.3 Temperature Measurements

Another benefit of our sensor is its ability to record temperature. Body temperature is an important physiological indicator of health and plays a significant role in IOP homeostasis. However, since the device is placed on the back of the rat, and not subcutaneously, the temperature read by the sensor's chip does not directly correspond to body temperature. The relationship between chip and core temperatures was explored by placing a heating blanket under an anesthetized rat and varying its settings while monitoring the animal's status with a rectal thermometer and the implantable sensor simultaneously. Figure 5.9 shows the temperature calibration of 3 sensors using linear regression analysis. The mean slope of the curves was 1.39 ± 0.059 with an offset of -4.77 ± 2.16. The linearity of every curve allows the user to estimate body

temperature based on the chip's temperature. While the slopes did not considerably differ between sensors, the offsets presented greater variability, probably due to slight differences in sensor placement and fitting of the vest across animals. Although this conversion may not yield absolute temperatures in every animal, the similarity in slopes indicates that relative variations in body temperature can be obtained. More exact pressure records for a particular rat could be obtained by calculating the mean temperature of an implanted sensor over time and setting it equal to a mean body temperature of 37°C. Since the curve's slope does not change, it is possible to solve for the offset of that particular sensor, which provides a complete calibration curve. For instance, if a sensor reads an average of 30°C while the animal is awake, setting this equal to a body temperature of 37°C and using a slope of 1.39, the offset of the sensor comes out to be -4.7 °C.

Temperature fluctuations had a noticeable effect on IOP. Figure 5.10A shows an experiment in which an implanted animal was placed under isoflurane anesthesia while its temperature was varied using a heating blanket. In the first stage, the animal was awake and IOP oscillated around 14mmHg, with temperature readings at 37.6 °C. After anesthesia was induced (first dashed line), core temperature dropped to 36.3 °C while IOP levels decreased to 9.50mmHg. When a heating pad (HP) was placed under the animal (second dashed line), body temperature rose to its original awake level but IOP remained low. However, when a small heating pad was place on top of the implanted eye (EP), IOP quickly rose to ~13.5mmHg. To serve as a control experiment, the same procedure was repeated in a rat in which the cannula had been pulled out of the anterior chamber and was exposed to atmospheric pressure (figure 5.10B). In this case, pressure readings had a mean value of -0.71 ± 0.60 mmHg with the animal on the core heating pad only and 0.46 ± 0.78mmHg when both pads were on. Although pressure

readings experienced an increase of ~1mmHg when the eye pad was used, the same action resulted in a 4mmHg IOP in the implanted animal. Pressure increase in the control experiment may be due to heating of the fluid line or a small electronic response to the heating source. Such device-dependent fluctuation should be further characterized and taken into account when performing future research. Commonly used anesthetic agents have been reported to have a lowering effect on intraocular pressure (Jia, 2000). To our knowledge, however, the effects of ocular temperature on IOP while under anesthesia have not been explored. These results are preliminary and further experimentation is necessary to draw definitive physiological conclusions. Nevertheless, the data shows the added value of the system when providing temperature data and its relationship to IOP, which could be an important research tool.

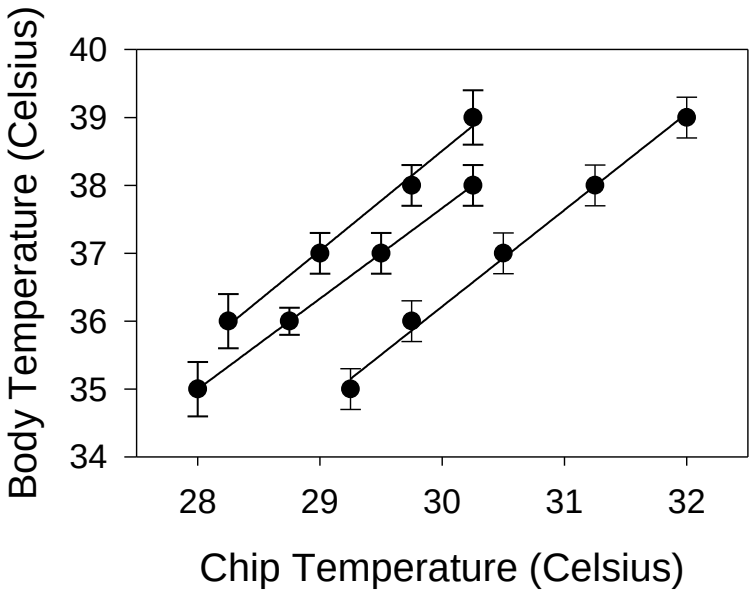

Figure 5.9 Sensor temperature vs. body temperature. Body temperature of 3 implanted animals was varied using a heating blanket, while core temperature was monitored using a rectal thermometer and sensor temperature was transmitted wirelessly to a computer. Data was fitted to the signal $f(x) = f_0 + ax$. Regression analysis showed that all sensors presented a slope of ~1.39, but offsets varied between devices.

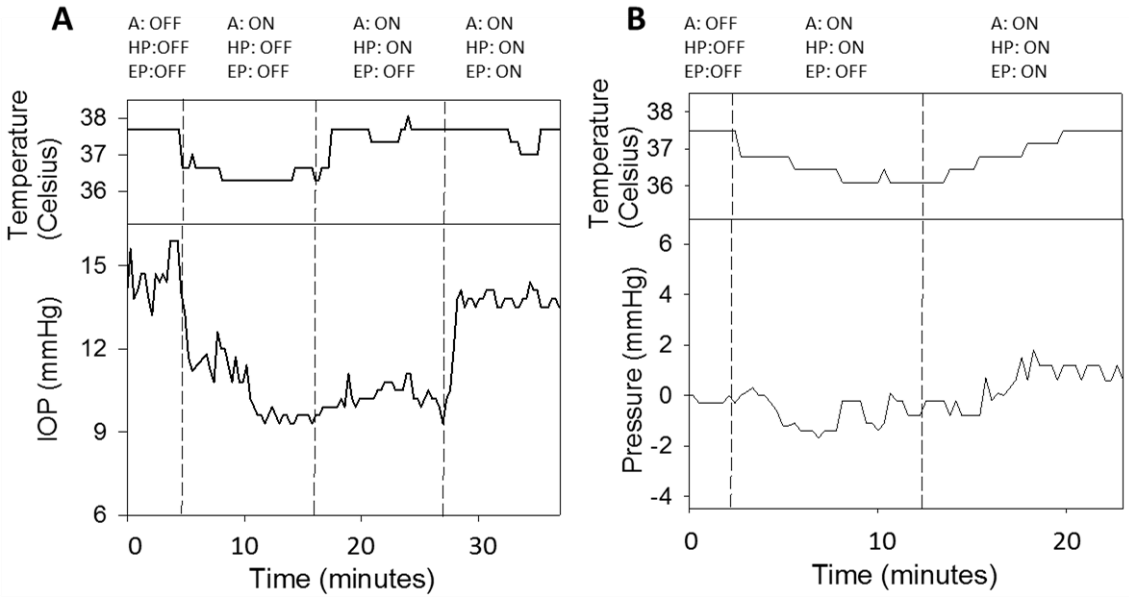

*A: isoflurane anesthesia; HP: heat pad; EP: eye pad.

Figure 5.10 Temperature effects on IOP. (A) Body temperature determined based on sensor temperature of a rat (top). IOP record of an implanted rat before and after anesthesia (bottom). Dashed lines indicate a change in anesthesia or heating of the animal. IOP was at 14mmHg while awake and decreased to 9.5mmHg with anesthesia. IOP remained low until a warming eye pad was used. (B) Control experiment. Animal was implanted but the cannula was pulled out of the eye. Temperature effects on pressure readings were diminished.

5.6 Discussion

In this chapter we presented the development of an implantable sensor to continuously monitor intraocular pressure in rats. IOP remains one of the most studied factors in glaucoma research, but as has been discussed throughout this manuscript, fully integrated commercial sensors present several limitations. Our device was designed specifically for glaucoma applications and aims to provide the researcher with the most accurate and reliable IOP data. Commonly used IOP sensors present accuracy levels of ± 3 mmHg (McLaren, 1996), which in most cases is problematic when compared to normal IOP values ranging between 12-22mmHg. Sensors with better accuracy levels are available (Downs, 2011) but their size limits their use to

higher order animals. Our system presents accuracy levels of ± 0.2mmHg when implanted in a rat eye. Similarly, other systems are subjected to electronically induced pressure drifts ranging from 2 (Akaishi, 2005; McLaren, 1996) to 17mmHg/month (Downs, 2011), which may require recurrent and invasive calibrations procedures. The special voltage-regulating circuitry we employ prevents such drifts from occurring, keeping the sensor's performance stable and comparable to a line-powered sensor (figures 19A and 19B). The installation of our device in a wearable vest makes the sensor easily accessible to the user and allows for simple troubleshooting and battery replacement, which extends the operational lifetime of the device to meet the needs of the researcher. Moreover, the system's circuitry is equipped with a second pressure sensor which can be used to record other physiological parameters (e.g. blood or intracranial pressure) simultaneously. Table 5.2 compares the characteristics of the implantable sensor to that of other available technologies. In all, we believe that our sensor is the most complete IOP sensor ever designed for use in rats.

Table 5.2 Implantable Sensor vs. Other Technologies

Feature	Our Sensor	DSI	Konigsberg	Implant Data	Tonometer
Accuracy (mmHg)	± 0.27	± 3	± 0.5	± 0.81	± 3.94
Drift (mmHg/month)	0.07	2-5	6-17	0-2	N/A
Temperature	Yes	No	Yes	No	No
Volume (cc)	6.25	4.5	70	N/A**	N/A
Multi-channel Sensing	Yes	No	Yes	No	No
Transmission Distance	500cm	45 cm	300cm	5cm*	N/A
Animal Feasibility (size)	Rodents, rabbits, monkeys	Rodents, rabbits, monkeys	Monkeys	Rabbit, monkeys	Any

* requires an operator; ** system is inside the eye

5.6.1 Current Limitations of the Technology

To ensure the proper functioning of the implantable sensor some issues must be considered. The most common cause of system failure is clogging of the cannula tip due to bacterial or fibrotic growth. Although such complications can be prevented, special care must be taken in maintaining aseptic condition during implantation. Additionally, flushing of the cannula in consecutive post-operatory days is crucial to preserve the cannula's integrity over time. Additional actions are sometimes required to replace the wearable vest when significant signs of wear-and-tear appear. Switching vests can be done under isoflurane anesthesia and does not affect the functioning of the sensor. Placement of the sensing elements in the back of the animal creates a small hydrostatic pressure difference between the transducer and the eye. This error can be corrected during calibration, but movement of the animal's head can create acute pressure changes. The protective spring that surrounds the connecting tubing diminishes the amplitude of these changes. However, natural IOP variations are greater than those seen by just tubing dynamics (figure 5.4B), which ensures the validity of the data. Lastly, implementation of the implantable sensor in bigger animals, in which the use of the vest is not viable, may require a redesign of the attachment elements and sensor placement.

CHAPTER 6: WIRELESS POWERING OF MOVING BIOLOGICAL SENSORS

6.1 Introduction

Telemetry has been become vastly popular in the medical field as a tool to wirelessly monitor or alter physiological functions. Its implementation extends from hospital patient monitoring, to clinical treatments and research applications. Implantable biomedical devices have been reported in areas such as: pacemakers (Wong, 2004), hearing aids (Kin, 2006; Neuteboom, 1997), intraocular pressure measurement (Downs 2011; McLaren, 1996) and body area examination (Gyselinckx , 2005), among others. However, most biomedical sensor nodes available today operate with batteries, which presents substantial drawbacks. Firstly, they add significant size and weight to the overall system, which in most cases are critical requirements. Secondly, the lifetime of the device depends on the capacity of the battery and can severely limit their usage. Lastly, when lacking electronic compensation, battery drainage can result in electronic artifacts that compromise data reliability (Downs 2011; McLaren, 1996). These limitations can diminish the effectiveness of the systems and, in some cases, hinder technological and medical advances.

To overcome the limitations of battery-powered devices, research efforts have shifted towards developing self-powering telemetry. Energy harvesting technology has been used to transduce optical (Paradiso, 2005), vibrational (Amirtharajah, 2000; Roundy, 2005), thermoelectric (Leonov, 2007), piezoelectric (Xu, 2010), glucose (Chaudhuri, 2003; Rapoport, 2012) and bio-potential (Mercier, 2012) energy into usable power. In most cases, these methods

are application-specific and generate low power densities. Alternatively, several others have employed near-field inducting coupling techniques to power their devices (Leonardi, 2009; Wang, 2006; Weiland, 2004; Wu, 2008). This approach works by using an external coil to induce a magnetic field that transfers energy to a built-in receiver. Electromagnetic coupling is highly useful in compliant patients, but can be hard to implement on animal research due to range limitations between the transmitting and receiving coils. Additionally, magnetic coupling often requires and operator to obtain measurements, which impedes around-the-clock data collection (Leonardi, 2009; Todani, 2011).

This chapter focuses on the development and implementation of a novel system to wirelessly power biomedical devices in a moving animal. The system employs radio frequency (RF) energy transfer to generate and maintain high power levels regardless of animal movements and positioning. The powering system was integrated into the implantable sensor described in chapter 6, enhancing its research applications even further. Data is presented on: i) stability, ii) power reception and iii) the ability of the system to maintain energy over time.

6.2 System Overview

The wireless powering system consists of: i) a radio frequency (RF) energy harvester, ii) an energy storage unit, iii) a battery monitor, iv) a voltage regulator and v) a custom power antenna. These components are integrated with the microcontroller, sensors and data transmission module described in chapter 5 (figure 6.1A). Two RF transmitters (TX91501, 1Watt at 915MHz, Powercast, Pittsburg, PA) are strategically placed orthogonal to each other on top of the animal's cage to serve as a remote power source. The RF waves emitted by the transmitters are collected by the specially designed power antenna, and converted to a DC voltage using the energy harvester (RFD102, RF Diagnostics LLC, Albany, NY). The custom

shape of the antenna and the arrangement of the transmitters allow the system to collect adequate amounts of energy at all times, regardless of the positioning and movement of the animal. The resulting DC voltage is redirected to the energy storage unit, where special circuitry regulates the amount of voltage delivered to the rest of the system, maintaining a constant 3V power supply. The same sleep/active alternating cycle described in chapter 5 is used for this version of the device. During active mode circuitry becomes active, IOP data is collected and transmitted along with the system's temperature and the voltage level currently stored in the system (sampled by the battery monitor). The receiver displays and stores collected data using a custom Labview program (figure 6.1B).

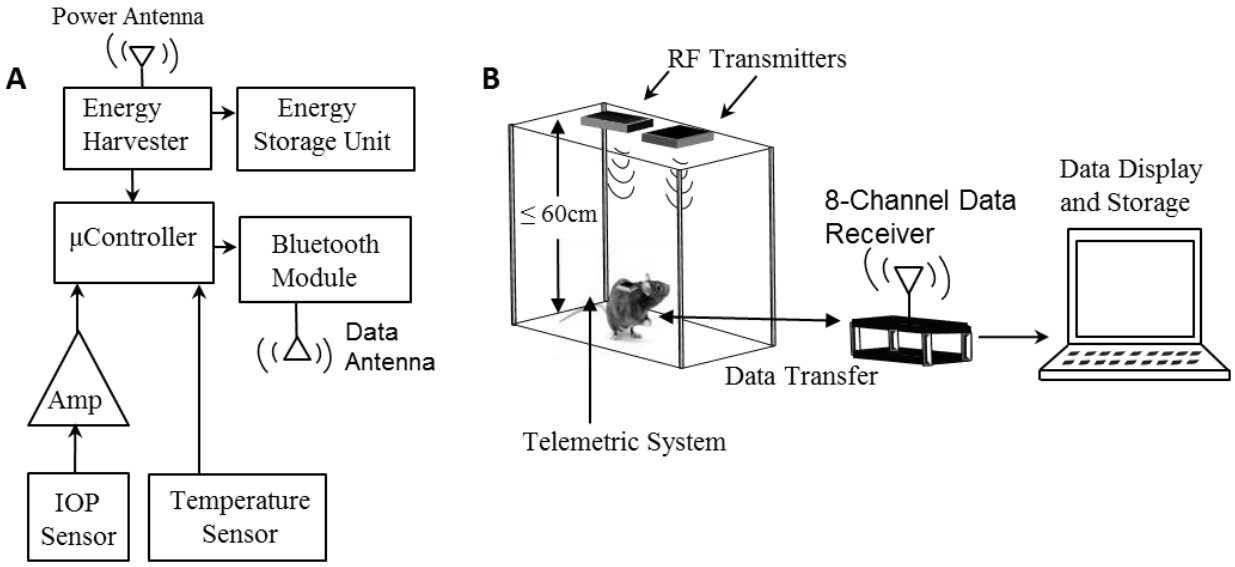

Figure 6.1 Wireless powering system. (A) Block diagram of the device. RF waves are collected with a power antenna and transduced to a DC voltage using an energy harvester. An energy storage unit maintains energy levels and regulates supplied voltage. IOP data is collected and amplified, along with temperature readings, before being digitized by the microcontroller. Data is transmitted wirelessly using Bluetooth technology. (B) System set-up. The powering and telemetric systems are worn by the rat. Two RF transmitters set at 1W and 915MHz are placed orthogonal to each other on top of the animal's cage. A single receiver can synchronize with up to 8 telemetric systems at a time. Data is displayed and stored in a PC.

6.3 Electronic Description

Figure 6.2 shows the schematics of the wirelessly-powered telemetric system. The system is equipped with i) wireless power transmission circuitry. ii) a microprocessor. iii) pressure and temperature sensing elements. All components were carefully selected or customized in order to provide high accuracy, low power consumption and operate with a single power supply. The following section covers the function of each component individually.

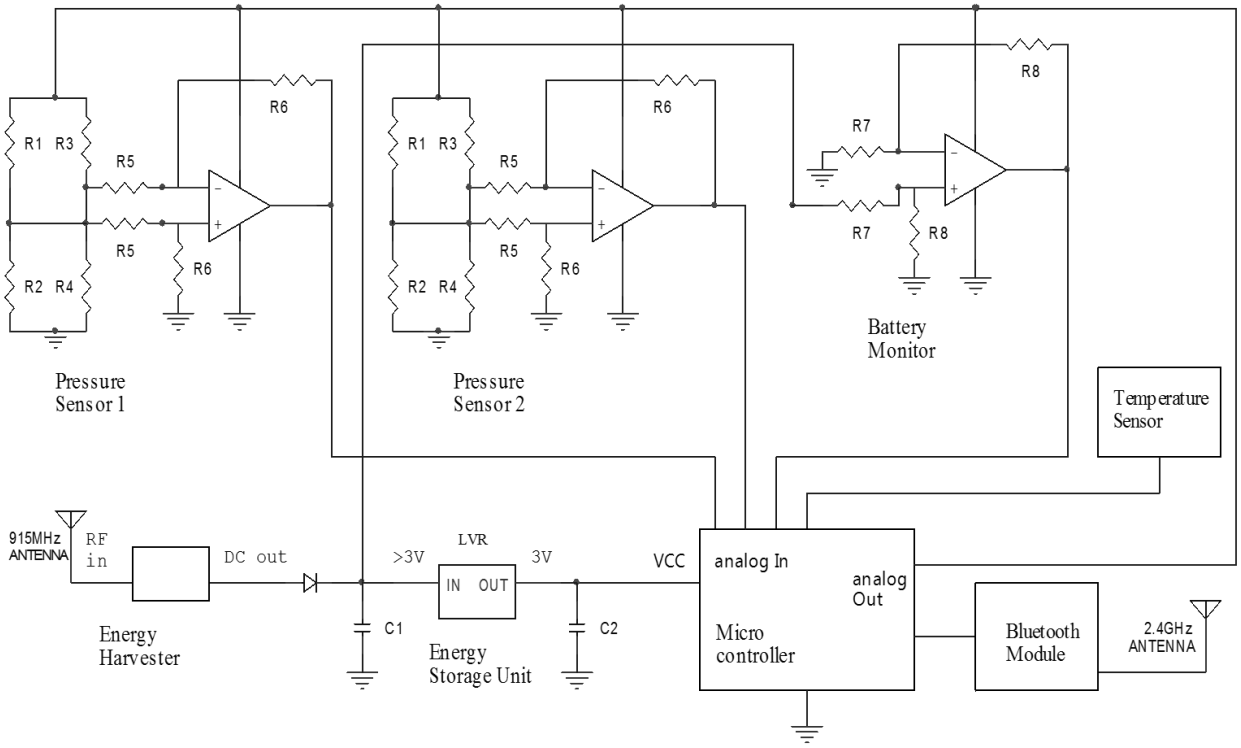

Figure 6.2 Electronic schematics of the wirelessly powered IOP sensor. A specially designed dipole antenna collects RF waves at 915MHz. Energy is converted to DC using a harvester, stored in two supercapacitors and linearly regulated to 3V. The microcontroller is digitally programmed to activate one or two pressure sensors in a smart cycle. A battery monitor continuously samples the amount of energy stored in the supercapacitors. Pressure signals are amplified x1000. IOP and temperature data are wirelessly transmitted using low power Bluetooth.

6.3.1 Wireless Power Transmission

6.3.1.1 RF-DC Converter

The energy harvester (RFD102A, RF Diagnostics LLC, Niskayuna,NY) is a small unit capable of turning RF waves ranging from 60Hz to 6GHz into a DC voltage. A 915MHz power signal was selected in this application due to increased efficiency of the module at this frequency. Optimization tests for matching network values were performed using specialized software (Advanced Design System, Keysight Tech., Santa Rosa, CA), but the results yielded output values similar to that of the stand-alone harvester (data not shown). The lack of a matching network reduces the number of components and overall size of the PCB. Additionally, operation in the 915MHz band prevents interference with the data transmission frequency (2.4GHz) due to the overall difference in wavelength between the two. According to the manufacturer, the harvester is able to deliver up to 18mA and offers a 53% peak efficiency when the input power reaches 11dBm or higher. The input power should be kept under 32dBm for reliable operation. For optimal performance, the harvester is paired with a Schottky diode, a custom-designed dipole antenna and stimulated using two RF transmitters.

6.3.1.2 Schottky Diode

The diode is connected between the DC output of the RF-module and the voltage regulator. The schottky diode (PMEG2005AEA, 115, NPX Semiconductor, Netherlands) is designed to increase efficiency and counts with a low forward voltage of 150mV, which allows for most of the voltage generated by the RF-DC converter to be stored. Under ideal conditions all energy stored in the capacitor would remain there until it is needed. However, under real conditions, current could flow backwards, enter the RF-DC module and dissipate energy through

the reverse leakage resistance present in most electronic components. The diode acts as a switch that prevents current from flowing towards the harvester, thus avoiding any losses.

6.3.1.3 Power Receiving Antenna

The antenna is a custom-designed, half-wavelength, dipole that attaches directly to the input and ground pins of the harvester. The antenna is made with a coated, thin copper wire. Each leg of the dipole must be precisely cut to match the receiving frequency following the equation:

$$\lambda = \frac{c}{f}$$

where λ is the wavelength, c is the speed of light and f is the desired frequency. For a half wavelength antenna, each leg must be 8.2cm long. Further trimming of the legs to achieve a length of 0.48λ creates a fully resistive antenna with an impedance of 70Ω, which increases efficiency. The antenna works best when it is completely straight and aligned with the RF field. The length of the poles, however, creates a challenge for implantation. In most biological applications, an 8.2cm long straight wire is not suitable to be placed subcutaneously and leaving the wire exposed can lead to unwanted bending of the antenna that could disrupt energy reception or overall damage of the wire. Therefore, a second challenge is presented when the shape of the poles is modified to allow them to fit within the dimensions of the system. In order to secure the antenna to the animal, a custom vest was designed to fit tightly around the back and chest of the animal. An innovative 3D architecture pattern (figure 6.3A) was developed to bend the antenna in such a way that it creates maximum alignment of sections of the antenna with the two RF fields being generated by the transmitters, while staying within the confines of the vest. The antenna connects to the rest of the circuitry, encased in a small plastic box that attaches firmly to the vest (figure 6.3B). From there, there are routed out of the box and embedded within

the fabric of the vest in order to protect it from contact and maintain the original shape. Originally the antenna was simulated using ADS, but an experimentally based design was necessary due to the software's inability to simulate the animal's presence, which greatly affects the antenna's performance. Other antenna patterns are possible, however the one presented here generated outstanding results.

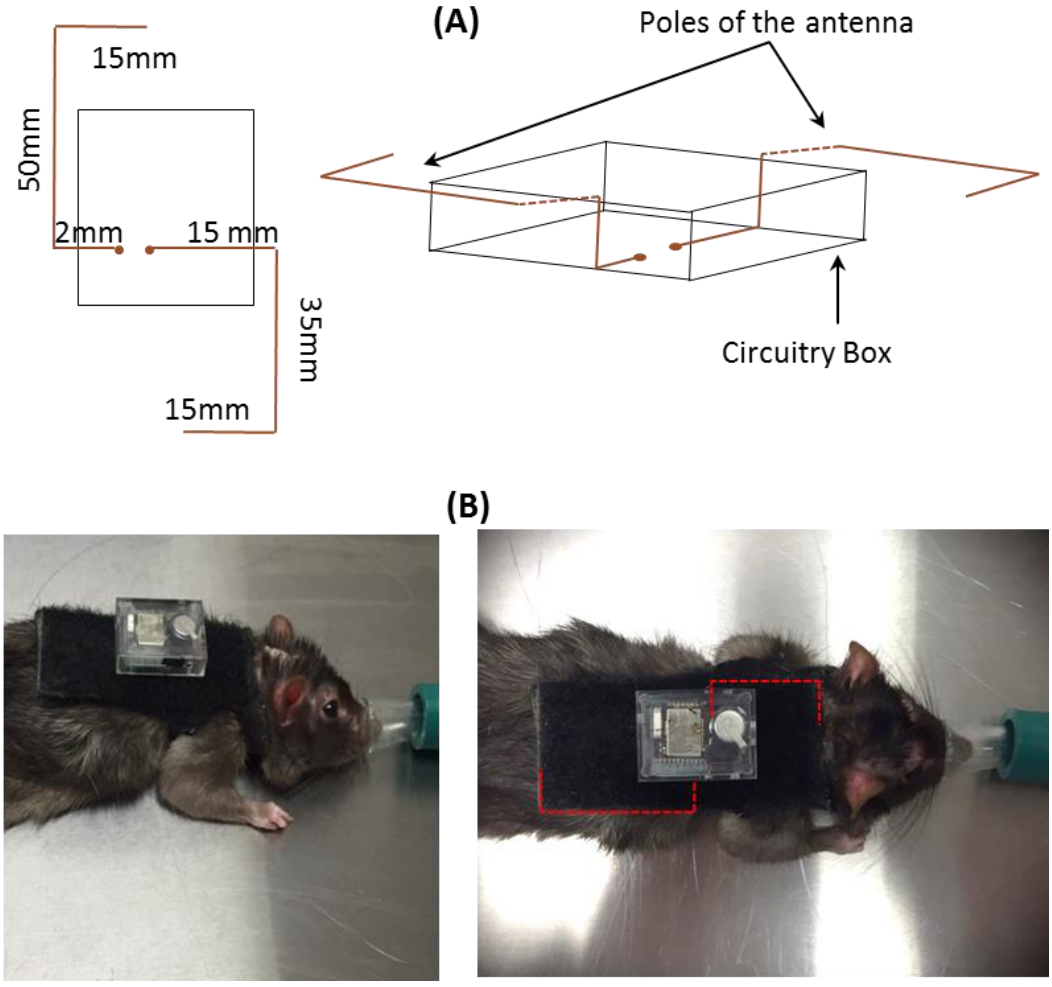

Figure 6.3 Power antenna design. (A) Antenna architecture. Top view of the antenna (left). 3D diagram of the antenna and circuitry box (right). (B) Antenna placement in the animal's vest. The telemetric system is attached to the vest using Velcro (left) and the antenna is embedded within the fabric of the vest (right).

6.3.1.4 RF Transmitters

Two RF transmitters (TX91501, Powercast, Pittsburg, PA) are placed, orthogonal to each other, on top of the animal cage. The transmitters operate with a fixed output of 1W (30dBm) at 915MHz. Each transmitter has dimensions of 6.75x6.25x1.63 inches, occupying approximately half of the rat's cage. The orthogonal positioning ensures that there is an energy field oriented along the width and the length of the cage at all times, which maximizes the alignment opportunities between the antenna and the field, this increasing power reception. The transmitters are approved by the Federal Communications Commission (FCC) and are equipped with a proximity detection system. If at any point the animal is at within harmful distance from the transmitter (e.g. while feeding or exploring roof of the cage), power output is momentarily paused until the animal returns to a safe distance. This instances are few, if any, at the dimensions employed in our cages, and guarantee the safety of the animal regarding energy radiation.

6.3.1.5 Energy Storage Unit

After energy is collected and transformed into a DC voltage it must be stored and regulated to drive the rest of the electronics. The unit consists of two super capacitors and a linear voltage regulator (figure 6.2) .The first supercapacitor, C1, serves to store most of the voltage generated by the harvester so that is it available for the active cycle of the system. It has a capacitance of 0.47F, an internal resistance of 50Ω and a voltage rating of 5.5V. The large capacitance in combination with the small leakage resistance allows the system to store charge for long periods of time. Smart circuitry adjusts the power consumption of the system to regulate the voltage across C1 to a maximum of 85% of its rating capacity, as discussed later in this chapter, in order to extend the life of the capacitor. The linear voltage regulator (LVR) serves to

rectify the supply voltage delivered to the microprocessor, which ensures data accuracy and eliminates electronically induced drifts in the pressure records. When the V_{C1} > 3V, the LVR outputs a constant 3V signal. For the system to operate effectively, the voltage across V_{C1} must be kept above 3V. The LVR has a low drop out voltage of 10mV and can output a currents up to 100mA. The second super capacitor, C2, serves to stabilize the output signal of the LVR, eliminating noise created by voltage fluctuations in the first capacitor. C2 has a capacitance of 0.33F and an internal resistance of 20Ω.

6.3.2 Microcontroller

The same microprocessor described in chapter 5 is used in this instantiation of the device. Once again the system is run in alternating active/sleep mode cycles. During sleep mode, all sensors and amplifiers are turned off and the stand-by current consumption of the device is decreased to 4μA, allowing for most of the energy harvested to be stored. During the active cycle, the controller uses one of its GPIOs to output an analog voltage that turns the sensors and amplifiers ON, data is then collected and transmitted wirelessly to a nearby computer. To further ensure data accuracy, the active cycle is split into data collection and data transmission and the microcontroller runs the device in a 4 step looping cycle: i) sleep mode ii) data collection iii) sleep mode and iv) data transmission. By splitting the active cycle the system avoids large spikes in current consumption that could pull the system's voltage below the lower operating threshold of 3V.

Additionally, the microprocessor runs the telemetric system in a smart power cycle, which uses the information provided by the battery monitor to automatically adapt the data sampling rate according to the amount of energy available. When $V_{C1} \leq 3V$, the system goes into continuous sleep mode, preventing the device from falling below operating levels. When 3.1>

$V_{C1} \geq$ 4.5V the system samples IOP at a low frequency (e.g. 1 data point every 4 seconds). Finally, when V_{C1} = 4.5V, the system continuously samples IOP at 250Hz for 10 seconds. Each high frequency reading decreases V_{C1} by approximately 100mV, ensuring that V_{C1} never goes above 4.5V (approximately 85% of the maximum voltage rating of $V_{C1)}$. Maintaining the capacitor's voltage below 85% of maximum capacity at all times extends its operating life and avoids overcharging that can damage the unit. The sampling rates as well as the unused GPIO ports are fully programmable and can be adapted depending on the application. The data receiver consists of a second identical microcontroller connected to a computer via a USB port. After the receiver collects the wirelessly sent data, it prints the low frequency information to the serial port of the computer, where it is read, plotted and stored by a custom-written LabVIEW program. The high frequency data is saved to a microSD memory card stacked to the receiver. High frequency data is not printed to the serial port to avoid data losses due to timing discrepancies (data is received faster than data is printed). A receiver must always be present to ensure system operation. If at any point the receiver is disconnected or absent, handshaking protocols are disrupted and the sensor is unable to regulate power consumption, causing the voltage stored in the system to deplete rapidly.

6.3.3 Code

The data transmission and reception codes were written in C++ and loaded into the microprocessors using a stack-up USB module and an open source prototyping software (Arduino, Italy). The sensor and receiver communicate wirelessly via Bluetooth using a wireless transmission protocol (Gazelle, Nordic Semiconductor, Norway). An especial library (RFduinoGZLL.h) is loaded into the code to allow protocol implementation. Data is transmitted following two different protocols: i) *low-frequency* information is sent using a single packet of

data. An especial structure (*struct*) is defined using 12 bytes. As IOP, voltage levels and temperature are sampled, they are assigned to a section of the struct. ii) *high-frequency data* are sent byte-by-byte when available. On the transmitter side, the code begins by turning the system ON and sampling the voltage level stored in the supercapacitor. If the voltage is < 3.2V, the sensor sends a low-power flag (*lp, 2 bytes*) to notify the user that energy is scarce and enters into sleep mode for 4 seconds. The process is then repeated. Otherwise, if voltage is between 3.2 and 4.5V, 20 IOP data points are collected at 50Hz and its sum is calculated (average is calculated at the receiver to optimize transmission speed). IOP sum, temperature, voltage stored and the device's ID are then sent in a single packet, as previously described. Else, if voltage levels are >4.5V, a high frequency flag (*hf_flag, 7 bytes*) notifies the receiver that single byte data will soon be sent. A 100ms delay is implemented to allow time for the receiver to prepare for high frequency data reception. The sensor then samples IOP at 250Hz for 10 seconds. Each data point is sent individually. The number of data points (*N_DATA_POINTS*) and the delay between points can be modified to change the length of data collection and sampling frequency. After high frequency is collected all antennas are digitally disabled to avoid battery depletion in case of hand-shaking errors. The antennas settings are restored before the next cycle.

On the receiver end a special library (*SPI.h*) was coded to allow for optimal data processing when collecting high frequency information. This library is different from the traditional SPI library included in the coding software, therefore is a new version of Arduino is installed the SPI library must be replaced. Similarly, another library (*SD.h*) is loaded to allow the microprocessor to access the external memory. The system uses the length of the data received to identify if any flags are present. If the length of data available is 2 bytes, the device identifies it as a low power flag and prints a string containing the device's ID and the notification to the

serial port (e.g. Rat:1 LP). A LabVIEW program records the date and time at which the flag was received. Conversely, if the data length is 12 bytes, the receiver identifies it as a packet of data (low frequency), copies it to the internal memory and prints information to the serial port (e.g. rat:1 cap:3.8 iop:300 temp:30). In this case the LabVIEW interfaces computes the average IOP and uses the markers (*rat*, *cap*, *iop* and *temp*) to break the data into substrings that are individually plotted and saved into a text file. Otherwise, if data length equals 7 bytes, the system closes any open files and creates a new file on the SD memory card. File names are assigned based on a counter that increases the file index every cycle (e.g. HF_data_1). Every time a new file is created in the card a bogus "0" is printed to it. This entry initializes the data file and the writing algorithm of the microcontroller. Initialization prior to data arrival minimizes data losses due to mismatches between the internal clock of the processor and data frequency. The receiver then prints the ID and file name to the serial port where a LabVIEW programs saves the file name and time received to a text file. Once the file is created and opened, the receiver prepares for byte-by-byte reception. As individual data points arrive they are printed into the SD's opened file. This remains true until the length of data is not equal to 1 byte (a different flag was received). LabVIEW records low power and high frequency flags, with their respective dates and times, into a single text file, while low frequency measurements are saved into a different text file. To read high frequency data, files must be transferred from the SD card to the computer and opened using a byte-reader LabVIEW program.

6.3.4 Sensing Elements

6.3.4.1 Pressure Transducer

The same pressure sensors used in chapter 5 are employed in this system. The printed circuit board (PCB) has two 4-pin connections set up for any sensor that operates in a

Wheatstone bridge configuration. In cases when only one sensor is necessary (e.g. IOP measurements) a single transducer is connected, which makes the system more power efficient. The pressure sensors (TBPDANS005PGUCV, Honeywell, Morristown, NJ) are piezoresistive strain gauges with a range of 0-250mmHg, an overpressure capacity of 1500mmHg and temperature compensation between 0-85 °C. The sensors are powered using a 3V supply and draw a nominal 300µA current. The PCB has integrated connections for shunt resistors that allow for external biasing of the sensing bridges in order to reduce their offset and maximize data resolution.

6.3.4.2 Differential Amplifiers

Each sensor is connected to a differential amplifier that maximizes data accuracy and resolution. The amplifier selection was based on two main features, the ability to operate using a single rail (e.g. single power supply) and low power consumption. The selected op-amp (LPV521, Texas Instruments, Dallas, TX) was specially designed for remote sensor nanopower applications, consuming 350nA when powered by a single 3V cell. Moreover the amplifier has integrated electromagnetic interference (EMI) protection, which attenuates RF noise picked up by the PCB and running through the pins of the op-amp. The amplifier attenuates RF waves resonating at 900MHz and 2.4GHz by more than 120dB. Since both of these frequencies are used for power transfer and data transmission, the EMI rejection properties of the amplifier ensure cleaner data. A gain of 1000 was used for data amplification.

Stored voltages are expected to oscillate between 3.2 and 4.5 V, which is out of the input range of the microprocessor (0-3V). The battery monitor consists of a factional amplifier with a gain of 0.3. The positive input of the amplifier is connected to the storage supercapacitor (C_1),

while the negative input is grounded. The output is transmitted and rescaled at the receiver to display actual voltage levels.

6.3.5 Printed Circuit Board (PCB)

Figure 6.4 shows the especially designed multilayer PCB for implementation of the wirelessly powered IOP sensor. The bottom layer (figure 6.4A) provides metal pads for surface mount versions of all the necessary components, with the exception of the microprocessor, which is located in the top layer. The *metal free area* marked on the PCB corresponds to the region underneath the data transmission antenna, which must be kept free of electronics to ensure proper data transfer. The PCB has 2 other middle layers. The first one is fully covered by a copper sheet that occupies the whole extent of the PCB (except for the metal free portion) and it is used as a floating ground to which all components are referenced. The second one contains routing vias for component interconnections.

Components were reflowed in placed using a programmable oven (T962a, Sanvn, China). Since the PCB contains components on multiple layers, the reflow process must be done in two stages. The bottom layer is assembled before the top layer to avoid double heating of the microprocessor. In order to avoid component detachment during the second round of reflow, two different soldering pastes are used. The first one, used in the bottom layer, has a melting temperature of 250°C. The second one liquefies at 160°C. In each case, the oven is programmed to follow the reflow profile of each paste. Figure 6.4B shows a picture of the assembled PCB. The sensor is manually soldered to the pins located on the side of the board. The supercapacitors and antenna pins are positioned on the upper side of the bottom layer (figure 6.4A). In cases of high energy reception (>25dBm) an RF diode can be placed in the metal pads between the antenna pins to limit the amount of RF energy that enters the harvester.

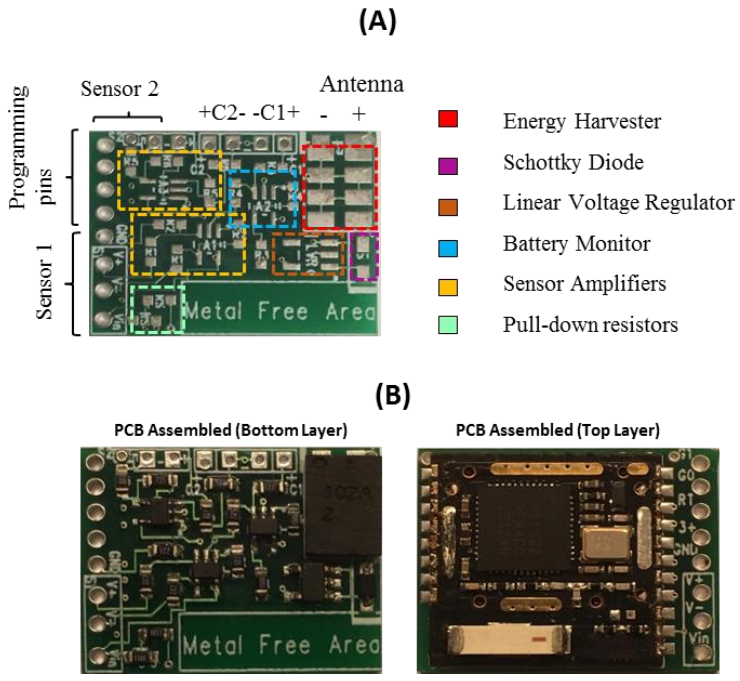

Figure 6.4 Printed circuit board of the telemetric system. (A) Unassembled bottom layer of the PCB. It includes all elements except for the microprocessor and Bluetooth module. Sensors and capacitors are manually soldered to the indicated pins. Programming pins are used to load digital algorithm to the microcontroller. (B) Assembled picture of the bottom (left) and top (right) layers of the PCB. Elements at set in place under a microscope and reflowed using a specialized oven.

6.4 Materials and Methods

6.4.1 Characterization of the Wireless Powering Technology

Similarly to the procedure described in chapters 3 and 5, a hydrostatic source was used to apply constant pressure to the sensor in order to assess the existence of artificial pressure drifts while the sensor was wirelessly powered. The system was fixed ~15cm away from an RF transmitter while pressure and energy stored in the unit were recorded. Once again fluid levels were maintained constant throughout the experiment. Drifts in data were calculated by linear regression and compared to the results obtained when the sensor was powered by a battery or

line voltage. The ability of the system to collect energy in different locations and positions within the cage was evaluated by mapping power reception inside the cage and its surroundings. The system was mounted on a cadaver rat to recreate actual operating conditions. A 60x60cm work area was divided into 36 squares of 10x10cm, the two transmitters were placed in the center of the grid, first at a height of 60 cm and then at 20cm. The telemetric system was moved along the grid, rotating the animal until a full revolution was completed at each location. The power received by the antenna was monitored using a portable spectrum analyzer (N9915A, Agilent Technologies, Santa Clara, CA). The maximum and minimum power received at each location were recorded.

6.4.2 Performance of the System in Awake Animals

The ability of the system to continuously power the sensor was evaluated in 3 awake rats for 7-15 days. The sensor was exposed to atmospheric pressure for the duration of the experiment. The average of 20 pressure points sampled at 50Hz were transmitted every 4 seconds with occasional transmissions of data sampled at 250Hz for 10 seconds. Each data transmission also included temperature and voltage stage stored readings.

6.4.3 Animal Housing and Training

Animals were kept in adapted plastic cages that featured an all-plastic feeding rack and water bottle (RS1-H, Innovive Inc. San Diego, CA). Standard metal feeding racks would cause reflection of the RF signal and impede wireless powering.

6.4.4 Data Analysis

Statistical significance was assessed by a two-sample *t*-test with an alpha level of 0.05 using SigmaPlot software. Results are expressed in terms of mean ± standard deviation.

6.5 Results

Repeating the experiments conducted in chapters 3 and 5, electronic drifts were assessed by hydrostatic pressure exertion. Figure 6.5A shows the pressure recorded by a sensor exposed to 40mmHg for 90 days, while powered by a constant 3V line voltage. Regression data showed an average slope of -0.01 ± 0.046 mmHg/ week (n=3). Figure 6.5B illustrates the same process while powering the sensor with the battery regulated technology outlined in chapter 5. Data was obtained every 4 seconds. As previously discussed, the experiment presented a regression slope of 0.01 ± 0.024 mmHg/week (n=3). At this sampling rate the average battery life was 28 ± 2.65 days (n=3). Lastly, figure 6.5C shows a plot of a wirelessly powered sensor exposed to 40mmHg for 90 days. In this case data was again collected every four seconds. Regression analysis yielded a slope of 0.0021 ± 0.001 mmHg/week (n=3). The data indicated that the wirelessly powered sensor presented negligible drift over 90 days, not significantly different from line powered (p=0.672) or battery regulated (p=0.599) pressure sensors. However, the system did offer substantially longer operational lifetime than a battery powered version of the sensor (figure 6.5B) while avoiding the wiring of the line powered device.

The key to avoiding drift artifacts lies in harvesting more energy than the sensor consumes at any point in time. Figure 6.6 shows the power received by a static antenna when located ~15cm directly below the source. When the antenna is perfectly aligned with the RF field, the power received is 13.43dBm (22mW) at a center frequency of 914.8MHz. On the other hand, the sensor consumes ~12mW while active (data collection and transmission) and just 12µW during sleep mode (figure 6.7). This is equal to 1.7 mJ of energy consumption during every active cycle. The static harvester can generate 8.8mJ over the same period of time. This surplus of energy is what allows system to maintain voltage levels well above minimum levels,

yielding stable pressure records (figure 6.5C). Under these conditions (fixed and aligned), the system could power the sensor continuously without the need of a sleep mode.

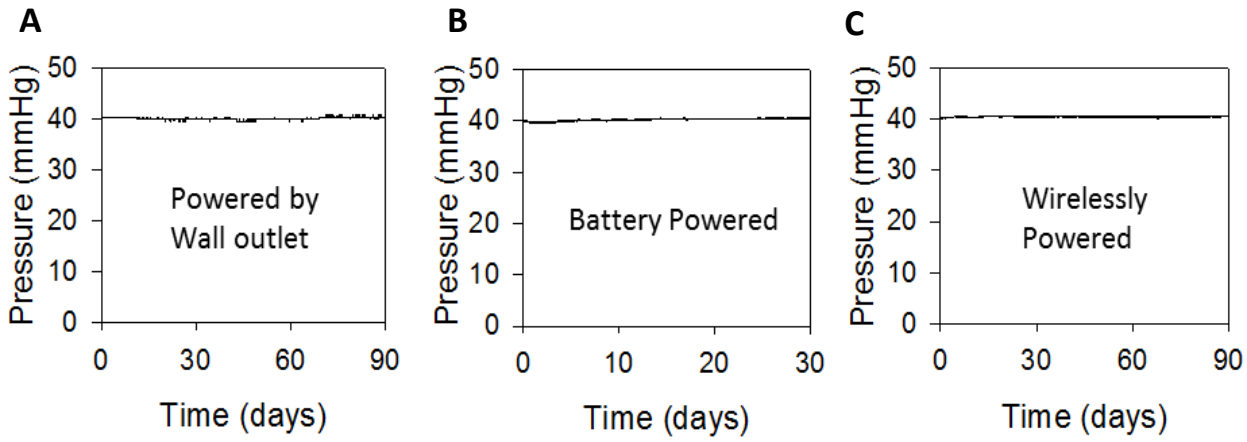

Figure 6.5 Pressure drift assessment of wirelessly powered sensor. (A) Hydrostatic pressure signal recorded using a line powered sensor. Data was fit to the line f(x) = 40.1 – 0.0014x. (B) Hydrostatic signal obtained using the battery regulated implantable sensor described in chapter 5. Regression yielded the equation f(x) = 40.05 + 0.0014x (C) Constant pressure signal measured using wirelessly powered sensor. Regression of this experiment revealed a fit f(x)=40.43+0.0003x. The wirelessly powered performed as well as the battery and line powered sensors but offers increased operational lifetime and full implantation.

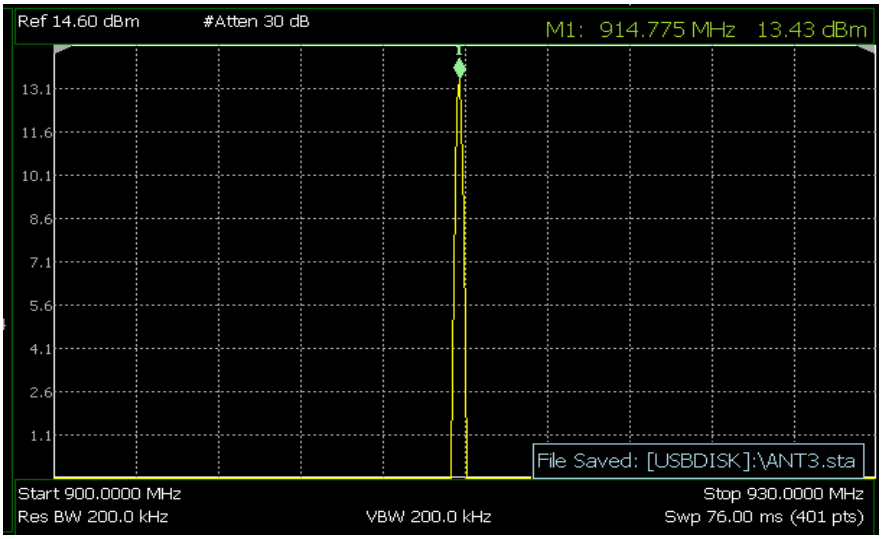

Figure 6.6 Antenna power reception. Power levels were monitored and recorded using a portable spectrum analyzer. When aligned with the RF field, and located at a distance of 15cm from the transmitter, the antenna receives 13.43dBm (22mW) of power at a center frequency of 915MHz.

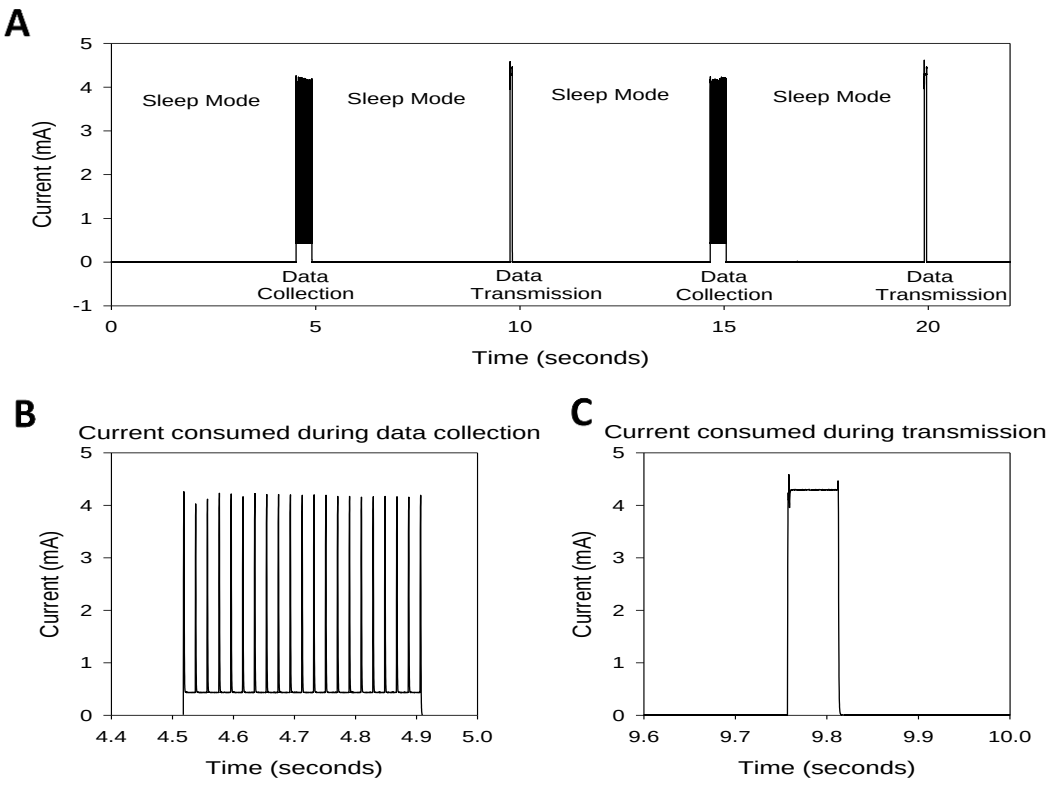

Figure 6.7 System's current consumption profile. (A) Data collection, data transmission split cycle. The device enters sleep mode between data collection and data transmission actions to avoid large current draws that may drop the capacitor's voltage below the operating thresholds. (B) Current consumption during data collection. 20 IOP data points are collected at 50Hz. Each data point draws approximately 4.2mA. Current consumption drops to 0.5mA in between data points. (C) Current consumption during data transmission. Bluetooth connectivity draws a steady 4.3mA for 30ms.

While the system is able to easily power a static sensor, a moving device presents additional challenges. The presence of the rat can attenuate power reception as animal tissue can absorb RF waves, reducing their availability. Moreover, animal movements along the length and width of the cage continuously alter antenna alignment, which plays a major role in power reception. Power distribution was tested by dividing the cage and its surroundings in blocks and moving an animal wearing the system along the grid, while recording the antenna's reception.

Figure 6.8A shows the minimum power detected at each location when the transmitters are located 60cm away from the bottom of the cage. Power levels under these conditions varied between 0.150 and 1.5mW. Conversely, the maximum power levels at this distance (figure 6.8B) ranged from 0.5 to 5mW. The weakest points were located in the surroundings of the cage, while the strongest energy locations corresponded to instances directly underneath the transmitters, where the animal's cage is located (black square). Figures 6.8C and 6.8D show the minimum and maximum power reception when the distance between the transmitters and the bottom of the cage is reduced to 20cm. Under these conditions, the antenna received minimum power levels between 1 and 4.5mW and maximum ratings ranging from 2.5 to12mW within the dimensions of the cage.

Based on these results, our system must be placed within 20cm of the RF- transmitters in order to ensure continued operation of the sensors. While the 60 cm separation between the transmitting and receiving antennas may not be adequate to run the system at the sampling rates proposed in this study, the power reception attained at this distance is comparable to previously reported wirelessly powered sensors (Ho, 2014). This distance may be suitable for research in which slower sampling rates can be used or for adaptation to sensors with a lesser power demand. Animal movements and positioning are unpredictable, which makes it impossible to determine the minimum sampling rate at which the sensor would operate continuously. Nevertheless, based on the minimum power reception at a distance of 20cm, obtaining a data point every 2.5 seconds (minimum of ~2.5mJ harvested) should provide the sensor unlimited battery life. The smart power cycle programmed into the device will increase the sampling rate when high energy levels are available and decrease it when the animal is located in a reduced energy location.

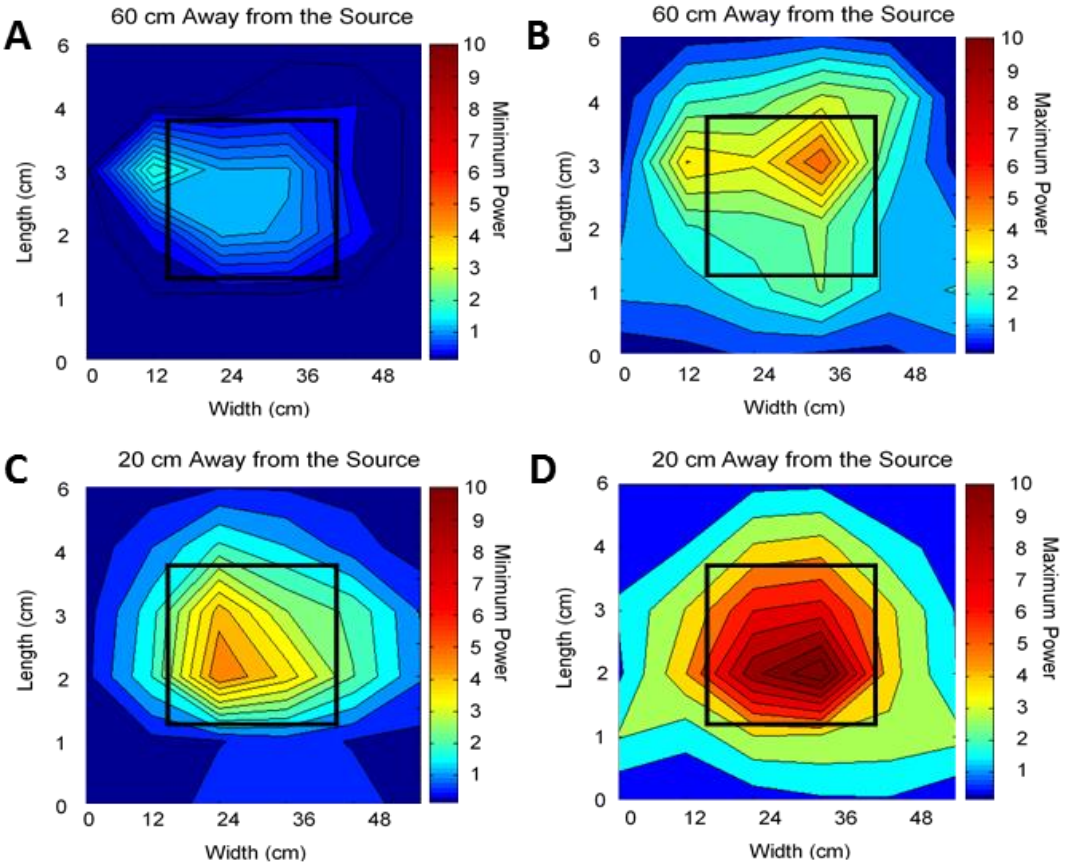

Figure 6.8 Power availability around a rat's cage. Black square represents the cages location in every figure. Measurements were taken with system mounted on a dead rat using a network analyzer. (A) Minimum power levels when sensor is located 60cm away from the RF source. Power levels ranged from 0.150 and 1.5mW. (B) Maximum power levels when sensor is located 60cm away from the RF source. Power levels ranged from0.5 to 5mW (C) When distance is reduced to 20 cm, minimum power levels increased to 1- 4.5mW. (D) Maximum power levels at 20 cm ranged between 2.5 and 12mW.

Further testing of the system's ability to continuously record pressure while wirelessly powered was performed by monitoring the voltage stored in a device implanted in a fully awake rat. Pressure data was recorded every 4 seconds while voltage levels oscillated between 3.2 and 4.5V and at a rate of 250Hz when they exceeded 4.5V. If at any point voltage levels drop below 3.2V, the system sends a *low-power* notification to the computer and enters in sleep mode configuration until energy levels once again surpass this lower threshold. During sleep mode no

data is collected. Figure 6.9A shows a 2 week record of the voltage stored in an implanted sensor. The mean voltage level through the two weeks was 4.4 ± 0.06V, never reporting low-power status during the experiment. On the other hand, the device was able to obtain high-frequency pressure measurements approximately every 2 minutes, on average. This experiment was repeated in 2 other animals and the results are summarized in Table 6.1. Only one of the tested animals was ever subjected to low energy levels. In this case the average voltage stored in the system was 4.3V but two instances of *low-power* were reported in the course of 1 week. The longest time the device stayed under sleep mode operation was 33 minutes. Along with IOP and voltage measurements, temperature of the device was also recorded. Figure 6.9B shows a comparison between the temperature record of a wirelessly-powered and a battery-powered sensor while mounted on an alert animal for 2 weeks. The two records superimposed each other, ranging between 29 and 32 °C. The wirelessly powered version of the device exhibited a mean temperature of 30.3 ± 0.6°C, while the battery powered prototype showed values of 29.3 ± 0.6 °C. In a group of 6 rats there was no statistically significant difference between the temperature records of battery and wirelessly-powered sensors (p=0.480), which indicates that the use of RF microwaves for wireless powering is not causing overheating of the device and should not have an effect in the core body temperature of the rat.

Table 6.1 Wirelessly Powered Sensor Performance on Awake Rats

Animal	Mean voltage level (Volts)	Low power (times/week)	Maximum down time (minutes)	Ave. time between HF data (minutes)	Max time between HF data (minutes)
Rat 1	4.4 ± 0.06	0	0	1:51	65
Rat 2	4.3 ± 0.2	2	33	9:56	209
Rat 3	4.4 ± 0.1	0	0	2:16	43

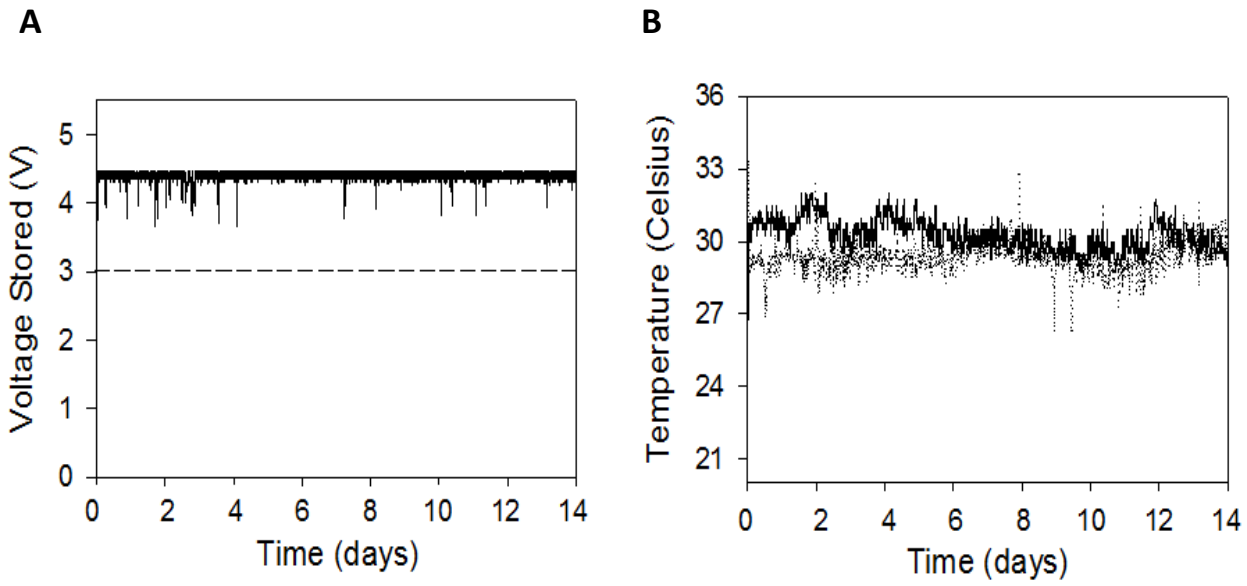

Figure 6.9 Wirelessly powered sensor performance on an awake rat. (A) Record of the voltage stored in the system for 2 weeks while mounted on a fully awake animal. Pressure data was obtained every 4 seconds at 50Hz when the voltage stored ranged between 3.1 and 4.49V. Additionally, 10 seconds of data were sampled at 250Hz when the voltage stored reached 4.5V. The device was programmed to enter sleep mode when voltage levels dropped below 3.1V. For 14 days the device never entered sleep mode and maintained an average voltage of 4.4 ± 0.06V, obtaining high frequency measurements every 1:51 minutes, on average. (B) Temperature record of a wirelessly powered sensor (black line) and a battery powered sensor (dotted line) for two weeks. The temperature difference between the two was not statistically significant (p=0.480), indicating that the presence of the RF transmitter is not causing a rise of body temperature in the animal.

6.6 Discussion

Powering of electronics is a major focus of the engineering process that takes place during the design phase of biological sensors. Most of the time, data reliability and success of experiments depend on a stable power source. While traditional batteries can provide adequate results in some cases, they add significant restrictions regarding size, lifetime and electronic drifts. Moreover, commonly used powering techniques, such as energy harvesting and electromagnetic coupling, often yield low power densities and are subjected to range limitations.

This chapter introduces a novel system that allows for the operation of moving biomedical sensors without the use of batteries. The device harvests RF waves and transforms them into a regulated DC voltage that keeps sensors running continuously while obtaining reliable data. The innovative power-antenna design, in combination with specialized circuitry, allows for collection and transduction of large amounts of energy, unlike any technology available today. This chapter presented the implementation of this technology to run an adaptation of the intraocular pressure sensor described in chapter 5.

6.6.1 Comparison to Existing Technologies

Remote power transfer has been explored by several research groups, many of which have specialized in operating biological sensors. Most of these technologies are based on electromagnetic or inductive coupling. When two coils are placed in close proximity to each other, energy can be transferred between them. The use of microcoils that operate in the near-field to power electronic implants have been reported. However, these technologies can only provide significant power when located at a maximum of ~ 3 cm away from the transmitting coil (RamRakhyani , 2011; Wang, 2006; Wu, 2008). Such distance limitations impede their use on implants embedded on freely moving animals. Mid-field coupling, which is less sensitive to distance attenuation (Kim, 2013), has been employed in awake rodents. Power levels of these devices range from a few hundred μWatts of power (Ho, 2014) to 1-3 mW when driven by a 1W transmitter (Montgomery, 2015). On the other hand, our device is able to generate 2-12 mW of power at all times, consistently staying in the upper edge of that range. The size of our device is considerably bigger than the implantable microcoils employed in mid-field coupling devices, which allows their systems to be fully implantable while ours remains wearable. The large amount of energy available when using our technology provides the user with additional

benefits. For instance, the excess power can be used to run multiple sensors simultaneously, operate electrical stimulators or drive electromechanical components. No other technology can provide such capabilities.

CHAPTER 7: CONCLUSIONS

7.1 Summary

This dissertation describes the design, development and characterization of two electronic devices for intraocular pressure (IOP) sensing and control. IOP is, to date, the only modifiable risk of glaucoma, a disease that claims the sight of millions of people worldwide. In most clinical cases, this disorder presents ocular hypertensive conditions that, over time, damage the cells responsible for relaying visual information to the brain. IOP is therefore fundamental in the diagnosis and management of the disease. Yet, little is known about the dynamics of IOP and its relationship to the onset and progression of glaucoma. Tonometry, the most commonly used IOP monitoring tool, lacks the accuracy and continuity necessary to carry out comprehensive research. Likewise, commercially available pressure sensors are subjected to unregulated battery drainage that compromises data accuracy and length of experiments. On the other hand, experimental models that aim to replicate the disease in animals offer limited controllability of IOP and are frequently ineffective in causing pressure elevation. The work presented throughout this document offers a solution to these problems.

The first device presented (iPump) employed a unique, patented, methodology to regulate pressure levels in the eye via a small cannula chronically implanted in the eye. The line continuously conducts pressure waves from the eye to a customized transducer. An especially designed control system uses microfluidic elements to manipulate intraocular volume levels based on the actual and desired pressure signals. The prototype built is tethered to the animal

using connecting tubing and sits next to the animal's cage. This process is the first glaucoma induction model to offer full controllability, nearly perfect success rate, and around the clock IOP measurements. The second device is an implantable IOP sensor for animal research. The system is attached to the animal's back and uses the same eye-cannulation procedure as the iPump to obtain measurements. The sensor can monitor IOP in a 24 hour basis with greater accuracy than any commercial sensor ever used to measure ocular pressure. Our design also eliminates commonly reported electronic drifts and offers, when paired with an innovative wireless powering technology (patent pending), unlimited operational lifetimes. The inventions developed in this project provide researchers with unique, pioneering tools that serve as enabling technologies to pave the way for future glaucoma research.

7.2 Original Contributions

The contributions of this project to the state of the art are summarized as follows:

- The iPump is the only ocular-hypertension induction mechanism available that offers the user full controllability over IOP. While traditional techniques to elevate IOP result in significant pressure variability throughout the experiments, the iPump maintains IOP within a programmable window of the set-point. By setting IOP to specific levels and exploring their correlation to glaucoma progression, researchers will be able to create more comprehensive glaucoma studies than ever before. Moreover, ocular hypertension induction using the iPump is effective 100% of the time, with pressure elevation seen within minutes. On the other hand traditional models are effective around 40% of the time and can take weeks to show signs of elevation.
- The mathematical model created to calculate ocular outflow parameters using the iPump provides accurate data while significantly shortening the duration of experiments. The

portability offered by the device also facilitates outflow measurements in any location without transporting the otherwise bulky and hard-to-set-up equipment traditionally used in these experiments. This becomes increasingly useful in laboratories where animals are housed in external vivaria and cannot be removed for survival experiments.

- The implantable sensor provides the user with continuous, accurate IOP measurements. Data obtained using this system is not subjected to artificial pressure drifts commonly seen in commercially available biomedical devices. These drifts generally require recurrent, invasive recalibration procedures. Unlike other IOP sensors, our system is fully programmable, which allows the user to collect data in a wide range of sampling rates.
- The wireless powering system for moving biological sensors (patent pending) developed to run the implantable sensor is able to produce 4-12mWatts at all times, regardless of the animal's movements. This power-availability level, in combination with the low power consumption of the implantable sensor, creates a surplus of energy that can be used to incorporate multiple sensors into the device, while providing unlimited battery life.

7.3 Recommendations for Future Research

7.3.1 Advancing this Technology

The most desirable system for glaucoma research is an implantable version of the iPump. The implantable sensor was developed with this in mind and should serve as an important stepping stone towards the final iPump iteration. The components of the current device were picked to provide a seamless transition towards miniaturization, yet the biggest challenge remains the efficient use of energy to power the pump, even with the wireless powering technology. Running the pump at full performance, as it is done in the experiments shown in this document, requires power levels beyond the capabilities of our energy harvesting system. The

pump's performance depends on two factors, the amplitude and the frequency of the PWM signal that is delivered to the pump's driver. Decreasing the signal's amplitude reduces the power consumption of the module, but also increases the sensibility of the pump to back pressure (e.g. IOP). As a result, IOP changes will cause a change in the flowrate, which in the current version is maintained constant. These changes may result in slower response times and could limit the maximum pressure level to which the system can raise pressure. A varying pumping rate would also impair the use of the constant-pressure perfusion method to calculate outflow facility. Changes in flow rate could be avoided by implementing a second closed-loop control system that regulates the voltage delivered to the pump's driver based on IOP levels. Along with the added controller, a new pump driver may be necessary to create the necessary power fluctuation to modulate flowrate. If the additional components resulted in an overall size beyond the requirements of the system, the mp6 pump could be substituted by the mp5 model. The mp5 is about half the size of the mp6, but it is only equipped with a single piezo-actuator, which further increases its susceptibility to backpressure.

7.3.2 Glaucoma Research

While much has been accomplished to this point using the iPump and the implantable IOP sensor, there is still work to be done. The next step towards advancing glaucoma knowledge is to utilize these devices to fully characterize IOP dynamics, as well as the correlation between ocular hypertension and glaucoma development. The study of IOP's natural fluctuations is essential for clinical assessment of the disease. To implement adequate medical treatments we must first thoroughly understand the healthy physiology and behavior of the parameters that we wish to modify. Extensive statistical analysis of an increased number of animals implanted with our sensor can begin to create a comprehensive picture of the natural behavior of IOP. These

experiments will help define the amplitude and time scales of circadian rhythms to which the eye is exposed. Following the work done in rabbits by McLaren and his colleagues (McLaren, 1996), light cycles of the housing rooms can be altered to analyze its effect on the previously observed variations, which are underexplored in rats. Once normal IOP dynamics have been fully characterized, the iPump can be used to systematically bring IOP levels to different values to later correlate them to ocular cell damage. For instance, IOP can be kept at 25mmHg in one cohort of rats for several weeks, while other groups are maintained at 30 and 35mmHg. After the experiments are terminated, histological processing of the eyes can provide a comparison of final ganglion cell counts between the groups. The untreated eye can also be processed to serve as a control and provide information regarding the original cell count. The length of hypertension exposure can also be modulated to provide further characterization. Alternatively, in some animals pressure can remain unaltered throughout the day, except for periodic systematic elevations using ramp or see-saw inputs that can be coded into the device. The amplitude and time course of these functions can provide definitive answers about the damage induced by acute spikes vs mean elevations of pressure.

Not all forms of glaucoma are associated with elevated IOP. Some individuals have glaucoma even though their pressure falls within a normal range, while others have abnormally high pressure yet show no clinical sign of retinal or optic nerve damage based on optic disc inspection and visual field measurement (Klein, 1992; Shiose, 1991). The reasons for this are not yet understood. It is suspected that intracranial pressure (ICP) might play a role (Berdahl, 2008). Retinal ganglion cell axons exit the eye through the lamina cribosa at the optic nerve head. Since the optic nerve is bathed in cerebrospinal fluid, the lamina is subjected to a tonic pressure gradient that is driven on the anterior side by IOP and the posterior side by ICP. An abnormally

low ICP could thus conceivably cause glaucoma as well. The implantable sensor could potentially be used to continuously monitor ICP, simply by implanting the cannula in the intracranial space instead of the eye. Alternatively, the second pressure transducer of the system can be implemented to obtain IOP and ICP measurements in parallel. Such experiments could provide researchers, for the first time, with continuous data of the pressure gradient to which the ocular nerve is exposed. Once the normal IOP-ICP relationship has been characterized, the iPump can be used to chronically control the gradient at will. IOP can be lowered or raised while ICP remains unchanged, or vice versa. Then specific damage to the ocular nerve could then be fully mapped out to compression levels of the lamina cribosa based on pressure values.

Glaucoma has also been linked to other conditions. Several studies have shown a strong correlation between diabetes and increased IOP (Lee, 2002; Memarzadeh, 2008; Mitchell, 1997), suggesting that diabetic patients may be at higher risk for glaucoma. These findings, however, remain controversial as other studies have found no such correlation (Quigley, 2001; Tielsch, 1995). Some experts suggest that the increased number of glaucoma diagnoses among diabetic patients is due to the greater scrutiny to which they are subjected given their risk for other ocular conditions, such as retinopathy (Klein, 1984). These contradictory findings have left a gap in knowledge between the two diseases. However, the use of the implantable sensor could provide useful insight into this matter. For years, researchers have developed experimental animal models to study diabetic disorders (King, 2008; King, 2012; Kim, 2005; Vickers, 2011), and the implantable sensor has been proven to collect IOP data much more effectively than tonometry techniques, like those used during clinical studies (chapter 5). Researchers could, for example, use these models to correlate weight and insulin levels to IOP changes over time. The

implementation of our system in combination with controlled diabetic models could provide a definitive picture regarding the relationship between diabetes and glaucoma onset.

7.3.3 Other Medical Applications

Injection and drainage are common occurrences in the medical field. Several conditions require physicians or nurses to extract fluid out of the body or inject a substance into it. In most cases the fluid in question is enclosed within a compartment in the body, which is subjected to pressure changes as the fluid volume is altered. The ability to move fluid in and out of a chamber based on pressure readings is the idea around which the iPump was built. This opens a world of possibilities to the technology presented in this dissertation. A few of them are explored next.

For instance, survey studies have found an increased incidence of shoulder bursitis among elderly members of the general population (Bosworth, 1941). The condition is characterized by inflammation of the sac located between tissues in our joints (bursa). It can present itself in the shoulder, elbow, hip and knee due to chronic injuries or as a natural part of the aging process (Ghelman, 2008). The symptoms range from joint stiffness to acute pain in the area (Fauci, 2010). In chronic conditions where extreme inflammation is experienced by the patient, periodic drainage of the joint may be necessary. This process can be painful and requires recurrent visits to the doctor's office (Ghelman, 2008). Cortisone shots are often administered to treat the condition, offering significant relief. However, in most cases the symptoms return over time (Ghelman, 2008). In chronic cases, the symptoms could be potentially eased with the use of the iPump. The small cannula could be permanently implanted in the affected bursa to continuously monitor pressure in the joint. The controller would then use pressure information to infer when there is an excess of fluid and use the pump to progressively drain the area. The fluid could be dumped into a small disposable reservoir taped to the outside of the skin. The draining

process would be gradual so that fluid levels never reach the point of pain receptor stimulation. The patient could replace the reservoir daily, avoiding time consuming trips to the doctor and, more importantly regaining full mobility without pain.

Another potential application for the iPump is found in patients that experience urinary retention syndrome, or ischuria. Patients who suffer from this condition are partially or completely unable to empty their bladder. This condition is especially common among men, with studies concluding that 4.5 to 6.8 per 1,000 men over 40 years old present urinary retention (Jacobsen, 1997; Meigs, 1999). Statistical incidence significantly increases with age, as men over 70 present a 10% chance of developing the condition, while a man over 80 sees his odds increase to 30% (Jacobsen, 1997; Meigs, 1999). The condition presents an important clinical challenge as its management practices are poorly defined (Carlo, 2012) and most prospective trials are not properly inclusive in their subject selection (Doll, 1993), possibly due to high risk of complications (Carlo, 2012). These issues have left numerous patients across the globe without a viable solution. The condition occurs when an obstructive or inflammatory process impedes normal fluid flow through the urinary track (Rosenstein, 2004). The most common cause of urinary retention is benign prostatic hyperplasia (BPH), which accounts for 53% of the cases (Curtis, 2001; Rosenstein, 2004). In most chronic cases, patients must self-catheter multiple times a day in order to release the urine produced by their bodies (Rosenstein, 2004). This process can be highly uncomfortable and time consuming.

In these cases the iPump can serve as a clinical treatment rather than a research tool. Two cannulas can be chronically implanted: the first cannula is placed inside the bladder, while the second cannula is inserted in the urinary track passed the site of obstruction. The system effectively bypasses the portion of the pathway that is nonfunctional and allows the patient to

urinate normally. The circuitry can be worn on the patient's belt around the clock. The sensor continually monitors intra-bladder pressure to assess the urine volume levels. When values reach a certain level the iPump can be programmed to send a signal to a phone app or fitness tracker to notify the user. The patient can then go to the restroom and activate the pump to pull fluid from the bladder and pump it into the urinary track, effectively emptying it. This procedure is more effective than simply implanting a shunt between the bladder and the urethra, as only the iPump can offer full controllability as to when the drainage process is started. Similarly, patients with urinary incontinence can implement the iPump as a way to bypass the urinary track and prevent fluid from leaving the bladder involuntarily. The urethra can be surgically blocked during implantation to allow the iPump to have full control over fluid levels. As this process is implemented some design considerations must be acknowledged. Some of the original specifications of the pump may need redefining to allow for higher flowrates that would empty the bladder within an appropriate timeframe.

Note that the both the urinary retention and the bursitis drainage applications require an implantable system rather than a tethered version like the one presented in chapter 3. Nevertheless, the only impediment that we have faced for system miniaturization, in animal research applications, deal with power demands. The device requires greater energy harvesting capabilities or batteries whose size is not viable for implantation in a rodent. However, the specific sensing components have already been miniaturized for their application on the implantable sensor and pumping elements are manufactured in small sizes. For human applications, rechargeable batteries with much bigger capacities do not represent a challenge. These batteries are not bigger or heavier than those commonly found in small portable electronics and can be recharged daily in the same fashion as cellphones.

Other urological conditions can also be addressed using our technology. For instance, Conditions such as bladder cancer can permanently damage the ability of the bladder to perform as a urine reservoir (Porter, 2005). The disease requires patients to go through a surgical procedure to replace the bladder with an artificial reservoir or one made out of bowel tissue (Hautmann, 2003). An internal conduct, called a stoma, is implanted to provide external access to the new fluid pool. In most cases the patient is required to self-intubate through the stoma and manually empty the pouch every 4-6 hours (Skinner, 1989). Failure to do so can result in leakage or infection, which could lead to kidney failure and pouchitis (inflammation of the reservoir) (Skinner, 1989). To avoid these complications the patient must ensure that drainage is done in a timely manner, preferably before fluid levels reach high values. The implantable sensor developed in this project can be used to monitor fluid levels and notify the user when fluid drainage is necessary. A cannula could be implanted in the artificial reservoir to measure in pressure and estimate fluid levels. Once those reach a user defined threshold, the system can wirelessly transmit a signal to a phone app or fitness tracker to notify the patient. This procedure would avoid common complications and improve the quality of life of patients that have been subjected to the insidious consequences of cancer. Some considerations should be taken to ensure sterility of the conducts and cannulas. However, urinary diversion techniques have been employed for over 160 years as a mean to bypass nonfunctional urinary organs (Simon, 1852). These common practices have provided physicians with innumerable hours of experience regarding catheter implantation and management of aseptic conditions.

7.4 Concluding Remarks

The systems developed throughout this project have met the originally proposed aims. This technology has successfully met the requirements outlined in chapter 2 for an ideal

glaucoma research model, table 7.1 illustrates this comparison. The accuracy, continuity and reliability of the pressure readings obtained with our devices projects our systems to be the finest IOP monitoring technology ever made for animal research. Similarly, the robust pressure control obtained with iPump makes it the most complete glaucoma induction model ever designed. The applications of these devices extend well beyond glaucoma studies, with the potential to affect several areas of the medical field and positively affect the lives of millions of people. In all, the contributions made in this thesis could the change the current paradigms of glaucoma research.

Table 7.1 Our Systems vs. The Ideal Systems

Feature	Ideal Sensor	Our Sensor		Feature	Ideal Model	iPump
Continuous data	Yes	Yes		Success Rate	100%	100%
Accuracy	< 1 mmHg	0.2 mmHg		Sustained elevation	Yes	Yes
Drift	None	None		IOP controllability	Yes	Yes
Animal species	Rodents, rabbits, monkeys	Rodents, rabbits, monkeys		Bio-response	None	None
Transcorneal	No	No		Unilateral	Yes	Yes
Operational Life	> 3 months	Unlimited*		Reversible	Yes	Yes
Multi-sensor	Yes	Yes		Time before elevation	Immediate	Minutes
Pressure Unit	mmHg	mmHg				

REFERENCES

Abrams L S, Vitale S, and Jampel H D. Comparison of three tonometers for measuring intraocular pressure in rabbits. *Invest. Ophthalmol. Vis. Sci.* 37 940-944. 1996.

Akaishi T, Ishida N, Shimazaki A, Hara H, Kuwayama Y. Continuous monitoring of circadian variations in intraocular pressure by telemetry system throughout a 12-week treatment with timolol maleate in rabbits. *J. Ocul. Pharmacol. Therap.* 21 436-444. 2005.

Asrani S, Zeimer R, Wilensky J, Gieser D, Vitale S, Lindenmuth K. Large diurnal fluctuations in intraocular pressure are an independent risk factor in patients with glaucoma. *J. Glaucoma* 9 134-142. 2000.

Aihara M, Lindsey JD, Weinreb RN. Aqueous humor dynamics in mice. *Invest Ophthalmol Vis Sci*. 2003 Dec;44(12):5168-73. PubMed PMID: 14638713.

Barany EH. The mode of action of pilocarpine on outflow resistance in the eye of a primate (Cercopithecus ethiops). *Invest Ophthalmol.* 1962 Dec;1:712-27.PubMed PMID: 13966451.

Bello, SA., Malavade A, and Passaglia CL. Development of a Smart Pump for Monitoring and Controlling Intraocular Pressure. *Annals of Biomedical Engineering* (2016): 1-13.

Bengtsson B, Leske MC, Hyman L, Heijl A. Fluctuation of intraocular pressure and glaucoma progression in the early manifest glaucoma trial. *Ophthalmol.* 114 205-209. 2007.

Berdahl JP, Fautsch MP, Stinnett SS, Allingham RR. Intracranial pressure in primary open angle glaucoma, normal tension glaucoma, and ocular hypertension: a case-control study. *Invest Ophthalmol Vis Sci*. 2008 Dec;49(12):5412-8. doi:10.1167/iovs.08-2228.

Bosworth B. Calcium deposits in the shoulder and subacromial bursitis: a survey of 12,122 shoulders. *JAMA. 1941; 116*(22): 2477-2482.

Caprioli J, Coleman AL. Intraocular pressure fluctuation a risk factor for visual field progression at low intraocular pressures in the advanced glaucoma intervention study. *Ophthalmology*. 2008 Jul;115(7):1123-1129.e3. Epub 2008 Feb 20. PubMed PMID: 18082889.

Chauhan BC, Pan J, Archibald ML, LeVatte TL, Kelly ME, Tremblay F. Effect of intraocular pressure on optic disc topography, electroretinography, and axonal loss in a chronic pressure-induced rat model of optic nerve damage. *Invest Ophthalmol Vis Sci*. 2002 Sep;43(9):2969-76. PubMed PMID: 12202517.

Curtis LA, Dolan TS, Cespedes RD. Acute urinary retention and urinary incontinence. *Emerg Med Clin North Am*. 2001;19(3):591-619

Dawson WW, Brooks DE, Hope GM et al.Primary open angle glaucomas in the rhesus monkey. *British Journal of Ophthalmology*. 1993 vol. 77, no. 5, pp. 302–310

Doll HA, Black NA, McPherson K, Williams GB, Smith JC. Differences in outcome of transurethral resection of the prostate for benign prostatic hypertrophy between three diagnostic categories. *Br J Urol* 1993; 72:322–30

Downs JC, Burgoyne CF, Seigfreid WP, Reynaud JF, Strouthidis NG, Sallee V. 24-hour IOP telemetry in the nonhuman primate: implant system performance and initial characterization of IOP at multiple timescales. *Invest. Ophthalmol. Vis. Sci.* 52 7365-7375. 2011.

Downs JC, Turner D, Girkin CA; Evidence for the "White Coat Effect" on IOP Measured Using Continuous IOP Telemetry in Nonhuman Primates. *Invest. Ophthalmol. Vis. Sci.* 2016;57(12):6466.

Fauci, Anthony (2010). *Harrison's Rheumatology, Second Edition*. McGraw-Hill Professional Publishing; Digital Edition. p. 271. ISBN 9780071741460.

Fitt AD, Gonzalez G. Fluid mechanics of the human eye: aqueous humour flow in the anterior chamber. *Bull Math Biol*. 2006 Jan;68(1):53-71. Epub 2006 Mar 8.PubMed PMID: 16794921.

Frampton P, Da Rin D, Brown B. Diurnal variation of intraocular pressure and the overriding effects of sleep. *Am J Optom Physiol Opt*. 1987 Jan;64(1):54-61. PubMed PMID: 3826279.

Friedman DS, Wolfs RC, O'Colmain BJ, Klein BE, Taylor HR, West S, Leske MC, Mitchell P, Congdon N, Kempen J; Eye Diseases Prevalence Research Group.Prevalence of open-angle glaucoma among adults in the United States. *Arch Ophthalmol*. 2004 Apr;122(4):532-8. Erratum in: Arch Ophthalmol. 2011 Sep;129(9):1224. PubMed PMID: 15078671; PubMed Central PMCID: PMC2798086.

Gaasterland D, Kupfer C. Experimental glaucoma in the rhesus monkey. *Invest Ophthalmol.* 1974 Jun;13(6):455-7. PubMed PMID: 4208801.

Gautam N, Kaur S, Kaushik S, Raj S, Pandav SS. Postural and diurnal fluctuations in intraocular pressure across the spectrum of glaucoma. *Br J Ophthalmol*. 2016 Apr; 100(4):537-41. doi: 10.1136/bjophthalmol 2015-306861. Epub 2015 Aug 12. PubMed PMID: 26269532.

Ghelman, Vincent J. Vigorita ; with Bernard; Mintz, Douglas (2008). *Orthopaedic pathology* (2nd ed.). Philadelphia: Lippincott Williams and Wilkins. p. 719. ISBN 978-0-7817-9670-5.

Goldmann H. Out-flow pressure, minute volume and resistance of the anterior chamber flow in man. *Doc Ophthalmol*. 1951;5-6:278-356 .PubMed PMID: 14896880.

Grozdanic SD, Betts DM, Sakaguchi DS, Kwon YH, Kardon RH, Sonea IM. Temporary elevation of the intraocular pressure by cauterization of vortex and episcleralveins in rats causes functional deficits in the retina and optic nerve. *Exp EyeRes.* 2003 Jul;77(1):27-33. PubMed PMID: 12823985.

Ha D, de Vries WN, John SW, Irazoqui PP, Chappell WJ. Polymer-based miniature flexible capacitive pressure sensor for intraocular pressure (IOP) monitoring inside a mouse eye. *Biomed Microdevices*. 2012 Feb;14(1):207-15. doi: 10.1007/s10544-011-9598-3. PubMed PMID: 21987004.

Hautmann, Richard E. "Urinary diversion: ileal conduit to neobladder. *The Journal of urology* 2003: 169.3, 834-842.

Heijl A, Leske MC, Bengtsson B, Hyman L, Bengtsson B, Hussein M; Early Manifest Glaucoma Trial Group. Reduction of intraocular pressure and glaucoma progression: results from the Early Manifest Glaucoma Trial. *Arch Ophthalmol*.2002 Oct;120(10):1268-79. PubMed PMID: 12365904.

Ho JS, Yeh AJ, Neofytou E, Kim S, Tanabe Y, Patlolla B, Beygui RE, Poon AS. Wireless power transfer to deep-tissue microimplants. *Proc Natl Acad Sci*. 2014 Jun 3;111(22):7974-9. doi: 10.1073/pnas.1403002111. Epub 2014 May 19. PubMed PMID: 24843161; PubMed Central PMCID: PMC4050616.

Jacobsen SJ, Jacobson DJ, Girman CJ, et al. Natural history of prostatism: risk factors for acute urinary retention. *J Urol*. 1997;158(2):481-487

Jasien JV, Hethcox L, Turner D, Girkin CA, Downs JC. Comparison of the Effects of Injectable and Inhalant Anesthesia on IOP in Nonhuman Primates as Measured with Continuous IOP Telemetry.*Invest. Ophthalmol. Vis. Sci.* 201657(12)

Jia L, Cepurna WO, Johnson EC, Morrison JC. Effect of general anesthetics on IOP in rats with experimental aqueous outflow obstruction. *Invest Ophthalmol Vis Sci.* 2000 Oct;41(11):3415-9. PubMed PMID: 11006233.

John, SW. Mechanistic insights into glaucoma provided by experimental genetics. The Cogan Lecture. *Invest Ophthalmol Vis Sci* 2005, 39:951-62. PMID: 16043833

Johnson M, McLaren JW, Overby DR. Unconventional aqueous humor outflow: A review. *Exp Eye Res*. 2016 Feb 2. pii: S0014-4835(16)30016-1. doi: 10.1016/j.exer.2016.01.017. Review. PubMed PMID: 26850315; PubMed Central PMCID: PMC4970980.

Karyotakis NG, Ginis HS, Dastiridou AI, Tsilimbaris MK, Pallikaris IG. Manometric measurement of the outflow facility in the living human eye and its dependence on intraocular pressure. *Acta Ophthalmol*. 2015 Aug;93(5):e343-8. doi: 10.1111/aos.12652. Epub 2015 Feb 1. PubMed PMID: 25645503.

Kass MA, Heuer DK, Higginbotham EJ, Johnson CA, Keltner JL, Miller JP, Parrish RK 2nd, Wilson MR, Gordon MO. The Ocular Hypertension Treatment Study: a randomized trial determines that topical ocular hypotensive medication delays or prevents the onset of primary open-angle glaucoma. *Arch Ophthalmol*. 2002 Jun;120(6):701-13; discussion 829-30. PubMed PMID: 12049574.

Katsimpris JM, Theoulakis PE, Papadopoulos GE, Katsimpris A, Lepidas J, Petropoulos IK. Ocular pulse amplitude measurement using pascal dynamic contour tonometer in glaucoma patients. *Klin Monbl Augenheilkd*. 2014 Apr;231(4):363-7. doi: 10.1055/s-0034-1368220. Epub 2014 Apr 25. PubMed PMID: 24771168.

Kee C, Hong T, Choi K. A sensitive ocular perfusion apparatus measuring outflow facility. *Curr Eye Res*. 1997 Dec;16(12):1198-201. PubMed PMID: 9426951.

Kim S, Ho JS, Poon ASY. Midfield wireless powering of subwavelength autonomous devices. *Phys Rev Lett*. 2013;110:203905.

King AJ. The use of animal models in diabetes research. *British Journal of Pharmacology*. 2012;166(3):877-894.

Klein R, Klein BK, Moss SE, Davis MD, DeMets DL. The Wisconsin Epidemiologic Study of Diabetic Retinopathy: III. Prevalence and Risk of Diabetic Retinopathy When Age at Diagnosis Is 30 or More Years. *Arch Ophthalmol*. 1984;102(4):527-532.

Klein BE, Klein R, Sponsel WE, Franke T, Cantor LB, Martone J, Menage MJ. Prevalence of glaucoma:The Beaver Dam Eye Study. *Ophthalmology* 1992, 99:1499-1504.

Kolker AE, Moses RA, Constant MA, and Becker B. The development of glaucoma in rabbits. *Investigative Ophthalmology*. 1963. vol. 2, pp. 316–321.

Koutsonas A, Walter P, Roessler G, Plange N. Implantation of a novel telemetric intraocular pressure sensor in patients with glaucoma (ARGOS study): 1-year results. *Invest Ophthalmol Vis Sci*. 2015 Jan 22;56(2):1063-9. doi: 10.1167/iovs.14-14925. PubMed PMID: 25613949.

Lee JS, Lee SH, Oum BS, Chung JS, Cho BM, and Hong JM. Relationship between intraocular pressure and systemic health parameters in a Korean population. *Clinical & Experimental Ophthalmology*. 2002. vol. 30, no. 4, pp. 237–241.

Lei Y, Overby DR, Boussommier-Calleja A, Stamer WD, Ethier CR. Outflow physiology of the mouse eye: pressure dependence and washout. *Invest Ophthalmol Vis Sci.* 2011 Mar 29;52(3):1865-71. doi: 10.1167/iovs.10-6019. Print 2011 Mar. PubMed PMID: 21169533; PubMed Central PMCID: PMC3101677.

Leonardi M, Pitchon EM, Bertsch A, Renaud P, Mermoud A. Wireless contact lens sensor for intraocular pressure monitoring: assessment on enucleated pig eyes. *Acta Ophthalmol.* 2009 Jun;87(4):433-7. doi: 10.1111/j.1755-3768.2008.01404.x. Epub 2008 Nov 12. PubMed PMID: 19016660.

Leske MC, Connell AM, Wu SY, Hyman LG, Schachat AP. Risk factors for open-angle glaucoma. The Barbados Eye Study. *Arch Ophthalmol*. 1995 Jul;113(7):918-24. PubMed PMID: 7605285.

Levkovitch-Verbin H, Quigley HA, Martin KR, Valenta D, Baumrind LA, Pease ME. Translimbal laser photocoagulation to the trabecular meshwork as a model of glaucoma in rats. *Invest Ophthalmol Vis Sci.* 2002 Feb;43(2):402-10. PubMed PMID: 11818384.

Li R and Liu J H. Telemetric monitoring of 24 h intraocular pressure in conscious and freely moving C57BL/6J and CBA/CaJ mice. *Mol. Vision.* 2008; 14: 745-749.

Liu J, Roberts CJ. Influence of corneal biomechanical properties on intraocular pressure measurement: quantitative analysis. *J Cataract Refract Surg*. 2005 Jan;31(1):146-55. PubMed PMID: 15721707

Liu JH, Zhang X, Kripke DF, Weinreb RN. Twenty-four-hour intraocular pressure pattern associated with early glaucomatous changes. *Invest. Ophthalmol. Vis. Sci.* 44 1586-1590. 2003.

Luce DA. Determining in vivo biomechanical properties of the cornea with an ocular response analyzer. *J Cataract Refract Surg*. 2005 Jan;31(1):156-62. PubMed PMID: 15721708.

Mansouri K, Shaarawy T. Continuous intraocular pressure monitoring with a wireless ocular telemetry sensor: initial clinical experience in patients with open angle glaucoma. *Br J Ophthalmol.* 2011 May;95(5):627-9. doi: 10.1136/bjo.2010.192922. Epub 2011 Jan 7. PubMed PMID: 21216796.

Mansouri K, Medeiros FA, Tafreshi A, Weinreb RN. Continuous 24-hour monitoring of intraocular pressure patterns with a contact lens sensor: safety, tolerability, and reproducibility in patients with glaucoma. *Arch Ophthalmol*. 2012 Dec;130(12):1534-9. doi: 10.1001/jamaophthalmol.2013.1350. PubMed PMID: 23229696.

Mateijsen DJ, Rosingh HJ, Wit HP, Albers FW. Perilymphatic pressure measurement in patients with Menière's disease. *Eur Arch Otorhinolaryngol*. 2001 Jan;258(1):1-4. PubMed PMID: 11271426.

McLaren J W, Brubaker R F, and Fitzsimon J S. Continuous measurement of intraocular pressure in rabbits by telemetry. *Invest. Ophthalmol. Vis. Sci.* 37 966-975. 1996.

McNulty R, Wang H, Mathias RT, Ortwerth BJ, Truscott RJ, Bassnett S. Regulation of tissue oxygen levels in the mammalian lens. *J Physiol*. 2004 Sep 15;559(Pt 3):883-98. Epub 2004 Jul 22. PubMed PMID: 15272034; PubMed Central PMCID: PMC1665185.

Medeiros FA, Weinreb RN, Zangwill LM, Alencar LM, Sample PA, Vasile C, Bowd C. Long-term intraocular pressure fluctuations and risk of conversion from ocular hypertension to glaucoma. *Ophthalmology*. 2008 Jun;115(6):934-40. Epub 2007 Oct 15. PubMed PMID: 17936908; PubMed Central PMCID: PMC2848165.

Meigs JB, Barry MJ, Giovannucci E, Rimm EB, Stampfer MJ, Kawachi I. Incidence rates and risk factors for acute urinary retention: the health professionals follow up study. *J Urol.* 1999;162(2):376-382

Memarzadeh F, Ying-Lai M, Azen SP, and Varma R. Associations with intraocular pressure in Latinos: the Los Angeles Latino Eye Study. *American Journal of Ophthalmology*. 2008 vol. 146, no. 1, pp. 69–76

Mermoud A, Baerveldt G, Minckler DS, Prata JA Jr, Rao NA. Aqueous humor dynamics in rats. *Graefes Arch Clin Exp Ophthalmol*. 1996 Aug;234 Suppl 1:S198-203. PubMed PMID: 8871174.

Millar JC, Clark AF, Pang IH. Assessment of aqueous humor dynamics in the mouse by a novel method of constant-flow infusion. *Invest Ophthalmol Vis Sci*.2011 Feb 3;52(2):685-94. doi: 10.1167/iovs.10-6069. PubMed PMID: 20861483.

Mitchell P, Smith W, Chey T, and Healey PR. Open-angle glaucoma and diabetes: the Blue Mountains eye study, Australia. *Ophthalmology*. 1997. vol. 104, no. 4, pp. 712–718.

Montgomery KL, Yeh AJ, Ho JS, Tsao V, Mohan Iyer S, Grosenick L, Ferenczi EA, Tanabe Y, Deisseroth K, Delp SL, Poon AS. Wirelessly powered, fully internal optogenetics for brain, spinal and peripheral circuits in mice. *Nat Methods*. 2015 Oct;12(10):969-74. doi: 10.1038/nmeth.3536. Epub 2015 Aug 17. PubMed PMID:26280330.

Moore CG, Johnson EC, Morrison JC. Circadian rhythm of intraocular pressure in the rat. *Curr Eye Res*. 1996 Feb;15(2):185-91. PubMed PMID: 8670727.

Morrison JC, Moore CG, Deppmeier LM, Gold BG, Meshul CK, Johnson EC.A rat model of chronic pressure-induced optic nerve damage. *Exp. Eye Res.* 64 85-96. 1997.

Morrison JC, Cepurna WO, Guo Y, Johnson EC. Pathophysiology of human glaucomatous optic nerve damage: insights from rodent models of glaucoma. 2011. *Exp Eye Res*. 93:156-164

Morrison JC, Cepurna WO, Johnson EC. Modeling glaucoma in rats by sclerosing aqueous outflow pathways to elevate intraocular pressure. *Exp Eye Res*. 2015 Dec;141:23-32. doi: 10.1016/j.exer.2015.05.012. Epub 2015 May 21. Review. PubMed PMID: 26003399; PubMed Central PMCID: PMC4628875.

Nusbaum DM, Wu SM, Frankfort BJ. Elevated intracranial pressure causes optic nerve and retinal ganglion cell degeneration in mice. *Exp Eye Res*. 2015 Jul;136:38-44. doi: 10.1016/j.exer.2015.04.014. Epub 2015 Apr 23. PubMed PMID: 25912998; PubMed Central PMCID: PMC4466149.

Parasuraman S, Raveendran R. Measurement of invasive blood pressure in rats. *Journal of Pharmacology & Pharmacotherapeutics*. 2012;3(2):172-177. doi:10.4103/0976-500X.95521.

Porter, MP, and Penson DF. Health related quality of life after radical cystectomy and urinary diversion for bladder cancer: a systematic review and critical analysis of the literature. *The Journal of urology* 173.4 (2005): 1318-1322.

Quigley HA, Addicks EM. Chronic experimental glaucoma in primates. I. Production of elevated intraocular pressure by anterior chamber injection of autologous ghost red blood cells. *Invest Ophthalmol Vis Sci.* 1980 Feb;19(2):126-36. PubMed PMID: 6766124.

Quigley HA, Addicks EM, Green WR. Optic nerve damage in human glaucoma. III. Quantitative correlation of nerve fiber loss and visual field defect in glaucoma,ischemic neuropathy, papilledema, and toxic neuropathy. *Arch Ophthalmol*. 1982 Jan;100(1):135-46. PubMed PMID: 7055464.

Quigley HA, West SK, Rodriguez J, et al. The prevalence of glaucoma in a population-based study of Hispanic subjects: Proyecto VER. *Arch Ophthalmol*. 2001;119:1819e26.

Quigley HA, Broman AT. The number of people with glaucoma worldwide in 2010 and 2020. *Br J Ophthalmol*. 2006 Mar;90(3):262-7. PubMed PMID: 16488940; PubMed Central PMCID: PMC1856963.

RamRakhyani AK, Mirabbasi S, Chiao M. Design and Optimization of Resonance-Based Efficient Wireless Power Delivery Systems for Biomedical Implants. *IEEE Transactions on Biomedical Circuits and Systems*. Feb. 2011 vol. 5, no. 1, pp. 48-63. doi: 10.1109/TBCAS.2010.2072782

Ren R, Jonas JB, Tian G, Zhen Y, Ma K, Li S, Wang H, Li B, Zhang X, Wang N. Cerebrospinal fluid pressure in glaucoma: a prospective study. *Ophthalmology*. 2010 Feb;117(2):259-66. doi: 10.1016/j.ophtha.2009.06.058. Epub 2009 Dec 6. PubMed PMID: 19969367.

Rosenstein D, McAninch JW. Urologic emergencies. *Med Clin North Am*. 2004;88(2):495-518.

Ruiz-Ederra, J., M. Garcia, M. Hernandez, H. Urcola, E. Hernandez-Barbachano, J. Araiz, and E. Vecino. The pig eye as a novel model of glaucoma. *Exp. Eye Res*. 2005. 81:561–569.

Salt AN, Plontke SK. Endolymphatic hydrops: pathophysiology and experimental models. Otolaryngol Clin North Am. 2010 Oct;43(5):971-83. doi:10.1016/j.otc.2010.05.007. Review. PubMed PMID: 20713237; PubMed Central PMCID: PMC2923478.

Sappington RM, Carlson BJ, Crish SD, Calkins DJ. The microbead occlusion model: a paradigm for induced ocular hypertension in rats and mice. Invest Ophthalmol Vis Sci. 2010 Jan;51(1):207-16. doi: 10.1167/iovs.09-3947. Epub 2009 Oct 22. PubMed PMID: 19850836; PubMed Central PMCID: PMC2869054.

Shareef SR, Garcia-Valenzuela E, Salierno A, Walsh J, Sharma SC. Chronic ocular hypertension following episcleral venous occlusion in rats. *Exp. Eye Res.* 61 379-382. 1995.

Shields MB. Uveoscleral drainage device. US Patent US20040015140 A1. 2004.

Shiose Y, Kitazawa Y, Tsukahara S, Akamatsu T, Mizokami K, Futa R, Katsushima H, Kosaki H. Epidemiology of glaucoma in Japan - a nationwide glaucoma survey. *Jpn J Ophthalmol* 1991, 35:133-155.

Simon J. Ectopia vesicae; operation for directing the orifices of the ureters into the rectum; temporary success; subsequent death; *autopsy Lancet*, 2 (1852), p. 568

Skinner DG., Lieskovsky G, and Boyd S."Continent urinary diversion. *The Journal of urology*. 1989. 141.6 : 1323-1327.

Sommer A. Intraocular pressure and glaucoma. *Am J Ophthalmol*. 1989 Feb 15;107(2):186 8. PubMed PMID: 2913813.

Sommer A, Tielsch JM. Risk factors for open-angle glaucoma: the Barbados Eye Study. *Arch Ophthalmol*. 1996 Feb;114(2):235. PubMed PMID: 8573036.

Takumida M, Akagi N, Anniko M. A new animal model for Ménière's disease. *Acta Otolaryngol*. 2008 Mar;128(3):263-71. PubMed PMID: 17851960.

Tamm ER. The trabecular meshwork outflow pathways: structural and functional aspects. *Exp Eye Res* .2009, 88:648-655.

Tielsch JM, Katz J, Sommer A, et al. Hypertension, perfusion pressure, and primary open-angle glaucoma. A population based assessment. *Arch Ophthalmol*. 1995;113:216e21.

Todani A, Behlau I, Fava MA, Cade F, Cherfan DG, Zakka FR, Jakobiec FA, Gao Y, Dohlman CH, Melki SA. Intraocular pressure measurement by radio wave telemetry. *Invest Ophthalmol Vis Sci*. 2011 Dec 20;52(13):9573-80. doi: 10.1167/iovs.11-7878. PubMed PMID: 22039243.

Turner D, Girkin CA, Downs CA; IOP Elevations Associated with Eye Rubbing. *Invest. Ophthalmol. Vis. Sci.* 2016;57(12):6433.

Ueda J, Sawaguchi S, Hanyu T, Yaoeda K, Fukuchi T, Abe H, Ozawa H. Experimental glaucoma model in the rat induced by laser trabecular photocoagulation after an intracameral injection of India ink. *Jap. J. Ophthalmol.* 42 337-344. 1998.

Van Der Zypen E. Experimental morphological study on structure and function of the filtration angle of the rat eye. *Ophthalmologica*. 1977. vol. 174, no. 5, pp. 285–298.

Vickers SP, Jackson HC, Cheetham SC. The utility of animal models to evaluate novel anti-obesity agents. *Br J Pharmacol*. 2011 Oct;164(4):1248-62.

Walter P, Schnakenberg U, vom Bögel G, Ruokonen P, Krüger C, Dinslage S, Lüdtke Handjery HC, Richter H, Mokwa W, Diestelhorst M, Krieglstein GK. Development of a completely encapsulated intraocular pressure sensor. *Ophthalmic Res*. 2000 Nov-Dec;32(6):278-84. PubMed PMID: 11015039.

Wang G, Liu W, Sivaprakasam M, Zhou M, Weiland JD, Humayun MS. A Dual Band Wireless Power and Data Telemetry for Retinal Prosthesis. *Engineering in Medicine and Biology Society.* 2006 pp. 4392-4395.doi: 10.1109/IEMBS.2006.260470

Weber AJ, Zelenak D. Experimental glaucoma in the primate induced by latex microspheres. *J Neurosci Methods*. 2001 Oct 15;111(1):39-48. PubMed PMID:11574118.

Whitacre MM, Stein RA, Hassanein K. The effect of corneal thickness on applanation tonometry. *Am J Ophthalmol*. 1993 May 15;115(5):592-6. PubMed PMID: 8488910.

Wilensky JT. Diurnal variations in intraocular pressure. *Trans Am OphthalmolSoc*. 1991;89:757-90. Review. PubMed PMID: 1687295; PubMed Central PMCID:PMC1298639.

Wu L, Yang, Basham E, Liu W. An efficient wireless power link for high voltage retinal implant. *IEEE Biomedical Circuits and Systems Conference*. 2008 pp. 101-104. doi: 10.1109/BIOCAS.2008.4696884.

Yu W, Cao G, Qiu J, Liu X, Ma J, Li N, Yu M, Yan N, Chen L, Pang IH. Evaluation of monkey intraocular pressure by rebound tonometer. *Mol Vis*. 2009 Oct 27;15:2196-201. PubMed PMID: 19898690.

APPENDIX A:

COPYRIGHT PERMISSION

The following statement from Springer permits the reproduction of previously published content (i.e. Chapter 3) in this dissertation.

SPRINGER LICENSE
TERMS AND CONDITIONS

Oct 02, 2016

This Agreement between Simon A Bello ("You") and Springer ("Springer") consists of your license details and the terms and conditions provided by Springer and Copyright Clearance Center.

License Number	3961020906398
License date	Oct 02, 2016
Licensed Content Publisher	Springer
Licensed Content Publication	Annals of Biomedical Engineering
Licensed Content Title	Development of a Smart Pump for Monitoring and Controlling Intraocular Pressure
Licensed Content Author	Simon A. Bello
Licensed Content Date	Jan 1, 2016
Type of Use	Thesis/Dissertation
Portion	Full text
Number of copies	4
Author of this Springer article	Yes and you are the sole author of the new work
Order reference number	
Title of your thesis / dissertation	Continuous Intraocular Pressure Sensing and Control for Glaucoma Research
Expected completion date	Nov 2016
Estimated size(pages)	140
Requestor Location	Simon A Bello 13564 cypress glen ln apt 303 TAMPA, FL 33637 United States Attn: Simon A Bello
Billing Type	Invoice
Billing Address	Simon A Bello 13564 cypress glen ln apt 303 TAMPA, FL 33637 United States Attn: Simon A Bello
Total	0.00 USD
Terms and Conditions	

ABOUT THE AUTHOR

Simón Antonio Bello graduated from the University of South Florida with a B.S. in Electrical Engineering in 2011. Shortly after, he began his pursue of a Ph.D. in the same field. Simón joined the Ocular Neuroscience and Neuroengineering Laboratory as a Research Assistant in 2012 where he began to apply his background to developed specialized electronics for glaucoma research. In 2013, he received his M.S. in Electrical Engineering with a concentration in Biomedical Systems. During his tenure as a graduate student, Simón's work has been recognized in multiple occasions, being awarded 3rd place in both the 2014 and 2015 Healthcare Innovation Competition, and 2nd place in 2013 RF Diagnostics design competition. Simón also worked as a Teaching Assistant in the areas of Circuit Design and Control's Theory.